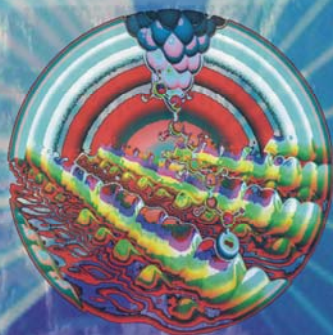# Gold- and Platinum Induced Nanowires on Ge(001);

Structure, Electronic Properties and Interaction with Simple Molecules
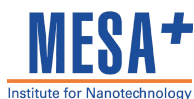
Daan Kockmann

Gold- and Platinum Induced Nanowires on Ge(001);

Structure, Electronic Properties and Interaction with Simple Molecules

Daan Kockmann

Goud- en Platina Geïnduceerde Nanodraden op Ge(001);

Structuur, Elektronische Eigenschappen en Interactie met Simpele Moleculen

Daan Kockmann

Samenstelling promotiecommissie:

Prof. dr. G. van der Steenhoven

Prof. dr. ir. H. J. W. Zandvliet

Prof. dr. ir. B. Poelsema

Dr. A. van Houselt

Prof. dr. ir. J. Huskens

Prof. dr. ir. J. W. M. Hilgenkamp

Prof. dr. B.-J. Ravoo

GOLD- AND PLATINUM INDUCED NANOWIRES ON GE(001); STRUCTURE, ELECTRONIC PROPERTIES AND INTERACTIONS WITH SIMPLE MOLECULES

PROEFSCHRIFT

ter verkrijging van,

de graad van doctor aan de Universiteit Twente,

op gezag van de rector magnificus,

prof. dr. H. Brinksma,

volgens het besluit van het College voor Promoties

in het openbaar te verdedigen op

vrijdag 9 juli 2010 om 13.15 uur

door

Daniel Kockmann

geboren op 16 juli 1978

te Feldkirch, Oostenrijk

Dit proefschrift is goedgekeurd door de promotores:

Prof. dr. ir. Harold J. W. Zandvliet

Prof. dr. ir. Bene Poelsema

Contents

Chapter One:

Introduction

General

In this dissertation some of the results that were obtained during this PhD-project are presented. The research of this PhD-project lies within the framework of *nano-electronics*. The main goal of this relatively new scientific field is to build device-components for the electronics industry with a size well below 100 nm. In this field a lot of effort is put into various topics, two of them are (1) the fabrication of (nano) template surfaces and (2) the use of (groups of) molecules as building blocks. More or less, the results presented in this thesis also deal with these two topics.

In this dissertation two different nanostructured substrate surfaces are discussed. Firstly, we have studied platinum (Pt) modified Ge(001) surfaces and secondly, we have studied gold (Au) induced nanostructures on Ge(001). Of both we have studied the structural and the electronic properties at two different temperatures, namely 293 K and 77 K. In addition, the formation of atomic chains of Pt on Ge(001) is discussed. Furthermore, these atomic Pt chains were decorated with two kinds of organic molecules after which the adsorption was studied. After the adsorption of CO the mutual molecular interactions were studied as well. In addition, after the adsorption of octanethiol we have studied single molecular properties.

Why?

Several reasons can be listed here to explain why there is such a massive interest in nanostructured surfaces, properties of individual molecules and a combination of both. Besides the fact that it is of fundamental interest to study elemental entities like atoms, molecules and surfaces, a lot of interesting physics exists within the small dimensions of *quantumland* [Ref. 1]. However, the most important reason that people are actually doing research in this field is, of course, related to industry (money).

In 1971 Intel launched their Intel® 4004 processor [Ref. 2], having 2300 transistors with an approximate size of $1x10^6$ m (1µm). In 2007, they introduced the Quad-Core Intel® Xeon® processor (Penryn) with 820.000.000 transistors of about $45x10^9$ m (45 nm) in size. So, an enormous improvement has occurred. This development was already forecasted by *Moore's Law*. In 1965, Gordon Moore (one of the three cofounders of Intel) observed/forecasted a doubling of the number density of transistors placed on an integrated circuit (IC) each 12 months [Ref. 3]; later this was adjusted to each 18-24 months. Up to now, this *law* still holds. Basically, the technique for the production of these transistor-chips (so-called silicon-technology, based on both the invention of the transistor by Shockley, Brattain and Bardeen in 1947/1948 and the invention of the IC by Kilby and Noyce in 1958), has never dramatically changed, but was only improved/modified in time. Although a further miniaturization is still possible by using this technique, there is a technological limit which is expected to be reached around 2020.

So, in order to prolong the coherence between Moore's prophetic words and reality till after 2020, a new technology has to be developed and this is why there is such a thrust in exploring a new generation of nanometer-scale electronic devices. Globally, there is an intensive search going on for new

materials and components, which can replenish or even replace the Si-technology in the coming years.

What?

In order to solve *Moore's law problem* several possible solutions have been proposed, many of those within the field of molecular electronics. Although this field is interdisciplinary (chemistry, physics, electronics, etc.), there is one coalescing goal: to use molecules or groups of molecules as building blocks for electronic components. The molecules should take over the tasks of conventional components such as wires, transistors, switches, memories and gain elements [Ref. 4] and possibly also expand the number of functionalities. The use of molecules as individual components for the use in electronics was first described in 1974. Then, Aviram and Ratner gave a theoretical illustration of a rectifier consisting of a single molecule: a single molecule rectifier [Ref. 5]. Note that purely organic electronic IC's will be an utopia for years.

In addition to (single) molecules with the desired properties to be used in an electronic device, there is a need for nano-structured surfaces. These nano-templates could act as molecular print boards; the functional (groups of) molecules should be attached to a pre-patterned surface. A decreased pattern size means a decreased device size, which means more devices on less material. Nano-sized structures have proliferated new pathways within the study of both their chemical and physical properties. However, building these extremely small entities via the bottom-up approach remains a challenge for scientists and engineers. For that reason, the study of (the formation of) nanostructures is a highly imperative field.

Outline

In Chapter Three the Pt-modified Ge(001) surface is discussed. Pt was evaporated onto Ge(001) and subsequent annealing resulted in three types of terraces. The most appealing type contains atomic chains of Pt. The formation of these chains is discussed. The structural and electronic properties are addressed as well.

The adsorption of CO on the atomic Pt chains is discussed in Chapter Four. The mutual interaction between co-adsorbed CO molecules was investigated and also a spatial map of the inverse decay length was made of the Pt/Ge(001) surface decorated with CO molecules.

In Chapter Five the results of the decoration of the atomic chains of Pt with octanethiol molecules are presented. Besides the adsorption geometry, some single molecule properties (after adsorption) are discussed.

As a second nanostructured surface we have studied Au-induced nanostructures on Ge(001), Chapter Six. Structural and electronic properties were studied both at 293 K and at 77 K.

All the results presented in this dissertation were acquired with a Scanning Tunneling Microscope (STM), an instrument which unlike a 'normal' microscope does not use light (photons) to image materials, but uses electricity (electrons). Some background information on this technique and the experimental procedures are given in Chapter Two.

References

[Ref. 1]   R. Gilmore, *Alice in Quantumland, an allegory of quantum physics* (Springer-Verlag, New York, 1995)

[Ref. 2]   http://www.intel.com/technology/timeline.pdf

[Ref. 3]   G. E. Moore, *Electronics* **38** (1965), p. 114

[Ref. 4]   J. M. Tour, *Molecular Electronics, Commercial Insights, Chemistry, Devices, Architecture and Programming* (World Scientific, New Jersey, 2003)

[Ref. 5]   A. Aviram and M. A. Ratner, *Chemical Physics Letters* **29** (1974), p. 277

Experimental techniques and procedures
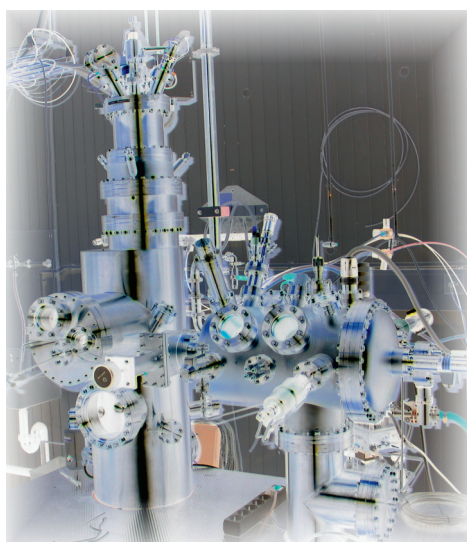
By inventing the Scanning Tunneling Microscope (STM), Binnig and Rohrer from IBM boosted the worldwide interest in nanostructures. The STM has become one the major tools in nanoscience. An STM can measure the topography and the electronic landscape of structures with very high spatial resolution. The combination of STM and STS has already proved to be very useful in probing the geometry and electronic structure of individual atoms and molecules. In this Chapter, the basic principles of STM will be described and the STM setup that was used will be elucidated.

History of STM

In the late 70's and early 80's of the past century Binnig and Rohrer from the Research Laboratory of International Business Machines Corporation (IBM) in Zurich were studying properties of inhomogeneous insulating layers between two metal plate-electrodes. Originally, they planned to study the electronic structure of these insulators locally, i.e. an area with a diameter of about 100 Å. However, apposite equipment was not available. Therefore, they replaced one metal plate-electrode by a moveable tip-electrode. Not much later, they realized that they had constructed a device that could not only probe the electronic structure (since the apex of the tip-electrode was sufficiently small), but in addition their device could obtain topographical information of the surface, just by transferring the tip-electrode over the surface plane. In 1982 they published the first results obtained with the so-called Scanning Tunneling Microscope (STM) [Refs. 1-3].

Nowadays, with an STM it is possible to image the topography of surfaces with atomic resolution, which makes the STM a unique tool already. Add to that the fact that an STM also allows you elucidate on the electronic landscape of the surface via various scanning tunneling spectroscopy (STS) techniques like current-voltage spectroscopy, inelastic electron tunneling spectroscopy and barrier height spectroscopy, again with atomic resolution [Ref. 4]. And finally, an STM can be used as a manipulation tool to create new structures and induce chemical reactions at the molecular level [Refs. 5-8 and references therein]. So, the invention of the STM was a major step within the eventual breakthrough of both nanoscience and nanotechnology (although the latter still has to undergo its real breakthrough). In addition, it was followed by the development of a complete new branch of techniques, scanning probe techniques. In the meanwhile, more than twenty of these

techniques have been developed [Refs. 4, 9]. The importance of the STM is clearly shown by the fact that its inventors were awarded the Noble Prize in Physics in 1986, only a few years after its development.

But how does it work?

Scanning tunneling microscopy is a surface probing technique, in which a very sharp metal electrode, the tip, is placed in very close proximity of the sample (which acts as the second electrode). Typically, the STM operates with a distance L between the tip and the surface of 0.4 – 0.7 nm [Ref. 9]. So there is no physical contact between tip and sample, they are separated by a vacuum. However, there might be *electronic contact* due to overlap of the electronic orbitals. When orbitals overlap, a possibility exists that electrons tunnel from one material to the other material. Tunneling is a quantum-mechanical phenomenon in which an electron with a certain kinetic energy E_k can pass a potential energy barrier E_p with $E_p > E_k$, which is forbidden according to classical (Newtonian) mechanics. A schematic view on electron tunneling is presented in Figure 2.1.

If the electron energy E in material 1 is sufficiently high, the travelling electron (wave) does not feel the energy barrier V, i.e. E > V and, hence, can simply pass the vacuum barrier. Whenever the energy of the electron is not high enough (E < V), according to classical mechanics the electron cannot pass the vacuum barrier. However, at such diminutive distance, the electronic wavefunctions of the tip and the sample respectively can overlap. And if so, there is a certain probability that the travelling electron tunnels through the vacuum barrier. Since, of course, free electron states should be available in the sample, a bias voltage should be applied to the tip/sample system. When

tunneling, the electrons decay exponentially within the (vacuum) gap. See Figure 2.1.
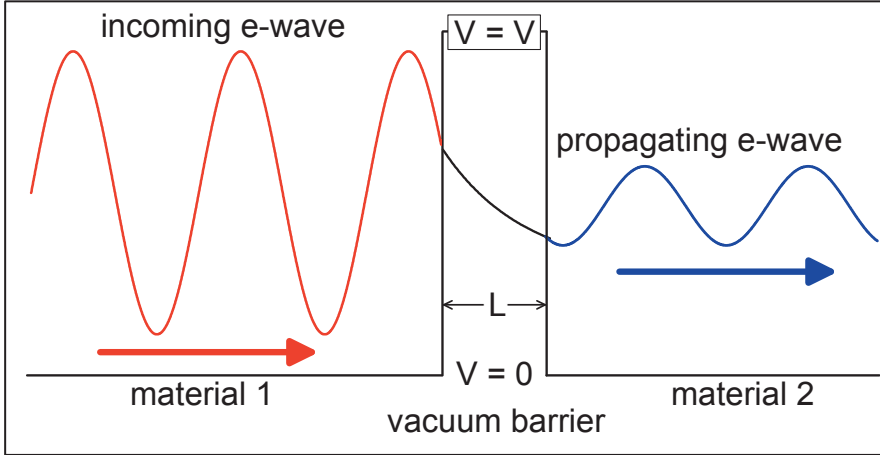
Figure 2.1: Schematic illustration of an incident electron wave (red), tunneling through a vacuum barrier, after which the electron wave propagates into the second material (blue). Within the vacuum barrier the electron wave decays exponentially (black).

More quantitatively, the probability for an electron to tunnel from tip to sample can be described by the decay of the wavefunction of the tip Ψ in the barrier [Refs. 4, 9]:

$$\left|\Psi(L)\right|^2 = \left|\Psi(0)\right|^2 e^{-2\kappa L} \tag{2.1}$$

with the width of the barrier L and the inverse decay length κ. The latter is defined by

$$\kappa = \sqrt{\frac{2m}{\hbar^2}\left(\frac{\phi_t + \phi_s}{2} - E + \frac{e|V|}{2}\right) + k_\parallel^2} \qquad (2.2)$$

with the local barrier height $\varphi_{t,s}$ of the tip and sample respectively, the mass of an electron m, Dirac's constant $\hbar$, the sample bias V and the parallel wave vector $k_\parallel$ [Refs. 10, 11].

Typically, a surface is raster-scanned by the tip of the STM at a fixed bias voltage and with a fixed tunneling current. The x-y-z motion is controlled with a piezo-scanner. As shown by Equation 2.1, the tunneling current exponentially depends on the separation distance between tip and sample (L). A small corrugation in the surface of the sample, thus has a large, and measurable, influence on the current. So, whenever the tip-sample distance changes, the accompanying change in current can be measured experimentally. An electronic feedback-loop is normally installed to monitor the tunneling current. With this the tunnel-current I (or the separation-distance z) can be controlled.

Regardless of the seemingly straightforward concept of STM, a major drawback comes with its advantages. The fact that the measured current is related to both the topographical landscape as well as the electronic landscape of the surface, makes it unclear whether a change in current is caused by a change in topography or by an electronic change.

The scanning tunneling microscope can also be used to obtain spectroscopic information of the sample. The motion of the tip is interrupted and the tip is positioned at a region of interest. Mostly the feedback of the electronics is put in the open-loop configuration. This keeps the tip-sample distance constant.

Subsequently, the current is measured as a function of voltage. This provides information on the local density of states.

The setup: an Ultra High Vacuum Low Temperature STM

A photographic image of the used Ultra High Vacuum (UHV) STM is displayed in Figure 2.2. This setup is designed for measuring at temperatures between 4 K and room temperature. The setup can basically be divided into three parts:

- The main chamber including the STM,
- the preparation chamber (including equipment), and
- the loadlock chamber.

Figuur 2.2: Photographic image of the LT-STM which was used during this research.

The loadlock chamber is used for insertion/removal of samples. After introduction of a fresh sample the loadlock is pumped by a 70 liter/second

turbo-molecular pump and a pre-pump (both from Varian) down to $\sim 1 \cdot 10^{-8}$ mbar. With a magnetic transfer arm the sample can be transferred to the preparation chamber. In addition, a Au-evaporator is mounted inside the loadlock.

The preparation chamber is equipped with the following facilities:

- Sample-stage for heating (by either e-beam bombardment or dc-current annealing) and sputtering the sample,
- an electron gun (Riber) used for sputtering with Ar^+,
- two leak-valves for controllably introducing gas into the chamber (one for 'clean' gases like argon and carbon monoxide and the second for organics from solid or liquid state),
- a home-build Pt evaporation source (tungsten wire wrapped with Pt),
- a quadrupole mass-spectrometer (Pfeiffer),
- a storage elevator for storing samples and tips.

The preparation chamber is pumped with a 180 liter/second turbo-molecular pump (Pfeiffer) and a rotary pre-pump (Leybold). The background pressure is typically below $5 \cdot 10^{-11}$ mbar.

The main chamber of the setup is equipped with an Omicron LT-STM scanner, which is controlled by Omicron SCALA electronics. The scanner-stage is mounted inside a vacuum chamber, surrounded with cryogenic equipment, namely two concentric bath cryostats. The inner cryostat can be filled with liquid nitrogen or liquid helium and serves for cooling the sample-stage. The outer cryostat can be filled with liquid nitrogen and serves as thermal shielding of the inner cryostat. The main chamber is pumped by a 400 liter/second ion getter pump with an embedded 1600 liter/second titanium sublimation pump. Typically the pressure in the main chamber is

below 2·10^{-11} mbar. The tips used in the STM are home-made, electrochemically etched tungsten (W) tips.

Sample preparation

The Ge(001) substrates were cut from nominally flat single-side polished n-type wafers into 5.0x10.0 mm^2 or 4.0x10.0 mm^2 samples. After placement into the UHV setup the samples were first slowly degassed. Degasification occurred via dc-current annealing up to about 250-300 K.

Subsequently, the samples were cleaned by cycles of alternating Ar$^+$ sputtering (25 minutes; 800 eV) and annealing (15 seconds; 1100 K) using a dc current. The cycle was repeated until the Ge(001) surface was atomically clean (typically 4-6 cycles were needed for this). The cleanness of the samples is checked by imaging the surface with STM.

For preparation of both the Pt-induced and the Au-induced nanostructured surfaces, we used home-build Au-or-Pt evaporators. Either high-purity Au or high-purity Pt was wrapped around a tungsten filament. By heating this filament using a dc-current the metal of interest was evaporated onto the Ge samples. After a cooling-period the samples were annealed up to 650 K (Au) or 1100 K (Pt). To measure the temperature of the samples during annealing a pyrometer (Wahl HeatSpy) was used. During annealing self-organization processes lead to surface nanostructures.

For the adsorption experiments we have used leak-valves, which allowed us to controllably introduce molecules into our preparation chamber. An additional vial was mounted to the leak-valve for chemicals that were in the liquid or solid phase at room temperature.

References

[Ref. 1]   G. Binnig and H. Rohrer, *Helvetica Physica Acta* **55** (1982), p. 726

[Ref. 2]   G. Binnig, H. Rohrer, C. Gerber and E. Weibel, *Physica B & C* **109** (1982), p. 2075

[Ref. 3]   G.Binnig, H. Rohrer, C. Gerber and E. Weibel, *Applied Physics Letters* **40** (1982), p. 178

[Ref. 4]   R. Wiesendanger, *Scanning Probe Microscopy and Spectroscopy, Methods and Applications* (Cambridge University Press, Cambridge, 1994)

[Ref. 5]   I. W. Lyo and P. Avouris, *Science* **253** (1991), p. 173

[Ref. 6]   G. A. Ozin, *Advanced Materials* **4** (1992), p. 612

[Ref. 7]   W. Ho, *Journal of Chemical Physics* **117** (2002), p. 11033

[Ref. 8]   S. W. Hla and K. H. Rieder, *Annual Review of Physical Chemistry* **54** (2003), p. 307

[Ref. 9]   C. J. Chen, *Introduction to Scanning Tunneling Microscopy* (Oxford University Press, New York, 1993)

[Ref. 10]   A. Stroscio, R. M. Feenstra and A. P. Fein, *Physical Review Letters* **57** (1986), p.2579

[Ref. 11]   R. M. Feenstra, J. A. Stroscio and A. P. Fein, *Surface Science* **181** (1987), p. 295

Formation and properties of Pt/Ge(001) nanostructures
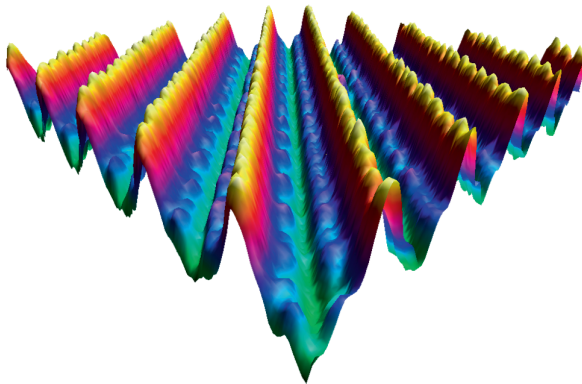
Via evaporation of Pt on Ge(001) and a subsequent annealing procedure, large arrays of Pt chains were formed. The formation of these nanostructures was studied, together with both the structural and electronic properties. The chains are dimerized, are perfectly straight, have a width of only one atom and the chain-to-chain separation distance is mostly 1.6 nm. Upon cooling from 293 K to 4.7 K most atomic chains undergo a doubling of the periodicity. This structural transition goes along with a change in the electronic properties of these chains and is attributed to a Peierls distortion.

Introduction

In order to prolong the coherence between Moore's legendary prophecy [Ref. 1] and reality, enormous effort is put into the development of potential substituent methods for the currently (and previously) used silicon-technology. Some of the suggested prospective methodologies might benefit from the use of nano-structured template surfaces. However, these nanostructures are not only of technological interest. Inasmuch as these nanostructures form the landscape of *quantumland* [Ref. 2], fundamentally appealing phenomena can occur. These phenomena cannot be explained with classical Newtonian physics. This makes it even more interesting to make and study nanostructured substrate surfaces.

To solve *Moore's law-problem*, these nanostructures ideally would be silicon (Si) based [Ref. 3]; however solutions based on Si's brother germanium (Ge) might be beneficial as well. Although Si is the base-element for use in electronics nowadays, Ge was used predominantly in electronics up to the 1970's. Since Ge has some unique properties relevant for electronics [Ref. 4], it is still being investigated widely in the race against the end of Moore's law. For that reason, we have studied Ge-based systems as well.

In our work, after evaporation of some precious metals (or platinum (Pt) or gold (Au)) on the Ge(001) surface and a subsequent annealing procedure, Pt/Ge or Au/Ge nanostructures are formed via self-organization. In this Chapter the formation mechanism of the Pt/Ge structures is addressed. In addition, the structural and electronic properties of the formed structures will be discussed. Here it will be shown that the Pt chains formed on Ge(001) undergo a structural phase transition when cooling down from room

temperature to 4.7 K. The Au/Ge nanostructure system will be discussed in Chapter 6.

Germanium

Similar to Si, Ge is a group IV semiconductor; both have a face centered cubic (bulk) crystal structure with a two-atom basis, also coined diamond structure, see Figure 3.1(a). When the lattice structure is cut along the (001) direction the surface atoms are left with two dangling bonds, Figure 3.1(b, c). Due to short-range interaction, dimers are formed by pairing of the dangling bonds of two neighbouring atoms, Figure 3.1(d).
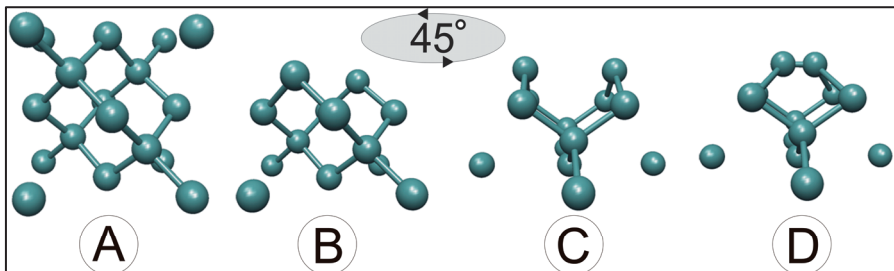
Figure 3.1: Schematic representation of the crystal structure of Ge (a); the crystal structure after cleavage along the (001) plane (b); crystal structure from (b) rotated by 45° (c); final structure after dimerization.

A weaker long-range interaction induces the reconstruction of the surface [Ref. 4]. These surface reconstructions reduce the free energy; the formation of a chemical dimer bond creates stability which outweighs the strain created during the rearrangement. The result is a nicely ordered surface consisting of dimer rows, well separated by troughs. The dimer row direction rotates by 90°

at each monatomic step as a consequence of the diamond structure of Ge. Commonly observed reconstructions are the $c(4\times2)$, $p(2\times2)$ and the $p(2\times1)$ reconstructions [Ref. 4]. For the $c(4\times2)$ and the $p(2\times2)$ reconstructions the dimers tilt out of the surface plane. Hence, the dimers consist of one atom that buckles upwards and one atom that buckles downwards.

Pt/Ge (001); the story so far

The main topic of this Chapter is the formation of atomic chains of platinum on the Ge(001) surface. The preparation of these structures was first described by Gurlu et al [Ref. 5]. They evaporated an equivalent amount of ~0.25 monolayer Pt on Ge(001) at room temperature. After subsequently annealing the sample to 1050-1100 K, room temperature STM measurements revealed that the surface consists of three different regions. The first type of terrace was coined the α-terrace. It is commonly thought that the α-terraces consist of both symmetric and asymmetric Ge dimers. Furthermore, α-terraces have a high concentration of vacancies. The second type of terrace found is the so-called β-terrace; it consists of both Ge-Ge dimers and Ge-Pt dimers. Again, a large number of vacancies was found here. However, in this case the vacancies are running along well defined crystal directions. Finally, they found patches of Pt atomic chains. These atomic chains were only observed on the β-terraces.

Following these observations, several interesting studies were devoted to the atomic chains of Pt on the Pt-modified Ge(001) surface.

In 2005 Oncel et al. performed scanning tunneling spectroscopy (STS) on the Pt/Ge(001) surface at both 77 K and 300 K [Ref. 6]. At the former

temperature they found one-dimensional (1D) electronic states on the Pt-modified terraces which were confined between the atomic chains. The distance between the chains determined the size of the 1D box. Local density of states measurements revealed one novel electronic state when the separation distance between the chains was 1.6 nm and two for the '*bigger box*' of 2.4 nm. Spatial maps of these states in the *bigger box*, recorded with STM, are nicely consistent with what one would expect, namely a maximum density in the middle of the box for the $n = 1$ state and a node in the middle accompanied by two off-centre maxima for the $n = 2$ state [Ref. 7].

Additionally, although it seems established that the formed atomic chains indeed are comprised of Pt dimers [Refs. 5-14], in literature some questions were raised by Vanpoucke et al. about the exact elemental nature of the atomic chains [Refs. 15]. Based on density functional theory calculations these authors concluded that the as-prepared atomic chains consist of Ge dimers instead of Pt dimers. In this Chapter we emphasize that the atomic chains are indeed comprised of Pt dimers.

In summary, this novel Pt-modified Ge(001) surface is a very attractive and interesting new material. For that reason, we have explored the formation and both the electronic and structural properties of the atomic Pt chains in more detail.

Experimental

Ge(001) substrates were prepared from nominally flat 7.6 cm x 0.5 mm, single-side polished, n-type wafers. Via laser-cutting (4.0 x 10.0) mm and (5.0 x 10.0) mm samples were made. The samples were first cleaned ultrasonically

in iso-propanol to remove contaminants. Subsequently they were mounted on molybdenum or tantalum sample-holders. To avoid metal-contamination of the Ge surface, contact of the samples with any other metal was avoided cautiously during the entire process.

After bringing the samples into the UHV setup, they were first carefully degassed. This degasification occurred via resistively heating of the samples, up to 500 K. Then the surface was cleaned by repeating a cycle of sputtering (800 eV argon ions) and annealing (resistively heating to 1100 K) treatments. After five to ten cycles the samples were clean; this was confirmed by imaging the samples with STM.

Ge(001), the α-terrace, the β-terrace and arrays of Pt chains

In Figure 3.2 a filled state STM image of a clean Ge(001) surface, measured at 77 K, is displayed. Clearly shown in Figure 3.2 is the $p(2 \times 2)$ dimer reconstruction of the Ge(001) surface. The right image shows a ball-and-stick model of the observed $p(2 \times 2)$ reconstruction. The (buckled) atoms are dimerized and are aligned in dimer rows. The resolution of the image in Figure 3.2 allows us to even see the 'down-atom'. Subsequently, a sub-monolayer amount of platinum was deposited onto the surface at room temperature. Platinum was evaporated by resistively heating a tungsten (W) wire wrapped with high purity Pt (99.995%). After Pt deposition, the sample was annealed at 1050-1100 K. Subsequently the sample was cooled down to room temperature by radiative quenching after which it was placed into the STM for observation.

In agreement with Gurlu et al. [Ref. 5], we observed three different types of terraces on the surface. Figure 3.3 shows an α-terrace, of which we believe that it consists of both symmetric and asymmetric Ge dimers.
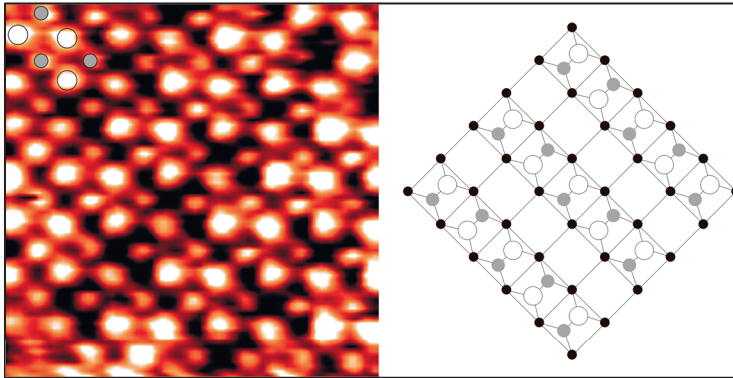

Figure 3.2: STM image (4nm x 4nm) of the p(2x2) reconstructed Ge(001) surface, scanned at 77 K. The image clearly shows the buckled registry of the dimer rows. The right image presents a ball-and-stick model of the p(2x2) reconstruction. The top layer atoms are shown as white and gray balls; the white balls are the 'up'-atoms and the gray balls are the 'down'-atoms. The black balls represent the second layer of Ge atoms; these are at their bulk positions and cannot be seen in the STM image.

The original Ge(001) dimer-row structure is still visible on the α-terraces. However, an excessive amount of dimer vacancy defects was found. Although we have found no evidence for the presence of Pt in the α-terrace, a possible explanation for this high vacancy density is that it is caused by the incorporation of Pt atoms beneath the surface. Similar vacancy defects have been observed for several other metal-contaminated group IV semiconductor surfaces, including Ni-doped Si(001) [Ref. 16] and Ge(001) doped with Pt [Refs. 5, 8], Pd [Ref. 17] or Au [Ref. 18]. These vacancy defects were

attributed to the metal atoms moving below the surface. So, in our case, in order to relieve the accompanying stress caused by the incorporated Pt atoms, the surface releases Ge surface atoms, hence creating dimer vacancy defects.
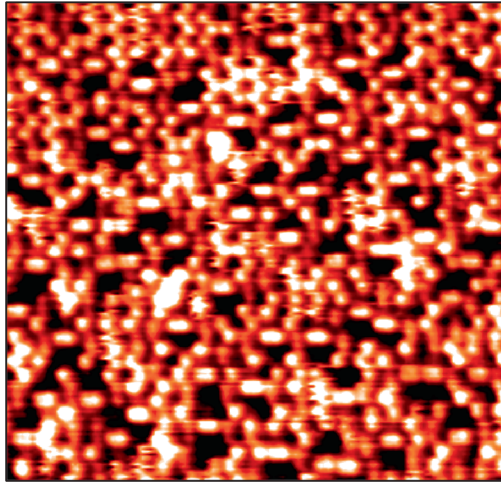
Figure 3.3: STM image (17 nm x 16 nm) of an α-terrace, recorded at 77 K with V_S = -1.5 V and I_T = 0.34 nA.

The second type of terrace is the so-called β-terrace, shown in Figure 3.4. The β-terrace also contains numerous missing-dimer-like defects. Yet, here the defects are clustered and mostly aligned in both the <310> and <110> directions, so showing up as line-defects. Like the α-terrace, we assume that the β-terrace is comprised of dimerized atom rows. However, in addition to Ge dimers, the β-terrace is also comprised of Ge-Pt dimers. The two types of dimers form the β-terrace on an alternating fashion.

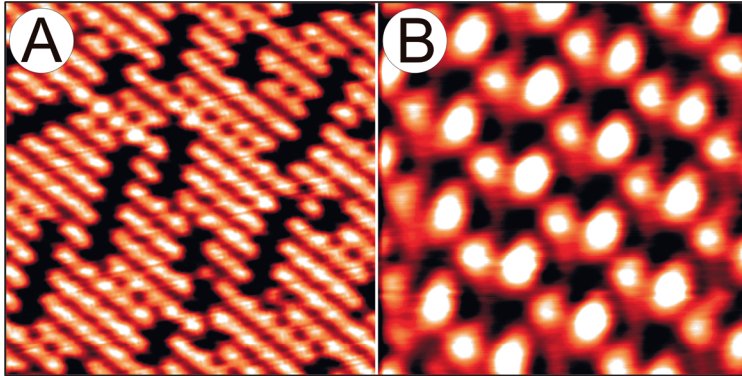**Figure 3.4:** STM images of the β-terrace recorded at 77 K. In (a) the dimer rows and the emblematic vacancy-lines are shown (11nm x 11nm; V_S = -1.4 V; I_T = 0.4 nA). Figure (b) shows the β-terrace at higher magnification (3.4nm x 3.4nm; V_S = -0.3V; I_T = 0.4 nA).

A third type of terrace consists of a β-terrace, but now covered with regions of well ordered structures. These structures consist of perfectly straight one-dimensional atomic chains, as presented in Figure 3.5. The chains consist of Pt dimers, aligned in the direction of the chain. Thus, the chains have a width of only one atom. Lengths of the chains can be up to a micron.

The chains were mostly found in patches; however, isolated chains were observed as well. Whenever the chains were found in patches the inter-chain distance was mostly 1.6 nm, see Figure 3.5(b), but occasionally also 2.4 nm or 3.2 nm. Figure 3.5(c) and (d) show higher magnification images of the Pt chains; (c) displays a filled state image and (d) shows an empty state image.
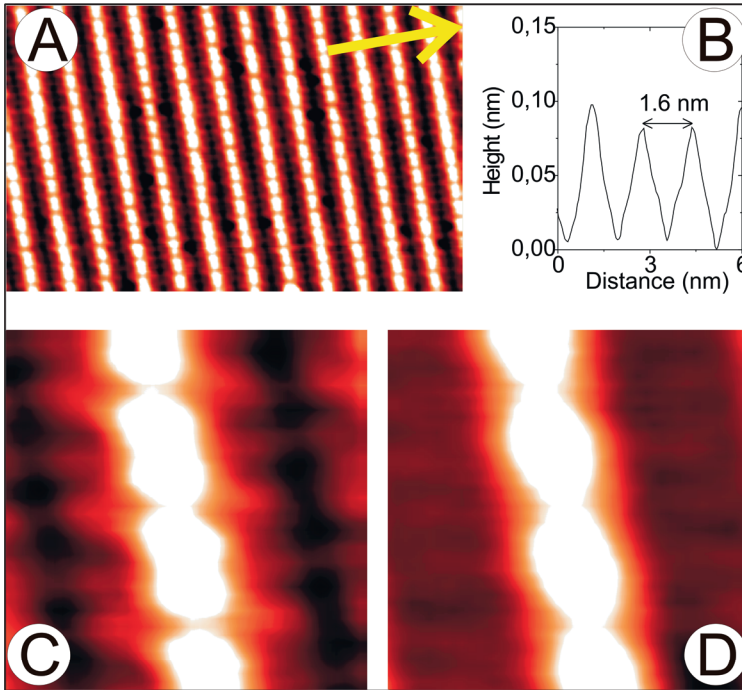
Figure 3.5: Filled state STM image ($21\,nm \times 12\,nm$) of atomic Pt chains (a); (b) shows a height profile taken along the yellow arrow in (a). Figures (c) and (d) show higher magnification STM images of the Pt chains; filled state (c) and empty state (d). Scan size of both (c) and (d) is $2\,nm \times 2\,nm$.

Chain formation via self-organization

Until recently the exact mechanism of the formation of the atomic Pt chains remained unclear. However, a further analysis of STM images recorded after Pt-evaporation and subsequent annealing revealed critical information about this formation process [Ref. 10]. Below some features are discussed that have been observed and which eventually led us to come up with a formation mechanism for the atomic chains.

Figure 3.6 shows two STM images of a β-terrace. At several positions the troughs in between the dimer rows have a width that is unmistakably larger than the width of normal troughs. These 'openings' of the troughs extend to about 1-2 nm and appear as dark elliptical features (depressions).

Since these trough-openings are only observed after evaporation of Pt and subsequent annealing, it is reasonable to assume that these are related to Pt atoms incorporated in the subsurface region of the sample. A schematic representation of such an opening is given in Figure 3.6(c). In this scheme the small ellipses represent the surface dimers, whereas the large ellipse represents the observed trough-opening.

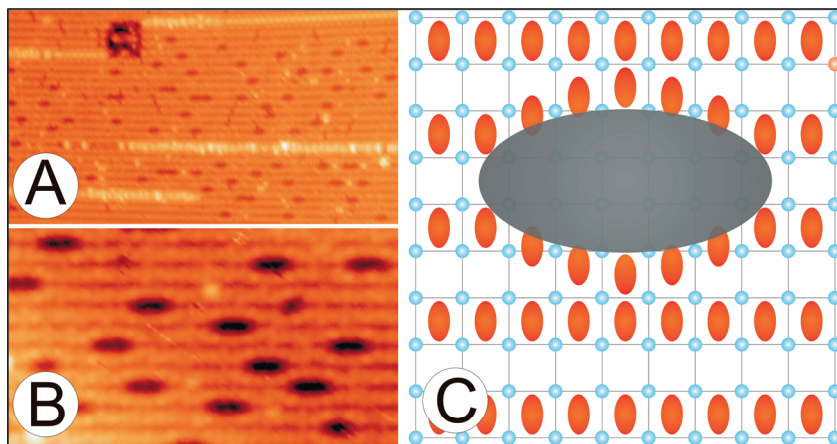**Figure 3.6:** STM image (39nm x 18nm) of a region of the β-terrace in which the troughs in between the dimer rows are locally widened elliptically (A). Also present in this image are some unfinished chains. In (B) a higher magnification of these widenings is presented (15nm x 7nm). A schematic illustration of such a widening is given in (C). The small orange ellipses represent the surface dimers.

Besides trough-openings of 1-2 nm, as displayed above, also openings with lengths up to 50 nm are observed; this is shown in Figure 3.7.
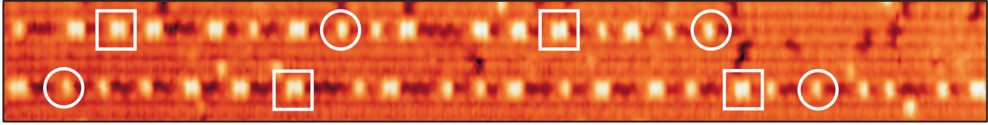

Figure 3.7: STM image showing two troughs which are widened over a length of 50 nm. Both troughs are partially filled with Pt dimers, either single dimers (circle) or in units of two dimers (square). Size = 50 nm x 6 nm.

Whereas the smaller openings are always 'empty', widening of the troughs over a larger extent is always accompanied by a partial filling of the trough with bright elliptical clusters. The orientation of the major axis of these clusters is perpendicular to the dimer-row direction; the transverse diameter is approximately 1 nm, while the conjugate diameter measures about 0.5 nm. Furthermore, these clusters are perfectly symmetrical along both the major and the minor axis. These clusters are only found in units of one (highlighted with a solid circle) or two (highlighted with a solid square).

These clusters are, as we will conclude, presumably Pt dimers. The size and shape of the clusters suggest that they are dimers. The possible dimer combinations are: Ge-Ge, Pt-Pt and Pt-Ge. The symmetrical appearance excludes that these clusters are mixed Pt-Ge dimers. In addition, in [Ref. 19] Zandvliet et al. performed a STM study on small Ge clusters on Ge(001); among these clusters were Ge ad-dimers. These Ge ad-dimers were observed at several different orientations with respect to the underlying Ge dimer rows. However, in none of these orientations the Ge ad-dimers had an appearance

similar to the clusters as observed in Figure 3.7. Therefore, it is assumed that the clusters that we have observed, like the ones in Figure 3.7, are not Ge dimers. Hence, from that respect the most plausible explanation is that these clusters are Pt dimers.

As said before, we have never observed more than two of these Pt dimers together. However, we did observe large arrays of atomic chains, which consist of hundreds of Pt dimers next to each other. How are these chains formed then? This can be made clear with Figure 3.8. Here, we see four popped up Pt dimers of which two are single dimers (marked 1 and 3) and the other two form a unit of two dimers (marked 2). The units of Pt dimers (1-3) are all in their 'original' popup orientation, i.e. their dimer bond perpendicular to the dimer-row direction. Near the single Pt dimer on the right (3) an additional Pt dimer is located (4). Shape and size are similar to the shape and size of the previously mentioned Pt dimers (1-3). However, this dimer is rotated by 90° with respect to the other dimers and, thus, in alignment with the dimers of the subsequent atomic Pt chain. We believe that this rotation only occurs if the local density of popped up dimers is sufficiently high. Since we have never seen units of three or more dimers, we assume that at this point the dimers rotate by 90° to form a chain in the direction of their dimer bonds.
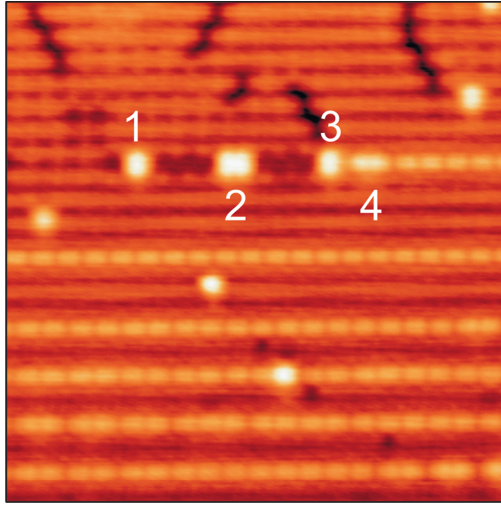
Figure 3.8: STM image showing the opening of a trough and five pop-up dimers. Two units of one dimer (1 + 3) and one unit of two dimers (2) are oriented perpendicular to the dimer row direction; the fifth dimer has rotated by 90° and is in alignment with the formed atomic chain.

For the development of the three different regions (α-terrace, β-terrace and β-terrace covered with Pt chains) the following idea is postulated. During Pt evaporation the Pt atoms dive into subsurface positions. Here the Pt atoms intermix with Ge. During annealing basically three different regions are formed, which differ in the density of (incorporated) Pt in the surface. The α-terrace has the lowest Pt density, the regions with atomic Pt chains have the highest density and the β-terrace has a Pt density which lies in between these two densities.

In the low density regime (α-terraces) the normal dimer reconstructed Ge structure is resembled very well and the incorporated Pt only causes vacancy-defects. In the intermediate regime (β-terraces) the Pt intermixes with the Ge

in a well ordered fashion; the β-terrace dimer rows consist of alternating Pt-Ge dimers and Ge dimers [Ref. 5].

In the high density regime (Pt chains) the β-terrace is formed, but the excess of Pt is driven out of the surface where it forms atomic chains. The dimer rows of the formed β-terrace widen during annealing, followed by Pt popping up as Pt dimers, oriented in the direction of the surface dimer bonds. Results published by Gürlü et al. [Ref. 20] and by Van Houselt et al. [Ref. 21] suggest that the widened configuration of the underlying surface remains present after formation of the chains. The idea of Pt density dependent terrace formation is in agreement with [Ref. 22].

Identification of atomic chains

In order to strengthen the idea that we are indeed dealing with Pt chains instead of Ge chains (the latter was mentioned in Ref. 15), we have conducted a selective adsorption experiment. This experiment is similar to an experiment performed by Oncel. He and his co-workers adsorbed small amounts (up to 4 Langmuirs) of carbon monoxide (CO) on the Pt/Ge(001) surface. Subsequently, they found that at 293 K the CO molecules adsorbed exclusively on the chains [Ref. 9].

CO is commonly known to react with Pt. On the other hand, CO does not adsorb on Ge. So, at least qualitatively, CO is a good reagent to use in a selective adsorption experiment to determine the nature of the atomic chains. Here, we exposed the Pt/Ge surface up to 2750 Langmuir of CO. Two different sample temperatures were used during CO exposure, about 175 K and 293 K. Subsequently, the surface was cooled down to 77 K and investigated with STM.

Figure 3.9 shows an STM image of the Pt/Ge surface after room temperature exposure to 2750 L of CO, recorded at 77 K.
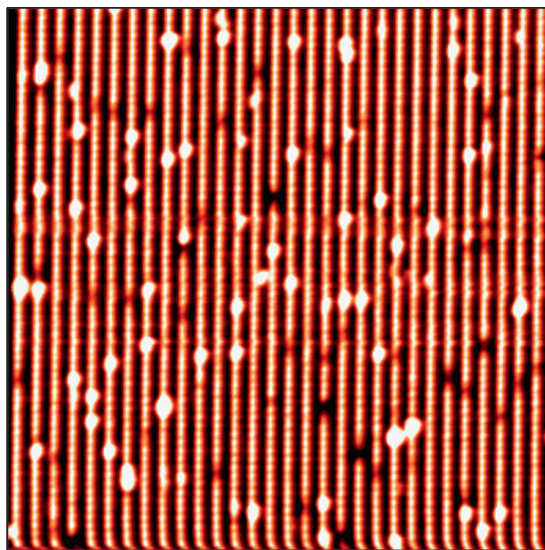
Figure 3.9: Empty state image of the Pt-modified Ge(001) surface, after exposure to 2750 Langmuir CO. The adsorbed CO molecules appear both as white protruding and dark depressed features, exclusively on top of the chains. This selective adsorption is indicative of the Pt-based nature of the chains. Scan size = 40nm x 40nm.

Clearly shown in the image are the atomic chains; however both bright (protruding) and dark (depressed) features are present on top of the chains. These features are attributed to the adsorbed CO molecules. We have explored several thousands of nm^2 and observed that virtually all CO molecules ($1000 \leq$) are adsorbed on the chains and not on the underlying

surface. Adsorption at a lower temperature (±175 K) did not influence these outcomes.

Although qualitatively investigated, this corroborates with the idea that the atomic chains are indeed comprised of Pt dimers and not of Ge dimers. A more detailed study of the adsorbed CO molecules on the atomic chains of Pt is discussed in Chapter 4.

A recent bias-dependent STM study by Zandvliet et al. supports the idea that the atomic chains are comprised of Pt dimers [Ref. 13]. They imaged a few atomic chains together with the neighbouring β-terrace using a sample bias voltage ranging from -1.5 V to +1.5 V with 0.2 V intervals. Between -1.5 V and +0.1 V one periodic unit (a single dimer) appears as two separate circular protrusions. From +0.3 V to +1.5 V the units appear as single elliptical protrusions. For a regularly adsorbed Ge dimer on the Ge(001) surface, one expects a single elongated protrusion located in between the surface atoms at negative bias; two separate protrusions on top of the surface atoms are expected at positive bias [Refs. 23, 24]. These findings are in favour of the interpretation that the chains are comprised of Pt dimers rather than of Ge dimers.

Periodicity doubling

As discussed in this Chapter previously, large arrays of very well ordered atomic chains of Pt atoms are formed after evaporation of Pt on Ge(001). These atomic chains are comprised of dimers aligned in the direction of the chain and form a quasi 1D system. The interest in 1D systems is driven by the fact that these systems can display an abundance of interesting physical phenomena, such as for instance a Peierls instability [Ref. 25]. Then, basically the periodicity of a 1D chain of metal atoms doubles resulting in an energy gap near the edges of the new Brillouin zone. At low temperature the chain is insulating and exhibits a double periodicity; at higher temperatures the chain loses its double periodicity and becomes metallic. For the ideal 1D scenario, the transition should occur at T = 0 K. Whenever the chain is coupled to the substrate or to neighbouring chains, however, the Peierls transition temperature shifts upwards. In order to investigate whether the Pt chains exhibit Peierls instability indeed, both the topographic and the electronic properties were studied at 4.7 K. Subsequently, these were compared with data recorded at 293 K.

Figure 3.10(a) shows a STM image of an array of atomic Pt chains, recorded at 4.7 K. Additionally, in (b) a similar array recorded at 293 K is presented. Clearly, the doubling of the periodicity is indicative of a Peierls distortion. Additional prove is needed, however. Maybe counterintuitive, but the lack of periodicity-doubling in the most left chain in (a) strengthens the idea of the occurrence of such a Peierls transition in the other chains. The chain at the edge of an array obviously has fewer neighbours and, thus, the neighbour-coupling is strongly reduced.
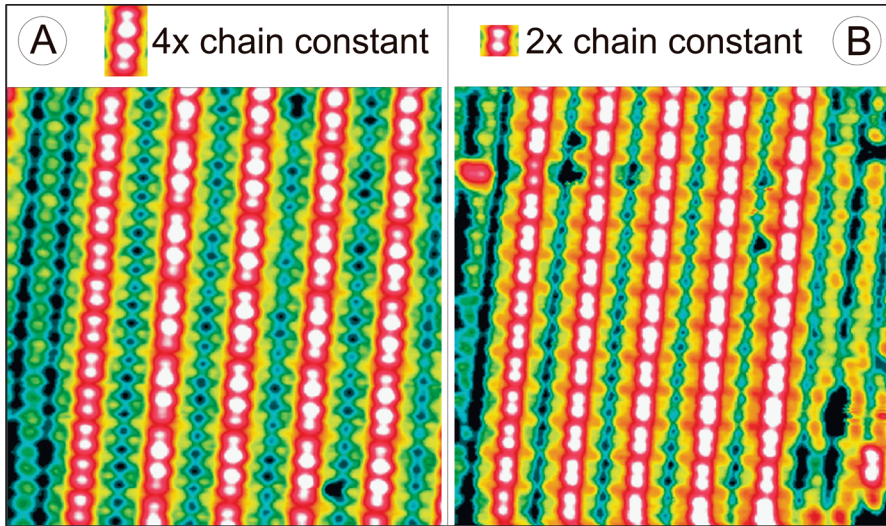
Figure 3.10: STM images of an array of Pt chains. The image on the left was recorded at 4.7 K; the image on the right was recorded at 293 K. Scan settings: V = -1.5V; I = 0.5 nA; size = 10nm x 10nm).

At this point it is not yet known, whether the chain-chain coupling is mediated through the substrate or is a direct coupling between the chains. With a weaker coupling, the Peierls transition temperature remains closer to the transition temperature of T = 0 K for an isolated 1D chain. So, for the chain at the edge of an array the transition temperature lies closer to 0 K than for the remaining chains in (a).

As shown in Figure 3.11(A), chains more remote from other chains keep the $2\times$ periodicity as well. The chain on the left in this figure is separated from another chain by 2.4 nm (instead of the commonly observed separation distance of 1.6 nm); the chain in the middle ends an array of Pt chains which continues to the right of the chain on the right. Like the chain ending the array, the chain 2.4 nm apart from the array also exhibits a $2\times$ periodicity.

Figure (B) shows the height profiles of the individual periodic units, measured as indicated by the black and red arrows respectively.
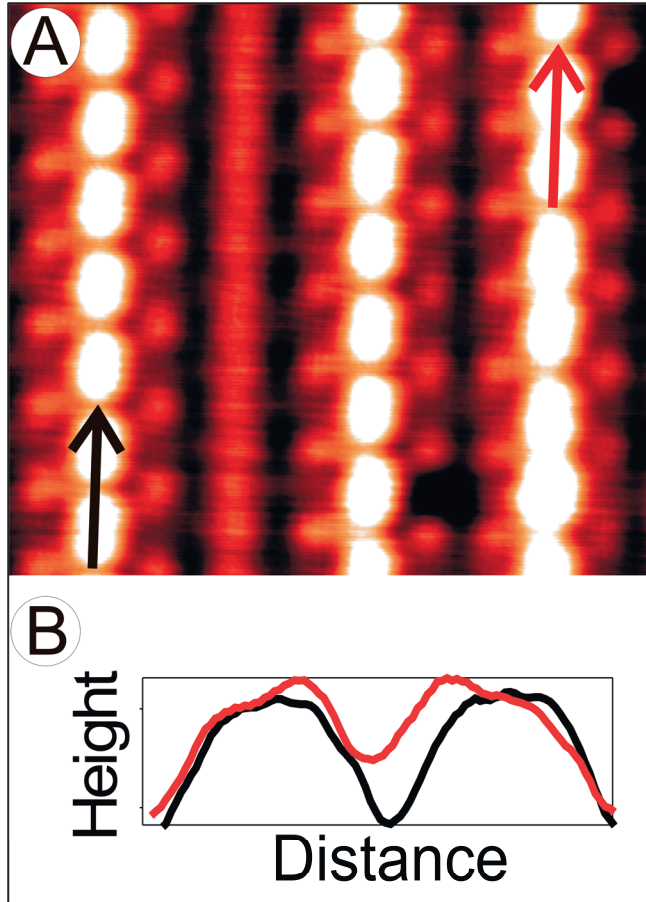
Figure 3.11: Filled state STM image (5.6nm x 5.0nm) of three Pt chains. The array of chains continues right next to the most right chain in the image. So, the chain in the middle is located at the edge of a Pt chain array. The chain on the left is separated from the chain in the middle by 2.4 nm. Both the chain on the left and the chain in the middle of the image exhibit the 2× periodicity, while the chain on the right exhibits the 4× periodicity. Two height profiles, measured as indicated by the arrows in the STM image, are presented in the inset of the figure. The image was recorded at T = 77 K.

Occasionally also single isolated chains were found. The isolated chains maintain their $2\times$ periodicity too [Refs. 11, 26]. Since the neighbour-coupling for a Pt chain remote from other chains is even lower than for the chains at the edge of an array, the Peierls transition temperature is expected to be even closer to T = 0 K.

A reduced differential conductivity

In case of a Peierls instability the structural transition is accompanied by a change in the electronic properties of the chain. Ideally, a metal-to-insulator transition occurs. Differential conductivity (dI/dV) plots measured at 4.7 K on top of both a $2\times$ periodicity and a $4\times$ periodicity chain are presented in Figure 3.12.

The minimum in the differential conductivity measured on the $4\times$ chain lies around 0.1 nA/V, whereas the minimum in the differential conductivity measured on the $2\times$ chain lies above 0.2 nA/V. So, around the Fermi level the structural transition from $4\times$ to $2\times$ gives an increase in the differential conductivity with a factor of about two.

At negative bias and around the Fermi level the (dI/dV) of the $2\times$ periodicity chain exceeds the (dI/dV) of the $4\times$ periodicity chain. This is in agreement with our previous findings. At positive bias, the (dI/dV) of the $4\times$ chain catches up with the $2\times$ chains and eventually also surpasses the (dI/dV) of the $2\times$ chain. This last observation is mostly likely due to the confined $n=1$ state, which is present between the atomic chains [Refs. 6, 7]. In order to derive conclusions about a possible Peierls transition from these data, additional experiments are a necessity, however.
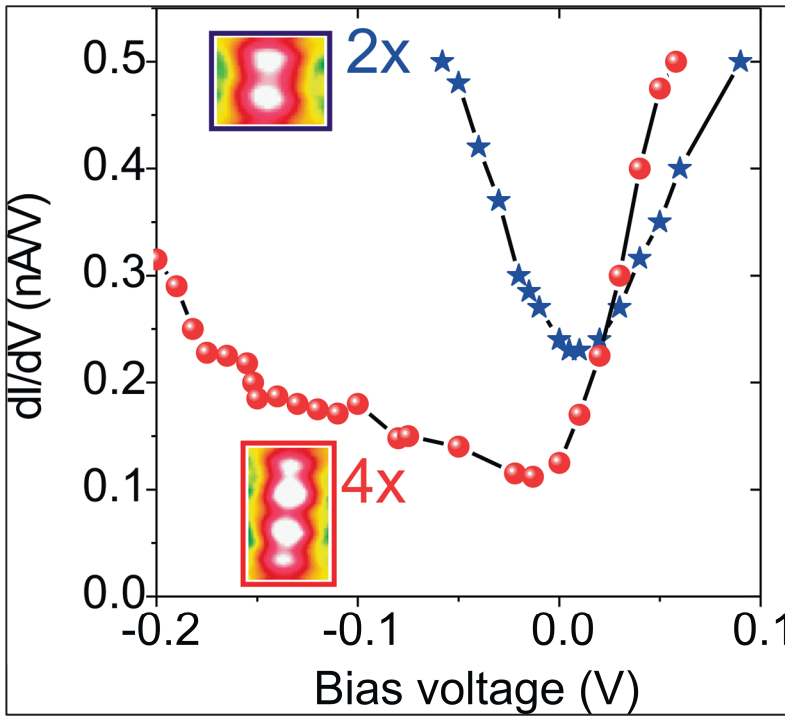
Figure 3.12: Differential conductivity curves recorded on-top of the Pt chains at 4.7 K. The data are recorded on the Pt chains with 2× periodicity (blue) and 4× periodicity (red).

The surroundings of the chains used for measuring the differential conductivity are different for the two types of chains. Since the surroundings can contribute to the tunneling current, it is required to separate the influence of the Pt chains to the tunneling current from the influence of the surroundings. In order to separate the input from the Pt chains from the input from the underlying surface (which is slightly metallic too) the inverse decay length, κ, was determined for both types of Pt chains. The inverse decay length provides information on the spatial origin of the tunneling electrons.

Wentzel, Kramers and Brillouin approximated the tunneling current to be,

$$I(V) = \int_0^V \rho(E)T(E,eV)dE \qquad (3.1)$$

where $\rho(E)$ is the density of states of the surface (assuming a constant density of states of the tip) and $T(E,eV)$ refers to the transmission probability [Ref. 27]. The latter is defined as

$$T(E,eV) = e^{(-2\kappa z)} \qquad (3.2)$$

Here, κ is the inverse decay length of the wave function, which is formulated as,

$$\kappa = \sqrt{\frac{2m}{\hbar^2}\left(\frac{\Phi_t + \Phi_s}{2} - E + \frac{e|V|}{2}\right) + k_{\parallel}^2} \qquad (3.3)$$

where Φ_t and Φ_s are the work functions of the tip and substrate respectively, V the applied voltage between tip and substrate, E the energy of the electronic state relative to the Fermi level, $k_{\parallel}$ the parallel wave vector, $\hbar$ Dirac's constant and m the mass of an electron [Refs. 28, 29].

It is evident from Equation (3.3) that a wave function decays more slowly into the vacuum, if the corresponding parallel wave vector, $k_{\parallel}$, is zero. The electronic states near the center of the surface Brillouin zone (Γ point) usually

have the largest contribution to the tunneling current because of their small inverse decay length. In most cases it is even justified to consider only the contribution of the electronic states near the Γ point. However, if no electronic state is present at the Γ point, other electronic states with nonzero parallel momentum and thus larger inverse decay lengths will dominate the tunneling current. This is for instance quite common for semiconductors where either an occupied state lying close to the Fermi level disperses upward in energy from the Γ point or a low lying unoccupied state disperses downward in energy from the Γ point [Refs. 27-29]. Conservation of energy requires that under these conditions tunneling occurs via electrons with nonzero parallel momentum.

For small sample bias, we can extract the inverse decay length, provided that we record *I–V* curves at two different heights, z_1 and z_2,

$$I_{1,2}(V) = e^{-2\kappa z_{1,2}} \int_0^V \rho(E)dE \qquad (3.4)$$

Hence,

$$\kappa = \frac{\ln(\frac{I_1}{I_2})}{2(z_2 - z_1)} \qquad (3.5)$$

Thus the natural logarithm of the ratio of the *I–V* curves, measured on the same spot at two different tip-sample separation distances, is directly proportional to the inverse decay length of the electronic state under study.

The inverse decay length is a slowly varying function of the sample bias [Ref. 29]. Therefore, large variations in the measured inverse decay length should be attributed to electrons that tunnel from other electronic states (slightly further away from the Γ point) with nonzero parallel momentum vectors.

Figure 3.13 shows the inverse decay length κ, versus sample bias as extracted from I–V curves recorded at different tip sample separation distances on-top of Pt chains that exhibit a $4\times$ periodicity (red trace) and a $2\times$ periodicity (blue trace).

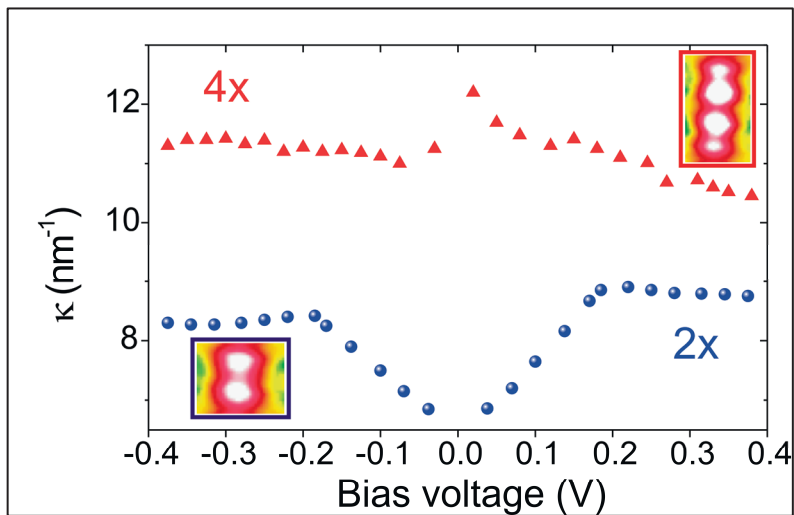**Figure 3.13:** Inverse decay length κ as a function of sample bias, recorded on-top of Pt chains with a 4× periodicity (upper trace) and a 2× periodicity (lower trace). Bias voltage is −1.0 V and tunneling current is 0.5 nA.

The inverse decay length of the Pt chains with a $2\times$ periodicity exhibits a rather broad minimum near the Fermi level (zero bias) which is indicative of a

metallic character of the Pt chains. For the chains with a $4\times$ periodicity the inverse decay length κ, is significantly larger. In addition, the $4\times$ curve does not display a minimum near the Fermi level. We interpret the absence of a clear minimum near the Fermi level as a strong indication that the metallicity of the $4\times$ chains has been reduced significantly as compared to the metallicity of the $2\times$ chains. The sudden jump in the inverse decay length just above the Fermi level of the $4\times$ Pt chains might be related to the development of novel electronic states between the Pt chains [Refs. 6, 7].

So, we conclude that the $4\times$ reconstructed chains are less metallic than the $2\times$ reconstructed ones. In a one-band model obviously a Peierls transition is leading to an insulator. However, in a multi-band case metallic behaviour can still survive if more than one band is crossing the Fermi level. In this case the Peierls transition will show up only as a reduction in the metallicity.

Conclusions

In summary, after evaporation of Pt onto Ge(001) and a subsequent annealing procedure three types of terraces are formed. We found so-called α-terraces and β-terraces and on the latter frequently large arrays of atomic Pt chains were observed. During Pt deposition, the Pt atoms first dive into subsurface positions. In the subsequent annealing step, the surface dimer-rows locally widen, allowing the subsurface Pt atoms to pop up as Pt dimers. At a certain Pt dimer density, the dimers rotate by 90° to form a well-defined chain of dimerized Pt atoms. The chemical nature of the chains was confirmed via selective adsorption of CO.

When cooling down from 293 K to 4.7 K the self-organized Pt chains experience a structural transition from a $2\times$ to $4\times$ periodicity. Isolated Pt chains and chains located at the edge of an array of Pt chains preserve the $2\times$ periodicity down to temperatures as low as 4.7 K. Scanning tunneling spectroscopy revealed that this transition is accompanied by a reduction in the differential conductivity of the Pt chains. Hence, we concluded that the transition is driven by a Peierls instability.

References

[Ref. 1]   G. E. Moore, *Electronics* **38** (1965), p. 114

[Ref. 2]   R. Gilmore, *Alice in Quantumland, an allegory of quantum physics* (Springer-Verlag, New York, 1995)

[Ref. 3]   H.J.W. Zandvliet, *Review of Modern Physics* **72** (2000), p. 593

[Ref. 4]   H.J.W. Zandvliet, *Physics Reports* **388** (2003), p. 1

[Ref. 5]   O. Gurlu, A.O.A. Adam, H.J.W. Zandvliet and B. Poelsema, *Applied Physics Letters* **83** (2003), p. 4610

[Ref. 6]   N. Oncel, A. van Houselt, J. Huijben, A.-S. Hallbäck, O. Gurlu, H.J.W. Zandvliet and B. Poelsema, *Physical Review Letters* **95** (2005), p. 116801.

[Ref. 7]   A. van Houselt, N. Oncel, B. Poelsema and H.J.W. Zandvliet, *Nano Letters* **6** (2006), p. 1439

[Ref. 8]   O. Gürlü, H. J. W. Zandvliet, B. Poelsema, S. Dag and S. Ciraci, *Physical Review B* **70** (2004), p. 085312

[Ref. 9]   N. Oncel, W. J. van Beek, J. Huijben, B. Poelsema and H. J. W. Zandvliet, *Surface Science* **600** (2006), p. 4690

[Ref. 10]   M. Fischer, A. van Houselt, D. Kockmann, B. Poelsema and H. J. W. Zandvliet, *Physical Review B* **76** (2007), p. 245429

[Ref. 11]   A. van Houselt, T. Gnielka, M. Fischer, J. M. J. aan de Brugh, N. Oncel, D. Kockmann, R. Heid, K.-P. Bohnen, B. Poelsema and H. J. W. Zandvliet, *Surface Science* **602** (2008), p. 1731

[Ref. 12]   D. Kockmann, B. Poelsema and H. J. W. Zandvliet, *Physical Review B* **78** (2008), p. 245421

[Ref. 13]   H. J. W. Zandvliet, A. van Houselt and B. Poelsema, *Journal of Physics: Condensed Matter* **21** (2009), p. 474207

[Ref. 14]   H. Pfnür, *Surface Science* **602** (2008) 1727

[Ref. 15]   D. E. P. Vanpoucke and G. Brocks, *Physical Review B* 77 (2008), p. 241308

[Ref. 16]   V. A. Ukraintsev and J. T. Yates, *Surface Science* **346** (1996), p. 31

[Ref. 17]   J. Wang, M. Li, and E. I. Altman, *Journal of Applied Physics* **100** (2006), p. 113501

[Ref. 18]   J. Wang, M. Li and E. I. Altman, *Physical Review B* **70** (2004), p. 233312

[Ref. 19]   H. J. W. Zandvliet, W. Wulfhekel, B. L. M. Hendriksen, B. J. Hattink and Bene Poelsema, *Physical Review B* **57** (1998), p. 1356

[Ref. 20]   O. Gürlü, A. van Houselt, W. H. A. Thijssen, J. M. van Ruitenbeek, B. Poelsema and H. J. W. Zandvliet, *Nanotechnology* **18** (2007), p. 365305

[Ref. 21]   A. van Houselt and H.J.W. Zandvliet, *Microscopy and Analysis* **22** (2008), p. S5

[Ref. 22]   J. Schäfer, S. Meyer, C. Blumenstein, K. Roensch, R. Claessen, S. Mietke, M. Klinke, T. Podlich, R. Matzdorf, A. A. Stekolnikov, S. Sauer and F. Bechstedt, *New Journal of Physics* **11** (2009), p. 125011

[Ref. 23]   W. Wulfhekel, B. J. Hattink, H. J. W. Zandvliet, G. Rosenfeld and B. Poelsema, *Physical Review Letters* **79** (1997), p. 2494

[Ref. 24]   T. M. Galea, C. Ordas, E. Zoethout, H. J. W. Zandvliet and B. Poelsema, *Physical Review B* **60** (2000), p. 60 7206

[Ref. 25]   C. Kittel, *Introduction to Solid State Physics* (8th edition, John
              Wiley & Sons Inc., New York, 2005)

[Ref. 26]   A. van Houselt, *Structural and electronic properties of Pt/Ge(001)
              and Au/Ge(001)* (Physical Aspects of Nanoelectronics & Solid
              State Physics Group, University of Twente, Enschede, 2007)

[Ref. 27]   D. A. Bonnell, *Scanning Tunneling Microscopy and Spectroscopy*,
              (VCH Publishers, New York, 1993)

[Ref. 28]   A. Stroscio, R. M. Feenstra and A. P. Fein, *Physical Review
              Letters* **57** (1986), p.2579

[Ref. 29]   R. M. Feenstra, J. A. Stroscio and A. P. Fein, *Surface Science*
              181 (1987), p. 295

A low temperature study
of CO molecules adsorbed
on atomic Pt chains
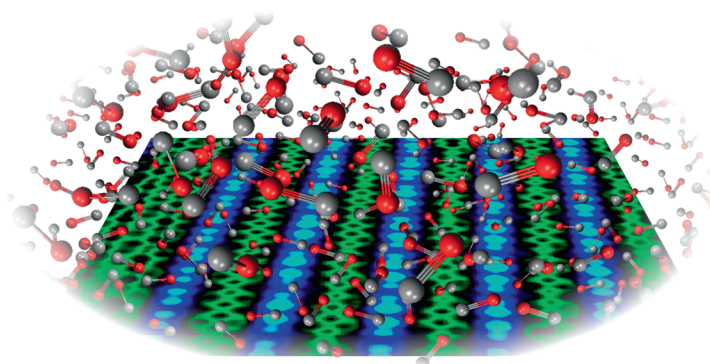
We have studied the adsorption of CO molecules on a Pt/Ge(001) surface at 77 K. The CO molecules preferentially adsorb on the Pt chains rather than on the troughs. We have identified two different adsorption sites: one either on the short-bridge site or on top of one of the atoms of a buckled Pt dimer, and the other one on the long-bridge site in between two Pt dimers. The CO molecules are immobile at 77 K. A statistical analysis of the nearest-neighbour spacing of the CO molecules reveals that adsorbed CO molecules interact repulsively along the Pt-dimer chains. This repulsive interaction, composed of electrostatic terms and a strain-mediated term, gradually fades away over a remarkably long distance of 3–4 nm. At adsorption sites the inverse decay length is small.

Introduction

The adsorption of molecules on surfaces is a key step in many important industrial processes, such as catalysis and metal organic chemical vapor deposition, and therefore, many studies have been devoted to this topic. Now, also in the field of molecular electronics there is interest in the adsorption of molecules on (nanostructured) surfaces. In molecular electronics nanostructured templates could serve as a molecular printboard for electronic devices. The ultimate goal is to use a single molecule as a device.

In terms of adsorption processes, the adsorption of carbon monoxide (CO) on platinum (Pt) is a model system; it is one of the most thoroughly investigated adsorption systems [Refs. 1–13]. Already in the early 1900's Langmuir studied the mechanism of a catalytic reaction involving CO and Pt [Ref. 1]. During the last decades, both experimental and theoretical studies have been performed in order to obtain a better understanding of the behavior of adsorbed CO on Pt [Refs. 2–13]. The majority of these studies, however, have been devoted to single crystal surfaces. The adsorption of CO on Pt(111) has been particularly well studied. At low coverage CO prefers to adsorb on atop sites, but at higher coverage the bridge site is occupied as well.

As mentioned before, most studies were performed on single crystal Pt surfaces. Studies on compound systems involving Pt have, however, attracted less attention. An appealing compound system to be used for the adsorption of CO is the Pt-modified Ge(001) surface. The Pt/Ge(001) system, as described in Chapter 3, can be used as a template surface on which (functional) molecules can be selectively deposited. The as-prepared Pt/Ge surface contains linear Pt dimer chains, with a cross section of just one atom.

The chains are virtually defect-free and can reach lengths up to a micron. The chain-to-chain separation distance is typically 1.6 nm. As described in Chapter 3, the CO molecules do adsorb on the atomic Pt chains. However, a more elaborate study is necessary to find out how the CO molecules are adsorbed exactly.

When the adsorption of CO to metals is simplistically discussed, typically three standard bonding modes are mentioned: a terminal mode, a bridging mode (μ_2-CO) and a threefold hollow mode (μ_3-CO). These are schematically shown in Figure 4.1. When connected through a terminal bond, the CO molecule is attached to only one metal atom, whereas the μ_2-CO and the μ_3-CO are connected to respectively two and three metal atoms. The bridging mode can be further divided into the so-called short-bridge (e.g. between nearest neighbour surface atoms) and long-bridge modes respectively.
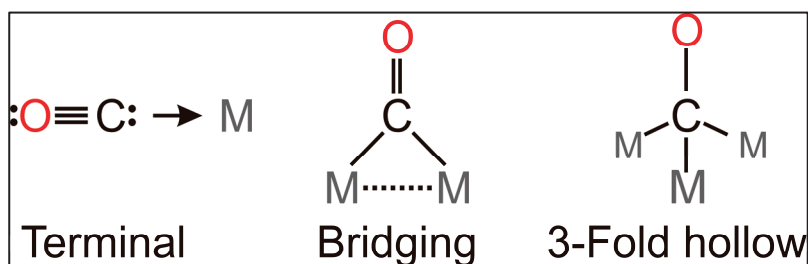

Figure 4.1: Three typical standard bonding modes known for the adsorption of CO on metal atoms.

Evidently, since we are dealing with a new kind of material, i.e. the Pt/Ge surface, it is not directly clear which adsorption sites will be relevant in case of CO adsorption. This issue will therefore be addressed first.

Additionally, we are interested in the mutual interaction between the adsorbed CO molecules. Despite an ongoing dispute on the exact nature of the mutual interaction between co-adsorbed CO molecules on Pt(111), it has been well established that CO molecules experience mutual repulsion. The range of this repulsive interaction is rather short. The occupation of nearest-neighbour sites is excluded but next-nearest occupations are allowed, yielding a repulsive range of only a few Ångströms. Some larger molecules on surfaces, as for instance, tetrathiafulvalene molecules on Au(111), exhibit repulsive interactions which have a much longer range of several nm [Ref. 14].

Though, in a study on the binding and diffusion of CO molecules on the Pt chains at room temperature, results indicated that the CO molecules possibly exhibited a higher repulsive interaction than anticipated [Ref. 15]. To investigate whether the co-adsorbed CO molecules indeed have a strong mutual repulsive interaction on the atomic Pt chains, we will measure the nearest-neighbour distribution of the adsorbed CO molecules at 77 K.

Experimental

We have studied the adsorption of CO on the Pt/Ge(001) system with an Omicron low-temperature scanning tunneling microscope (LT-STM). Nominally flat, single-side polished, slightly doped (n-type) Ge(001) wafers were laser-cut into 5.0x10.0 mm^2 substrates. The samples were first slowly

degassed after having been placed into the ultrahigh vacuum (UHV) setup. Subsequently, the samples were cleaned by cycles of Ar$^+$ sputtering (800 eV) and annealing at 1100 K using a dc current. These cycles were repeated until atomically clean Ge(001) surfaces were obtained. Imaging with STM was used to see whether the surfaces were properly cleaned.

Subsequently, a sub-monolayer amount of Pt was evaporated onto the Ge(001) surface, which was at room temperature, from a Pt wire wrapped around a tungsten filament. After evaporation the Pt/Ge(001) substrate was annealed at 1050-1100 K for 15 seconds and subsequently cooled to room temperature via radiative quenching. As discussed in more detail in Chapter 3, large regions with atomic Pt chains were formed via self-organization during this process.

In the next step the sample was exposed to CO at room temperature. The CO was introduced into the preparation chamber of the UHV system via a leak valve. Both exposure-time and pressure were monitored accurately. After exposure to CO, the samples were first imaged at room temperature to confirm the presence of adsorbed CO molecules. Subsequently the surface was cooled down to 77 K and imaged with STM.

Adsorption sites of CO on Pt/Ge(001) at 77 K

Figure 4.2 shows an empty state STM image of a Pt/Ge(001) surface after exposure at RT to 2750 Langmuirs CO, subsequently imaged at 77 K. In Figure 4.2, the imaged area is fully covered with monatomic Pt chains that are at a mutual distance of 1.6 nm. In comparison with a 'bare' Pt/Ge(001) surface (see inset in the Figure), it is immediately apparent that the chains are

now 'decorated' with two types of features. The underlying terrace remained virtually unchanged. Both types of features have not been observed before exposure to CO.

First, there are quite a number of dark features, appearing as depressions in the chain. Second, bright protruding spots on the chains are observed. For convenience we will now coin these dark and bright features D(ark) and B(right), respectively. Of both types, one example is highlighted by a yellow rhombus frame.
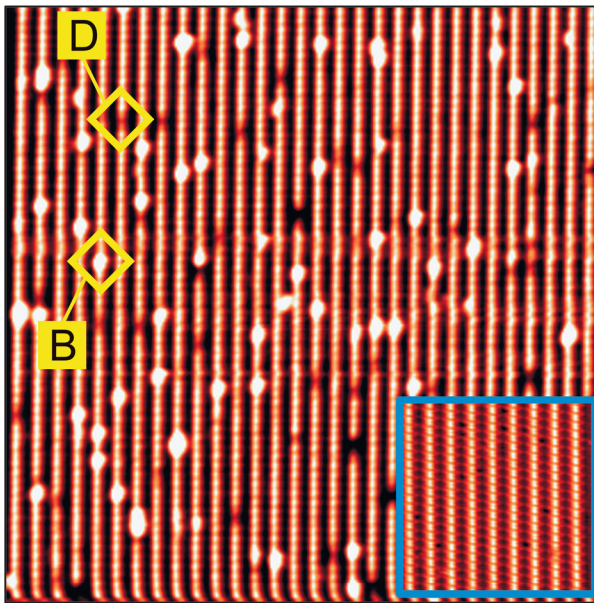

Figure 4.2: STM image of the Pt/Ge(001) surface, decorated with CO molecules. Scan settings: V_S = +1.8V, I_T = 0.5nA, size = 50nm x 50nm. The inset shows the surface before exposure to CO.

The background pressure was continuously monitored during the adsorption process and no gases other than CO were detected. As such, both features must be attributed to the adsorption of CO molecules on the Pt chains. First of all it appears that the abundance of D and B species is about equal.

The B-type adsorption site is not found at room temperature [Ref. 15]. Oncel et al. found only one type of adsorption site; the molecule appeared as a protrusion at negative bias and as a depression at positive bias. The CO molecule was positioned at an on-top adsorption site.

Since the abundance of the two species is about equal, it is likely that both adsorption sites, i.e., D and B, have similar binding energies. Since the Pt chains undergo a phase transition from a $2\times$ periodicity at room temperature to a $4\times$ periodicity at low temperatures [Chapter 3] it is tempting to relate the feature B to the adsorption on the $4\times$ Pt chains. The $4\times$ chains are comprised of buckled Pt dimers, whereas the Pt dimers of $2\times$ chains are unbuckled. However, the resolution of the STM images obtained after CO adsorption on Pt/Ge(001) prohibited giving a conclusive answer on this issue instantly. In addition, since CO was adsorbed at room temperature and the sample was cooled subsequently it is also unsure whether the $4\times$ buckled dimers actually form.

To elaborate on this, the B- and D-features were studied in more detail by monitoring them bias-dependently. The scan range was varied between -2V and +2V. In Figure 4.3 we show a D-feature measured both at +1.80 V and -1.80 V. The most prominent difference between the appearance at negative and positive bias is the fact that the D-feature shows up as a depression in the empty state image and as a protrusion in the filled state image.
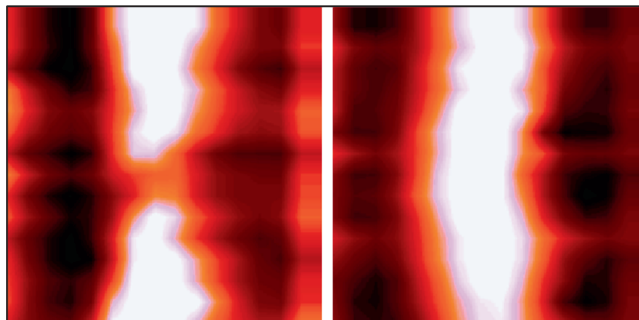
Figure 4.3: STM images (2.7nm x 2.7nm) of a CO molecule adsorbed on a Pt chain (feature D), imaged at 77 K, 0.50 nA, +1.80 V (left) and -1.80 V (right). This molecule shows up as a depression at +1.80 V and as a protrusion at -1.80 V.

Less prominent is a slight curvature along the chain that is observed at negative bias. These observations hold for the entire energy window, from -2 V to +2V.

These details are in agreement with the room temperature data published by Oncel et al. [Ref. 15]. They attributed these observations to a CO molecule adsorbed at a short-bridge site in the Pt-dimer chain. The latter is also in good agreement with a recent first-principles density functional study of the interaction between an isolated monatomic Pt chain and a CO molecule, by Sclauzero et al. [Ref. 16]. These authors compared the energies of different adsorption sites (bridge, substitutional, tilted bridge, and on top) and found that for an unstrained wire the bridge site is energetically the most favorable one. It should be pointed out here that the calculations in [Ref. 16] are for an isolated infinite Pt wire, whereas our experiments are performed on finite Pt wires that are grown on a Ge(001) substrate. Therefore, one should be somewhat cautious in comparing these two data sets.

In Figure 4.4 the height profile of a chain with an adsorbed D feature (taken from an empty state image) is superimposed on a height profile of an undecorated Pt chain. Each of the peaks in the black curve represents one Pt dimer. The centre of the molecule (the minimum in the red profile) is exactly positioned at a minimum of the profile of the bare Pt chain, i.e. in between two adjacent Pt dimers. This position is referred to as the long bridge adsorption site.
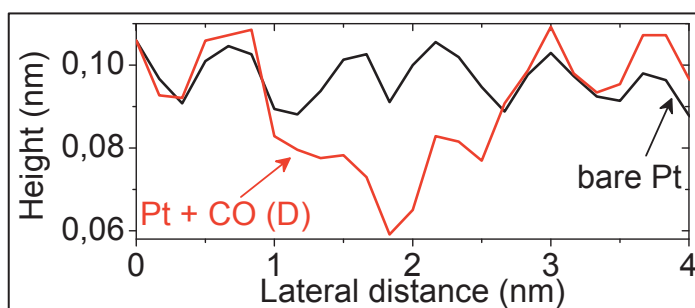
Figure 4.4: Height profiles taken along two different Pt chains at 77 K. The height profile of a chain decorated with the D-feature (red curve) is compared with an undecorated chain (black curve). Sample voltage is +1.8 V, sample current is 0.50 nA.

In Figure 4.5 a comparison is made between the empty state and the filled state appearance of the adsorbed B-feature. In contrast to the D-feature, the B-feature appears comparatively equal when imaged at reversed biases. Such a feature is not present in the room-temperature data of Oncel et al. [Ref. 15]. As will be shown later, also the D-feature is not related to the short-bridge adsorption site that is observed at room temperature.

Figure 4.5: STM images of a CO molecule adsorbed on a Pt chain (feature B). This molecule shows up as a protrusion at both negative and positive bias. Scan settings: Size = (2.7nm x 2.7nm); T = 77 K; I = 0.50 nA; V = -1.80 V (left), +1.80 V (right).
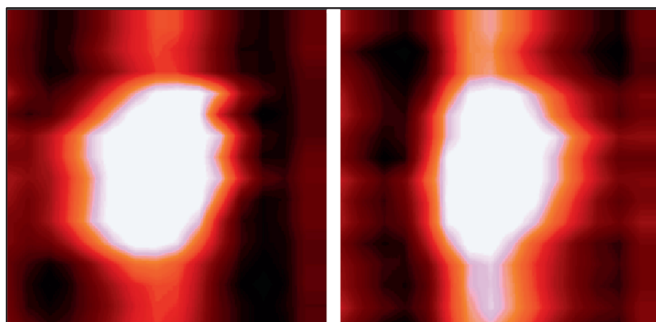
In Figure 4.6 we compare the height profile taken along the Pt chain with an adsorbed B-feature (red line) with the profile of a bare chain (black line). In comparison with the D-feature the situation for the profile of the B-feature is, however, less straightforward. First of all, we note that the feature exhibits two rather broad lobes. We emphasize that the mirrored situation, i.e., with the maximum intensity on the left-hand side occurs with about equal probability. The maximum is positioned above a maximum of the profile of the bare chain, i.e. on top of a Pt dimer. The two lobes and the asymmetric appearance of this feature indicate that the CO molecule is probably slightly tilted or adsorbed at one of the two atoms of the Pt dimer. As shown in Chapter 3, some of the Pt dimers are buckled at 77 K. Especially when a CO molecule is adsorbed, no clear distinction between an on-top adsorption site and a short-bridge adsorption site can be made. This buckling of the Pt dimers however, could possibly also explain both the two lobes and the tilt of the molecule. Another possibility for this tilt can be that a semi-bridging carbonyl is formed. In that case the CO is initially adsorbed on-top, but

subsequently it accepts electron density from a second metal center. Usually this is accompanied by distortions away from a linear M-CO (180°) or a symmetrically bridging CO (120°). Typical angles are around 150°. This is schematically shown in Figure 4.7. Actually, a semi bridged carbonyl is an intermediate form between the terminal and the bridging mode.
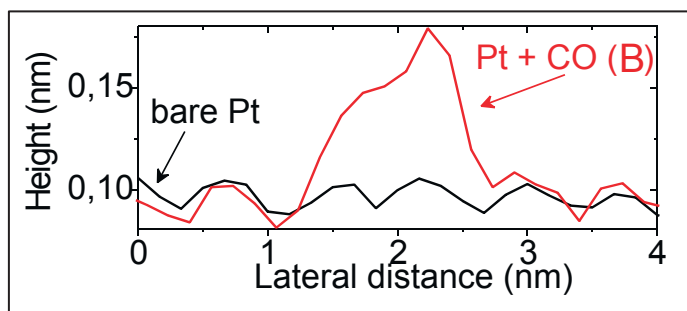

Figure 4.6: Height profiles of two different Pt chains at 77 K. The height profile of a chain decorated with the B-feature (red curve) is compared with an undecorated chain (black curve). Sample voltage is +1.8 V, tunneling current is 0.50 nA.

Figure 4.7: Schematic representation of on-top adsorbed carbonyl (left) turning into a semi-bridging carbonyl (right).

Summarizing, at room-temperature CO adsorbs at a short-bridge site, showing up as a depression at positive bias and as a protrusion at negative bias. At 77 K, this adsorption site is no longer present while two other adsorption sites appear. First, a long-bridge site shows up as a protrusion at negative bias and as a depression at positive bias. Second, we found a short-bridge, or on-top, site, which emerges as a protrusion at both negative and positive biases.

Repulsion of adsorbed CO molecules on atomic Pt chains

Oncel et al. studied the behavior of CO molecules adsorbed on atomic Pt chains at 293 K. At this temperature the CO molecules perform a random walk on the Pt chains [Ref. 15]. Furthermore, indications were found that the CO molecules might possess a strong mutual repulsive interaction [Refs. 15, 17]. By studying the distribution of the separation distance between adsorbed molecules, we tried to elucidate on this point. Nonetheless, experimentally it is easier when the molecules exhibit no translational motion at all. For that reason, more than 100 CO molecules were monitored during 90 minutes at 77 K. We found no indication for any thermally activated motion. So, at 77 K the CO molecules lack any mobility.

Using several low-temperature images, akin to the one shown in Figure 4.2, the distribution of the separation distance between adsorbed CO molecules on the same Pt chain was determined. For 390 adsorbed CO molecules the distance to their nearest-neighbour adsorbed CO molecule on the same Pt chain was measured.

In Figure 4.8 we have plotted the experimentally determined probability distribution. In addition, we have plotted the probability distribution that

one would expect in case neighbouring adsorbed CO molecules do not interact, given by Equation (4.1).
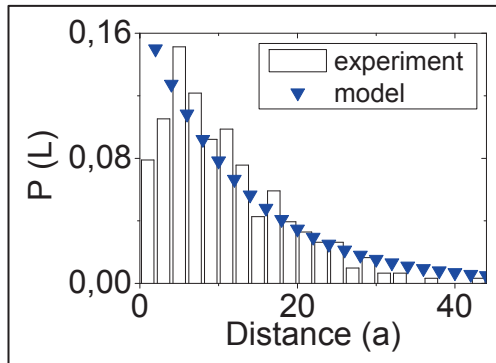
Figure 4.8: Normalized probability distribution for finding a CO molecule at a certain distance from another CO molecule on the same Pt chain; shown are both experimental data (bars) and a 'no-interaction'-model (triangles). In this plot the distance is normalized to the spacing between adjacent Pt dimers within a Pt chain (= 0.8 nm). Each bin represents 2a = 1.6 nm.

The probability of finding a CO molecule at any site on the Pt chain is given by p; p is the probability of finding a Pt-chain site covered and equals 0.078 in our experiment. The probability to find two neighbouring CO-occupied adsorption sites is thus simply given by p^2. The probability to find a separation by two lattice sites is then given by $(1-p) \cdot p^2$. The probability to find a separation of M lattice sites is $(1-p)^{M-1} \cdot p^2$. Finally, in order to

obtain a normalized distribution function, the above numbers have to be divided by p. Hence, the normalized distribution function is given by:

$$\frac{(1-p)^{M-1} \cdot p^2}{p} \tag{4.1}$$

It is immediately clear from the data in Figure 4.8 that the CO molecules adsorbed on the same Pt chain repel each other on a length scale up to about 4 nm. At distances higher than 4 nm there is good agreement between the no-interaction-model and the experimental data. At distances lower than 4 nm the no-interaction-model overrates the actual data. These two observations are indicative of mutual repulsive behaviour between CO molecules adsorbed at distances closer than 4 nm to each other. In comparison, CO molecules adsorbed on Pt(111) exhibit a repulsive interaction that vanishes within a distance of less than 0.5 nm [Ref. 18].

We have also examined the possibility of interaction between adsorbed CO molecules on neighbouring chains; this interaction is virtually absent. Therefore, the repulsive interaction along the chain cannot be solely electrostatic in origin.

We have fitted the repulsive interaction by taking into account two terms: a dipole-dipole term which decays as L^{-3} and a strain-mediated term which falls off logarithmically along the chain direction. Despite the fact that we have only a limited data set, the data can be fitted properly with a combination of an electrostatic dipole-dipole interaction and a strain-mediated interaction. Since we have two different CO adsorption sites on the Pt chains at 77 K, it is

important to compare the probability distribution for the nearest-neighbour separation of D-D, B-B, and D-B adsorption site pairs. Interestingly, the same characteristic long-range repulsive interaction is observed for all combinations, i.e. D-D, B-B, and D-B. As referred to above, we emphasize that we have also examined the interaction between adsorbed CO molecules on adjacent Pt chains. Our analysis reveals that this interaction is very weak if existent at all.

We accentuate that the range of the repulsive interaction between adsorbed CO molecules on the atomic Pt chains is unusually large, compared to the interactions between CO molecules on monocrystalline Pt surfaces [Ref. 18]. Tentatively, a qualitative explanation of this remarkable observation can be given by using the Blyholder adsorption model [Ref. 19].

The adsorption of CO on transition metal surface atoms is often described in terms of the Blyholder model [Ref. 19]. Blyholder extended the Dewar-Chatt-Duncanson model of the chemical bonding between alkenes and metals [Refs. 20, 21]. In this electron donation/back-donation model, electrons are donated from the highest occupied molecular orbital (HOMO) of CO, 5σ, to the $5d_{z^2}$ orbital of the metal. Subsequently, electrons are backdonated from the metal d_π orbital to the lowest unoccupied molecular orbital (LUMO) of CO, i.e. $2\pi^*$. This is illustrated in Figure 4.9. Of course, we are cautiously using the Blyholder model, since we are not dealing with a pure transition metal surface.

Within the Blyholder model the repulsive interaction between adsorbed CO molecules can be understood in a straightforward manner: the adsorbed molecules form a dipole with an estimated dipole moment of 0.9 D for Pt

[Ref. 12]. For a CO molecule that adsorbs at an on-top site, this dipole moment is aligned in a direction perpendicular to the surface. Due to this parallel alignment, neighbouring CO molecules undergo mutual repulsion. In addition, the adsorption induces local charge rearrangements that lead to electrostatic interaction as well [Ref. 18]. However, these interactions alone are insufficient to explain the unusually long range of the interaction since they decay very rapidly.
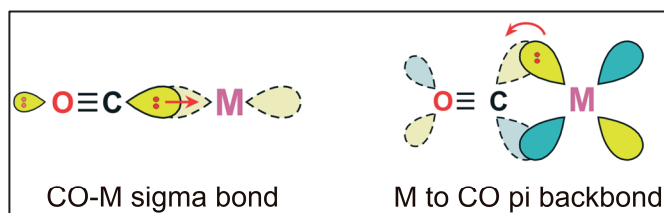
Figure 4.9: Schematic representation of the electron donation / back-donation model.

As mentioned before, this model basically consists of two parts. The second part, in which electrons are *backdonated* from the metal d-orbital into the LUMO of CO, can be larger than the first part. If so, the net result is that the electron density of the metal reduces. For our Pt/Ge(001) system we expect that in the vicinity of an adsorbed CO molecule there is a zone in which the electron density is significantly reduced. Thus, within a certain range the electron density of the neighbouring Pt dimers is depleted. It should be noted that we assume that the electrons predominantly come from the Pt chain and not from the underlying substrate.

Since we are dealing with atomic metal chains instead of a metal surface, the reduction in the electron density can have a larger influence that it usually has for normal metal surfaces. Compared to, e.g. Pt(111), the density of free electrons is strongly reduced and thus screening effects are much less effective leading to an enhanced lateral length scale for repulsion. Due to the asymmetric donation/backdonation model, the adsorption of a CO molecule will lead to a small dipole. Since all the dipoles are aligned perpendicular to the surface, an adsorbed CO molecule also hinders the adsorption of another CO molecule in its direct proximity.

Spatial maps of the inverse decay length of Pt/Ge(001) + CO

According to the Simmons model [Refs. 22, 23] the tunneling current is given by

$$I(V,z) = \frac{CV}{z} e^{-2\kappa z} \qquad\qquad (4.2)$$

in which C is a constant, V is the sample bias, z is the width of the tunneling barrier and κ is the inverse decay length.

Due to the fact that the exponential term in Equation (4.2) dominates the $1/z$ term, the tunneling current is often approximated by $I(V,z) \propto e^{-2\kappa z}$. The slope of the graph $\ln(I)$ versus z then gives -2κ. As said, the $1/z$ part of the Simmons model is neglected. Therefore a more exact method was

developed to obtain more accurate values of κ. In addition, the developed method is a much more time-efficient method.

The development of the so-coined κ-microscopy method is based on the parameters F_1 and $F_{2,}$ which are defined as:

$$F_1 \equiv \frac{1}{i}\frac{di}{dz} = -2\kappa - \frac{1}{z} \tag{4.3},$$

$$F_2 \equiv \frac{1}{i}\frac{d^2 i}{dz^2} = \left(-2\kappa - \frac{1}{z}\right)^2 + \frac{1}{z^2} \tag{4.4}.$$

For κ this eventually results in

$$\kappa = \frac{-F_1}{2} - \frac{\sqrt{F_2 - F_1^2}}{2} \tag{4.5}$$

In the commonly used $I(z)$ spectroscopy technique, the first term of Equation (4.5) is used. However, the second term represents the normally neglected $1/z$ term. The use of a lock-in amplifier enables the measurement of both di/dz and $d^2 i/dz^2$ simultaneously with the topography. More experimental details are given in Appendix A.

In Figure 4.10 the result of the newly developed κ-microscopy method is shown. Simultaneously, the topography (a), a F_1 map (b) and a F_2 map (c) of a Pt/Ge(001) surface decorated with CO molecules were recorded at 77 K. In Figure (a) the adsorbed CO molecules are visible as bright, circular

protrusions on the atomic Pt chains (circled). Clearly, the lock-in signals displayed in (b) and (c) track the topography of the surface very well. Via a combination of the F_1- and F_2-maps the spatial map of the inverse decay length is acquired (d). The CO molecules are now observed as dark spots. The latter indicates that at sites where CO molecules are adsorbed the inverse decay length is small.
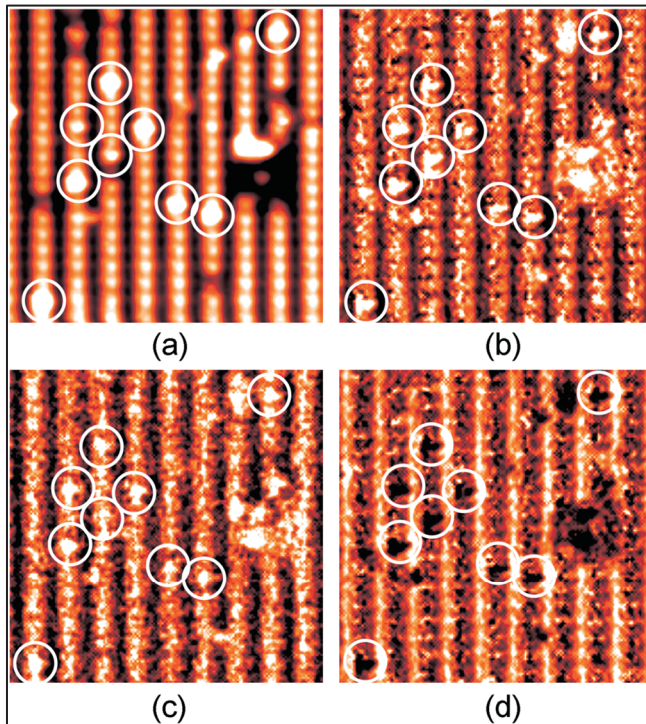

Figure 4.10: (a) Empty state STM image of a Pt modified Ge(001) surface. Adsorbed CO molecules are encircled in white. Sample bias is +1.5 V, tunneling current is 0.4 nA and image size is 15×15 nm^2. (b) F_1 map of the area in (a). (c) F_2 map of the area in (a). (d) Spatial map of κ for the area in (a).

Conclusions

We have adsorbed CO molecules on the Pt/Ge(001) surface at room temperature; subsequently this system was studied at 77 K. Our study revealed that CO binds preferentially, if not exclusively, to the Pt chains.

At this temperature CO occupies two different adsorption sites. A long-bridge site showed up as a protrusion at both positive and negative bias. An on-top or short-bridge site showed up as a depression at positive bias and as a protrusion at negative bias.

The distribution of the separation distance between adsorbed CO molecules was determined and compared with a no-interaction model. From this we found that CO molecules repel each other. The range of this repulsion is spectacular: CO molecules show a mutual repulsion at distances as large as 3–4 nm.

A spatial map of the inverse decay length κ of a Pt/Ge(001) surface decorated with CO molecules was recorded at 77 K. On the κ-map the CO molecules showed up as dark depressed features. This is indicative of a small inverse decay length κ.

References

[Ref. 1]   I. Langmuir, *Transactions of the Faraday Society* **17** (1922) p. 621

[Ref. 2]   M.-L. Bocquet and P. Sautet, *Surface Science* **360** (1996), p. 128

[Ref. 3]   M. T. M. Koper, R. A. van Santen, S. A. Wasileski and M. J. Weavers, J. *Chemical Physics* **113** (2000), p. 4392

[Ref. 4]   J. Yoshinobu, N. Tsukahara, F. Yasui, K. Mukai and Y. Yamashita, *Physical Review Letters* **90** (2003), p. 248301

[Ref. 5]   E. H. G. Backus, A. Eichler, A. W. Kleyn and M. Bonn, *Science* **310** (2005), p. 1790

[Ref. 6]   T. Takaoka and T. Komeda, *Physical Review Letters* **100** (2008), p. 046104

[Ref. 7]   S. E. Mason, I. Grinberg and A. M. Rappe, *Journal of Physical Chemistry C* **112** (2008), p. 1963

[Ref. 8]   R. B. Shumbera, H. H. Kan and J. F. Weaver, *Journal of Physical Chemistry C* **112** (2008), p. 4232

[Ref. 9]   G. Ertl, H. Knozinger and J. Weitkamp, *Handbook of Heterogeneous Catalysis Vol. 1-5* (Wiley-VCH, Weinheim, 1997)

[Ref. 10]   B. Poelsema, S. T. de Zwart and G. Comsa, *Physical Review Letters* **49** (1982), p. 578

[Ref. 11]   B. Poelsema, L. K. Verheij and G. Comsa, *Physical Review Letters* **49** (1982), p. 1731

[Ref. 12]   H. Steininger, S. Lehwald and H. Ibach, *Surface Science* **123** (1982), p. 264

[Ref. 13]   H. Froitzheim, H. Hopster, H. Ibach and S. Lehwald, *Applied Physics* **13** (1977), p. 147

[Ref. 14]   I. Fernandez-Torrente, S. Monturet, K. J. Franke, J. Fraxedas, N. Lorente and J. I. Pascual, *Physical Review Letters* **99** (2007), 176103

[Ref. 15]   N. Oncel, W. J. van Beek, J. Huijben, B. Poelsema and H. J. W. Zandvliet, *Surface Science* **600** (2006), p. 4690

[Ref. 16]   G. Sclauzero, A. Dal Corso, A. Smogunov and E. Tosatti, *Physical Review B* **78** (2008), p. 085421

[Ref. 17]   N. Oncel, *Scanning tunneling microscopy and spectroscopy studies on Pt-modified Ge(001) and metallic (Pd, Au)-quantum dots on self-assembled monolayers* (University of Twente, Enschede, 2007)

[Ref. 18]   S. E. Mason, I. Grinberg and A. M. Rappe, *Journal of Physical Chemistry B* **110** (2006), p. 3816

[Ref. 19]   G. Blyholder, *Journal of Physical Chemistry* **68** (1964), p. 2772

[Ref. 20]   M. J. S. Dewar, *Bulletin de la Société Chimique de France* **18** (1951), p. C71

[Ref. 21]   J. Chatt and L. A. Duncanson, *Journal of the Chemical Society* (1953), p. 2939

[Ref. 22]   J. G. Simmons, *Journal of Applied Physics* **34** (1963), p. 1793

[Ref. 23]   J. G. Simmons, *Journal of Applied Physics* **34** (1963), p. 2581

Octanethiol adsorbed on Pt chains
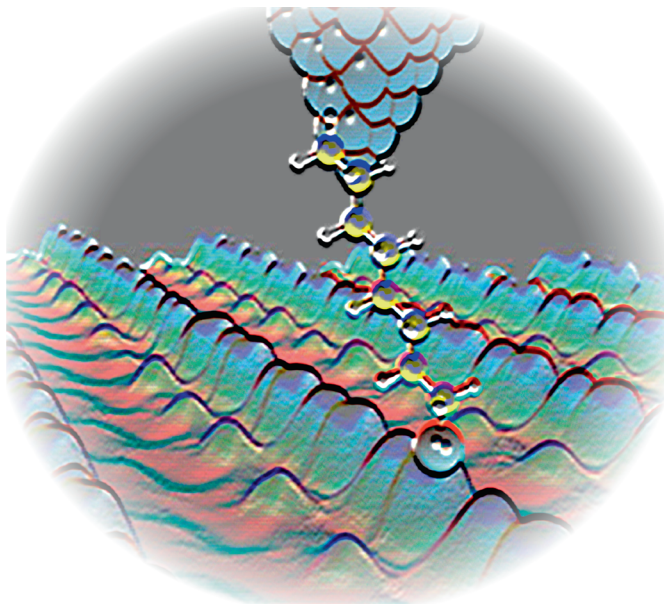
Octanethiol molecules adsorbed on Pt chains are studied with scanning tunneling microscopy and spectroscopy at 77 K. The thiol-head of the molecule binds to a Pt atom and the octane-tail is lying flat down on the chain. Open-loop current time traces reveal that the molecule wags its tail and attaches to the scanning tunneling microscopy-tip. This results in a dramatic increase of the current. We measured a single molecule resistance of 100-150 MΩ.

Introduction

As indicated in the opening words of Chapter 4, the adsorption of molecules on surfaces has been of interest for more than a century. Meanwhile the interest is boosted [Ref. 1], amongst others due to both the invention of the STM and Aviram and Ratner's 1974 landmark publication [Ref. 2]. In their article Aviram and Ratner put forward the idea to use a single (organic) molecule as a molecular rectifier. A single molecule that has a donor-spacer-acceptor like structure could behave as a p-n junction and thus exhibit rectifying current-voltage behaviour. At that time, the so-called top-down approach was the only way to create electronic components. However, Aviram and Ratner proposed a novel method; the so-called bottom-up approach. With this method electronic devices/components are assembled, taking individual molecules or atoms as a starting point.

Nonetheless, it took more than two decades before the physical and chemical properties of an individual molecule could be measured successfully. In particular the introduction of scanning tunneling microscopy, in the early 1980's [Ref 3-5], has given an enormous boost to this field. Meanwhile numerous papers are published on molecular electronics, demonstrating many intriguing and exotic phenomena. Single molecules, or small bundles of molecules, have been trapped between electrodes [Refs. 6-13] and researchers have measured Coulomb gaps and Coulomb staircases [Ref. 6], bi-stable switching [Ref. 7], current rectification [Ref. 8], negative differential resistance characteristics [Ref. 9], Kondo resonances [Ref. 10] and conductance switching [Ref. 11].

The use of alkanethiols in molecular electronics is now well-established since these molecules form densely packed and well-ordered self-assembled monolayers on metal surfaces [Ref. 14 and refs. therein]. An alkanethiol

molecule basically consists of three parts: a sulphur-hydrogen head, a hydrocarbon chain, and an end group. The basic picture used to explain the adsorption of an alkanethiol on a metal substrate, ending in self-assembly, entails physisorption followed by chemisorption [Ref. 15]. After physisorption, the molecule binds via the sulphur atom to the surface. The H atom is released and the alkanethiol transforms to an alkanethiolate. At low coverage the alkanethiolate molecules are flat-lying on the surface in ordered domains, referred to as the striped phase or lying down phase. This is shown in Figure 5.1(a). Upon increasing the coverage to one monolayer the alkanethiolate molecules will eventually convert to a standing-up phase, see Figure 5.1(b). By using nano-structured surfaces instead of normal metal surfaces as a template, one could construct or assemble more sophisticated nanostructures.
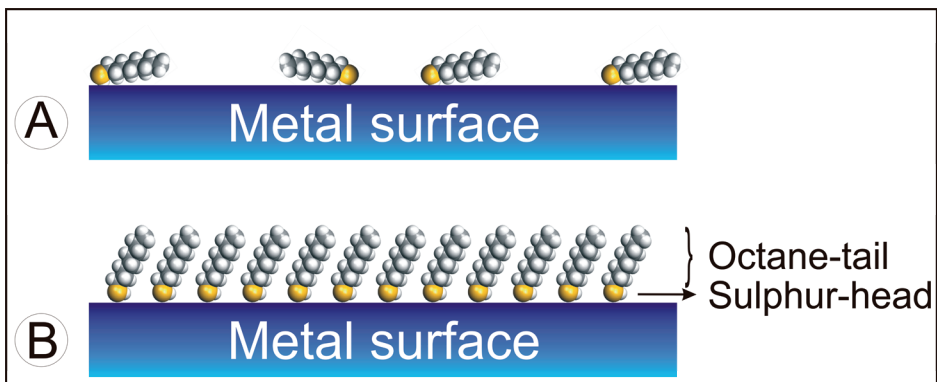

Figure 5.1: Octanethiolate molecules adsorbed on a metal surface forming a lying down phase at low coverage (a) and a self-assembled monolayer (b).

In this Chapter we report on the adsorption of octanethiol molecules on atomic Pt chains. These Pt chains were grown on Ge(001) via a self-organization process, as discussed in Chapter 3. The Pt/Ge(001) surface is a particularly attractive candidate to be used as a template in molecular electronics since it predominantly consists of arrays of dimerized, perfectly straight and virtually defect-free monatomic Pt chains.

The Pt/Ge(001) substrates were exposed to (various amounts of) octanethiol at room temperature and subsequently cooled down to 77 K. After adsorption and cooling down to 77 K the structural and the electronic properties of the adsorbed octanethiolate molecules were studied with STM and STS.

Experimental

Ge(001) substrates (5.0 mm × 10.0 mm) were cut from nominally flat, single-side polished n-type wafers. After rinsing with isopropanol, the samples were placed into the UHV LT-STM (Omicron). Here, they were slowly degassed. Subsequently, the samples were cleaned by sputtering with 800 eV argon ions and thermal annealing to 1100 K (using a dc current). This procedure was repeated several times before atomically clean Ge(001) surfaces were obtained. Imaging with STM at 77 K revealed that the surface predominantly consists of two different well ordered domain patterns: $p(2\times2)$ and $c(4\times2)$. Subsequently, we deposited a sub-monolayer amount of Pt onto the clean Ge(001) surface at room temperature. Pt was evaporated onto the surface using a simple home-built Pt evaporator; a high-purity Pt-wire was wrapped around a W filament. Evaporation occurs simply by heating the W filament via a dc current. After evaporation the Pt/Ge(001) substrate was

annealed up to 1050-1100 K and subsequently cooled down to room temperature by radiative quenching. Following this procedure, we found large patches of Pt chains. A more detailed description on the procedure and on the formation and the properties of the Pt chains is given in Chapter 3.

After formation of the Pt chains, the surface was exposed to octanethiol (Sigma-Aldrich). The octanethiol was introduced in the preparation chamber of our UHV system via a leak valve at room temperature. This valve allowed us to meticulously control the octanethiol-pressure in our preparation chamber. Samples were exposed to $10-16500$ Langmuirs of octanethiol. After each exposure step the UHV-setup was allowed to reach its normal background pressure ($p \leq 5 \cdot 10^{-11}$ mbar); then, the sample was transferred to the STM chamber for cooling down and imaging.

Adsorption of octanethiol on Pt/Ge(001)

To investigate whether or not, the octanethiol molecules adsorb on the Pt/Ge(001) surface, an octanethiol-exposure dependent series of STM scans was recorded at 77 K after room temperature adsorption. This series is presented in Figure 5.2.

The atomic Pt chains appear as almost vertical bars. The chains are comprised of Pt dimers, which are aligned in the direction of the chains. The width of a single chain is exactly one Pt atom and the distance to neighbouring chains is mostly 1.6 nm, but sometimes also 2.4 nm or 3.2 nm. Clearly present in the images (a), (b), (c) and (d) are many white circular spots located on top of the Pt chains. These spots were not present before exposure to octanethiol. The apparent size of the spherical features is consistent with the size of an octanethiolate molecule, i.e. $\approx 1\,nm$) [Ref. 16].

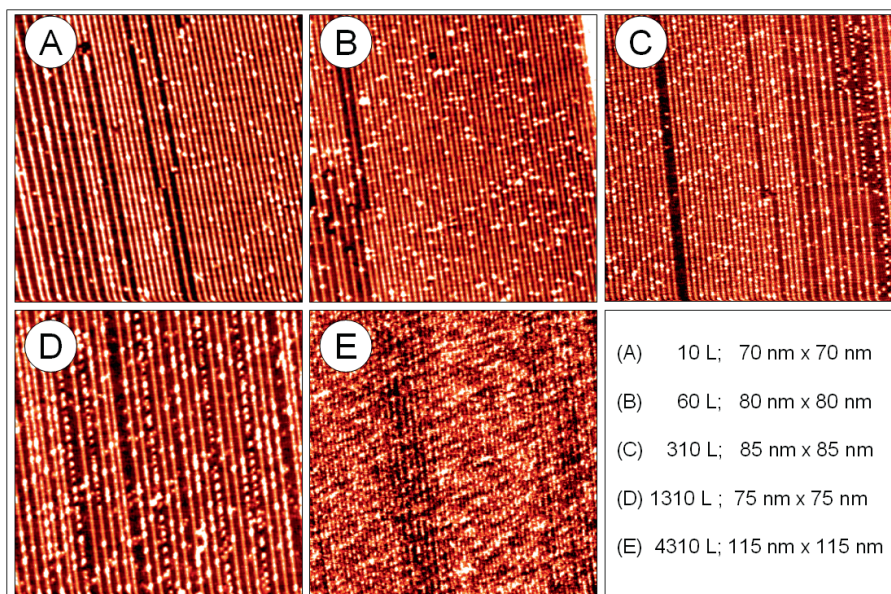|	
(A)	10 L; 70 nm x 70 nm
(B)	60 L; 80 nm x 80 nm
(C)	310 L; 85 nm x 85 nm
(D)	1310 L ; 75 nm x 75 nm
(E)	4310 L; 115 nm x 115 nm

Figure 5.2: Series of filled state STM scans of the Pt/Ge(001) surface after exposing it to different amounts of octanethiol at room temperature, ranging from 10 Langmuir (a) to 4310 Langmuir (e). The white circular features are attributed to the octanethiol molecules. In (e) the molecules are so densely packed that the individual molecules are no longer visible separately. Scan settings: $T = 77\,K$; $V = -1.6\,V$; $I_T = 0.5\,nA$.

The exposure of the Pt/Ge(001) surface to octanethiol varies from 10 Langmuirs in Figure 5.2(a) to 4310 Langmuirs in Figure 5.2(e). An increase of the exposure of octanethiol leads to an increase in the number density of these white spots. Therefore, we attribute these white spherical features to octanethiolate molecules adsorbed on the atomic Pt chains. Furthermore, from Figure 5.2 it is clear that at an exposure between $10 - 1310$ Langmuirs the octanethiol molecules adsorb on the Pt chains and virtually not on the underlying substrate. The density of these white spots increases with increasing exposure to octanethiol up to about 2000 Langmuirs. Above 2000 Langmuirs the density of white blobs on the Pt chains becomes so high that

we cannot recognize the separate molecules anymore. An example of this is shown in Figure 5.2(e).

Since the octanethiol molecules do adsorb on the Pt/Ge(001) surface, the next step is to focus on the adsorption geometry of the adsorbed octanethiol molecules on the Pt chains. Therefore, an additional Pt/Ge(001) surface was exposed to 60 Langmuirs of octanethiol.

In Figure 5.3 an STM image ($25\,nm \times 25\,nm$) of this Pt modified Ge(001) surface is displayed.
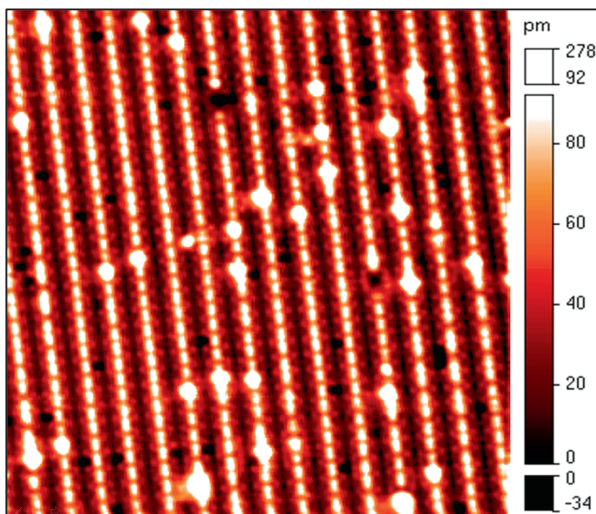
Figure 5.3: STM image ($25\,nm \times 25\,nm$; $V_S = -0.9\,V$; $I_T = 0.5\,nA$; $T = 77\,K$) of the Pt/Ge(001) surface after exposure at RT to 60 Langmuirs of octanethiol.

The surface was scanned at 77 K with a sample bias $V_S = -0.9\,V$ and a tunneling current of $I_T = 0.5\,nA$. The dimerized chains of Pt atoms are displayed as almost vertical dashed bars; the octanethiol molecules appear as

bright circular features adsorbed on the chains. In Figure 5.3 it is even more evident than in Figure 5.2 that the sticking coefficient of octanethiol on the atomic chains is much higher than on the underlying substrate surface.

The adsorbed octanethiol molecules were scanned at a bias range from $-1.5\,V$ to $+1.5\,V$. At both positive and negative sample bias the Pt chains are easily recognizable. Regarding the adsorbed octanethiol molecules a clear distinction can be made between negative sample bias (filled state) and positive sample bias (empty state) imaging. This is shown in Figures 5.4(a) and 5.5(a).

In Figure 5.4(a) we zoom in on one of the octanethiol molecules as presented in Figure 5.3.
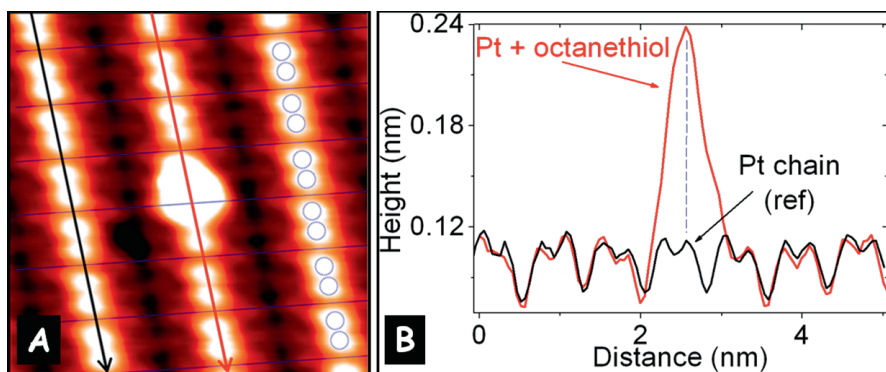
Figure 5.4: STM image ($5\,nm \times 5\,nm$; $V_S = -1.5\,V$; $I_T = 0.5\,nA$; $T = 77\,K$) of an array of Pt chains with in the center of the image an adsorbed octanethiol molecule (a). The molecule shows up as a bright protrusion; this is also clear from the height profiles shown in (b).

Figure 5.4(a) displays a filled state image (25 nm^2); a large white protrusion covers virtually one and a half Pt dimer. For convenience, we have added blue

circles on the most right Pt chain to indicate the atomic positions. The topographic centre of the molecule is positioned on one of the Pt atoms of the fully decorated Pt-dimer. More clearly this is shown in the height profile in Figure 5.4(b); this profile is taken along the Pt chain as indicated by the red arrow. As a reference profile we also plotted the height profile of a clean Pt chain, as indicated by the black arrow in (a).

Furthermore, when looking at the troughs flanked by the chains, there is no difference between the region near the adsorbed molecule and the regions further away from the adsorbed molecule.

From the area shown in Figure 5.4(a), also an empty-state image was recorded, Figure 5.5(a). This image shows that the adsorbed octanethiolate now exhibits a completely different shape. The protrusion, much smaller in size now, is located on one side of the Pt dimer. Additionally, on the other side of this dimer, the protrusion is accompanied by a small depression.
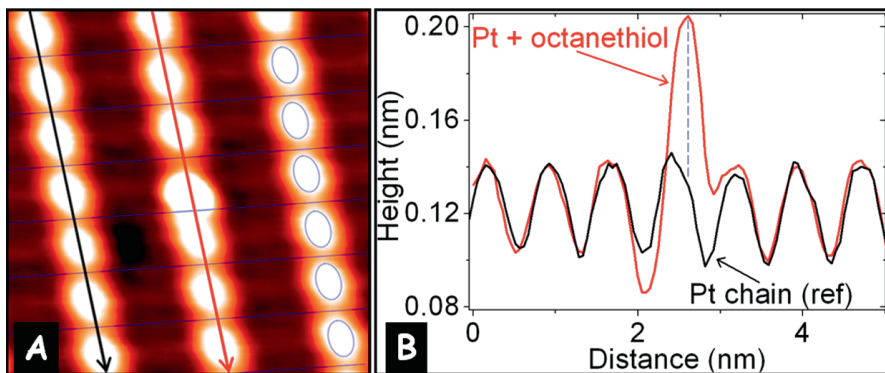
Figure 5.5: STM image ($5\,nm \times 5\,nm$; $V_S = +1.5\,V$; $I_T = 0.5\,nA$; $T = 77\,K$) of an array of Pt chains with in the centre of the image an adsorbed octanethiol molecule (a). The molecule shows up as a small protrusion accompanied by a small depression; this is also clear from the height profiles shown in (b).

The positive sample bias height characteristics of a bare Pt chain and a Pt chain decorated with an adsorbed molecule are presented in Figure 5.5(b); the profiles were recorded along the arrows as indicated in (a).

As mentioned before, alkanethiols are well-studied because of their ideal self-assembly properties on metal surfaces. The sulphur atom of the thiol headgroup binds to the surface and for a densely packed monolayer the alkane chains are standing upwards due to the intermolecular Van der Waals forces [Ref. 15]. At low coverage however, the alkane chains are lying flat down on the surface. Both based on these observations and the STM data shown here we assume that the octanethiolates are also lying flat down on the Pt chains, at least in the low coverage regime. In fact, if we take a closer look at the region in the troughs between the Pt chains, we see no difference between before and after adsorption of the octanethiolate molecules. Moreover, the region in the troughs between the Pt chains near an adsorbed octanethiolate molecule is virtually identical to a molecule-free trough region. Hence, the tail of the octanethiolate molecules must be located on the Pt chains rather than in troughs between the chains. Thus, on the basis of our STM data we conclude that the sulphur atom binds on-top to one of the atoms of the Pt dimer and the tail of the octanethiolate molecule lies flat on the Pt chain.

Spectroscopy of an adsorbed octanethiol molecule
In order to obtain more insight in the exact adsorption geometry of the octanethiolate molecule we have performed scanning tunneling spectroscopy; current-voltage characteristics were measured both on the head and the tail of

the molecule. It must be noted, however, that at this moment we do not know which part is the head and which part is the tail. In Figure 5.6 we show I(V) curves recorded on both parts of the octanethiolate molecule. In (c) the data acquisition locations are marked by the black dot (●) and the red triangle (▲). The tunneling current was measured with a sample bias between $-1.5\,V \le V_S \le +1.5\,V$. Figure 5.6(b) shows a closer look of the region from $0.0\,V$ to $+0.4\,V$.

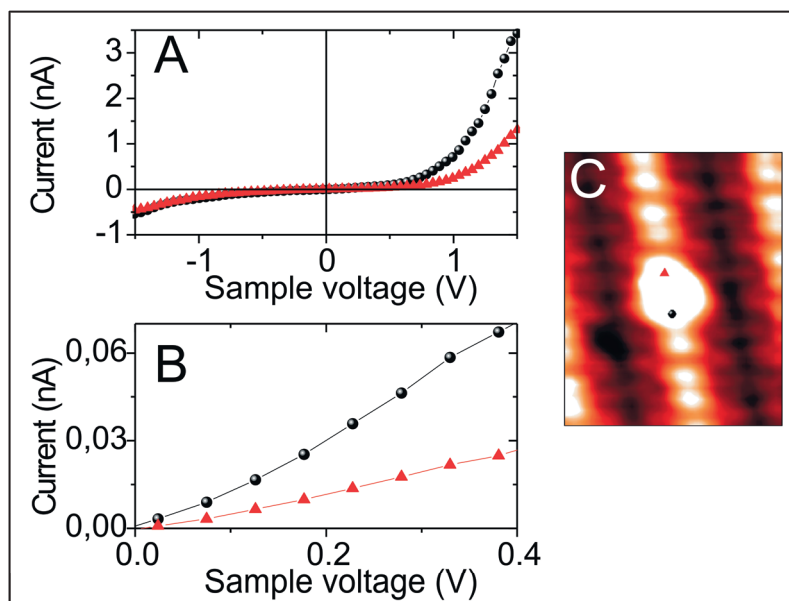**Figure 5.6:** I(V) characteristics taken on the two ends of an octanethiol molecule adsorbed on a Pt chain, as indicated by the black dot (●) and the red triangle (▲) in the STM image of (c). In (b) the voltage window from 0 V to 0.4 V is articulated. We ascribe the curve with the highest current ratio (black) to the sulphur-side of the molecule and the red curve to the octane-side of the molecule.

At negative sample bias the $I(V)$ curves measured at the two different ends of the molecule are virtually identical. At positive sample bias, however, the two parts of the molecule behave differently. The region marked with the black dot (•) in the STM image in (c), shows a much higher current than the region marked with the red triangle (▲). After superimposing the negative sample bias STM image of (c) onto its positive bias counterpart, we found that the red triangle (▲) is positioned on the small depression, similar to the one discussed at Figure 5.5. We ascribe the more metallic curve to the sulphur-head of the molecule (•) and the other curve to the organic (non-conjugated) tail of the octanethiolate (▲). So, while it is hard to discriminate between both the thiol- and the octanepart of the adsorbed molecule by just performing STM, the combination with STS on different parts of a molecule allows one to discriminate between the two parts. In Figure 5.7 we have illustrated the orientation of the octanethiol molecule adsorbed on the Pt chain, as derived from this combination of STM and STS.
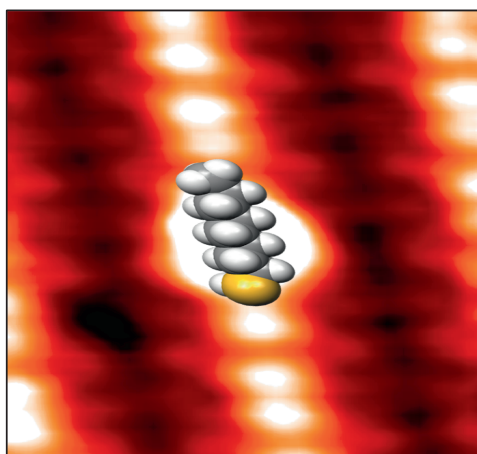

Figure 5.7: STM image of the octanethiol molecule adsorbed on the atomic Pt chain, with an illustration of the orientation of the adsorbed molecule.

Electron transport through a single molecule

In Figure 5.8 we have plotted three I(t) transients. The current was measured in time on top of the adsorbed octanethiol molecules. During these experiments the feedback of the electronics was in the open-loop configuration. So, the separation distance between the tip and the surface of the sample was kept constant within the timeframe of the experiment. So, if there is a change in the geometry of the adsorbed molecule, which is in between the tip and the surface of the sample, this will be immediately reflected in the measured current.
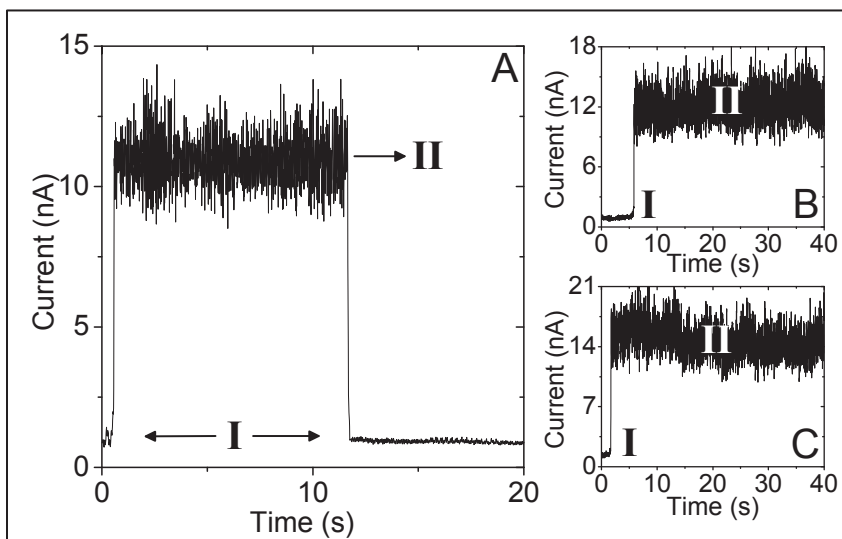
Figure 5.8: I(t) transients recorded on an octanethiolate molecule that was adsorbed on a Pt chain. The current traces were recorded at a constant height with a sample bias of 1.5 V. In (a) the current jumps back and forth between the current set point (1 nA) and a much higher current of 11 nA. We have measured high current residence times up to about 40 seconds, like (b) and (c) and high currents up to 10-15 nA, like (a), (b) and (c). The current jumps were caused by the octanethiolate molecule that wagged its tail and subsequently contacted the STM tip, as indicated by the schematic drawings in Figure 5.9.

The data presented in Figure 5.8 were acquired with a sample bias of $V = 1.5\,V$. Clearly shown in the chart of Figure (a) is the dramatic increase in the current from 1 nA to 11 nA. After being constant for more than ten seconds the current drops back abruptly to its original value of 1 nA. During other experiments, we even measured current jumps from 1nA to 15 nA, see (c) and also high current residence times up to about 40 seconds, see (b) and (c). In these experiments, however, we only observed a current jump upwards and no return to the starting value of 1 nA.

It must be mentioned that current traces as plotted in Figure 5.8 are not typical for this experiment. Sudden current jumps were only observed in about 15% of the executed experiments. In the other experiments, however, the current measured above an adsorbed octanethiol molecule stayed constant at the current setpoint (1 nA) during the entire measurement.

Although we have measured different maximum currents, and also different residence times at high current, we are dealing with the same process in all these cases. The simple fact that the current returns to its starting value (1nA) excludes a permanent change in the geometry of the adsorbed molecule. This is also confirmed by comparison of STM images taken both before and after recording the current-traces.

As the most plausible explanation of the sudden increase in the current signal the following scenario is proposed: during tunneling to the molecule, the tail of the octanethiolate molecule flips up and jumps into contact with the apex of the STM tip. Interestingly the length of the octanethiolate molecule ($\approx 1\,nm$) is slightly larger than the width of the tunnel gap, i.e. $\approx 0.7\,nm$ [Ref. 17]. Hence, the tail of the octanethiolate molecule is long enough to contact the STM tip. An artistic view of this occurrence is presented in Figure 5.9.

The fact that the current does not always return to its starting value, is most likely due to a difference in thermal drift of the tip.
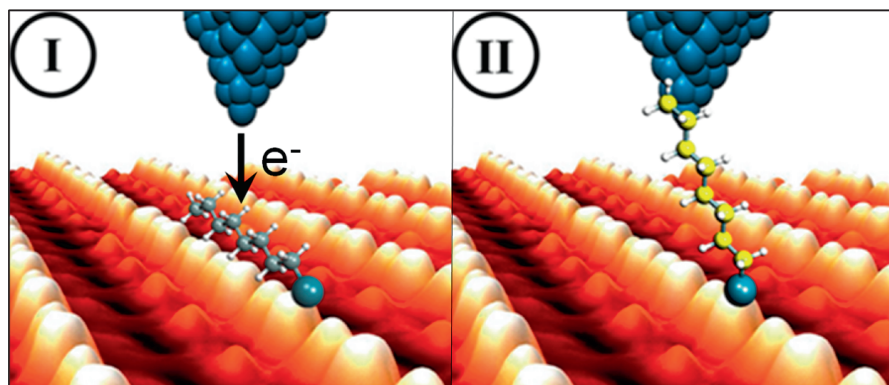
Figure 5.9: Artistic view of the observed current jumps as discussed above: they are caused by the octanethiolate molecule that wags its tail and subsequently contacts the STM tip. Firstly, electron tunneling occurs through the vacuum to the adsorbed molecule (I). Secondly, electrons flow through the molecule that has wagged its tail, thereby making contact with the tip (II).

Knowing both current and voltage, we extracted the resistance of a single octanethiol molecule trapped between the tip of the STM and the Pt/Ge(001) surface to be between $100-150\,M\Omega$. This value is in good agreement with values reported in literature [Ref. 14 and refs. therein]. It should be pointed out here that at the side of the tip of the STM we have not created a chemisorbed contact since the tail of the octanethiolate detaches typically after 10-40 seconds, leaving the molecule on its original adsorption site. Since the resistance we measured falls in the range of the reported values for both C6 and C8-thiolates [Ref. 14] we cannot determine whether the current flows through the whole molecule or just through a major part of the molecule.

Sudden current jumps due to flipping of an adsorbed molecule were reported previously [Ref. 18, 19]. However, in these experiments the current changes were much smaller and the average residence time of the molecule in contact with the tip was much shorter. It should be pointed out here that it does not make sense to vary the current set point, since an increase (decrease) of the current by a factor of ten results in a decrease (increase) of the tip-substrate separation distance of only 0.1 nm.
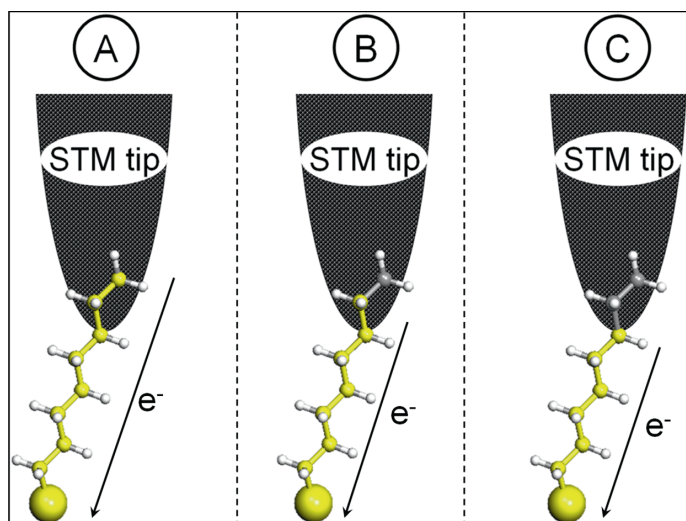
Figure 5.10: Illustration of the different motion paths as a result of the overlap between the adsorbed molecule and the apex of the tip. The resistance of the motion paths increases with increasing path length; as such the current increases from A to C.

Another peculiar feature in the data from Figure 5.8 is the large noise level at the high current levels (II in the Figure). An increase in current automatically gives rise to an increase in the noise level. However, the observed increase in noise is higher than anticipated. A possible explanation for this can be the

fact that the molecule overlaps significantly with the tip so that the molecule can have different adsorption configurations. We suggest that the end of the molecule jumps rapidly from one adsorption site to another adsorption site. The current then flows (alternately) through different parts of the molecule. This is illustrated in Figure 5.10, where the yellow parts indicate the electron paths. Since all adsorption configurations result in different resistances, a large noise band is observed.

Conclusions

In summary, we have studied the adsorption of octanethiol molecules on a Pt-modified Ge(001) surface with STM and STS at 77 K. The octanethiolate molecules adsorb highly preferentially on the Pt chains.

By measuring the I(V) characteristics on both the thiol-head and the octane-tail of the adsorbed molecule, we were able to discriminate between the two different parts. From that the adsorption geometry was determined.

I(t) experiments with the feedback of the electronics in the open-loop configuration above the adsorbed molecule were performed. Occasionally, the molecule then wagged its tail, hereby contacting the tip of the STM. We were able to keep contact between the tip and the molecule for tens of seconds. Throughout this contact we measured currents up to 15 nA. The fact that the molecule is attached to the tip of the STM enabled us to determine the resistance of a single octanethiol molecule adsorbed on the Pt chains, $100 - 150 \, M\Omega$.

References

[Ref. 1]   N. P. Guisinger, N. L. Yoder and M. C. Hersam, *Proceedings of the National Academy of Sciences* **102** (2005), p. 8838

[Ref. 2]   A. Aviram and M. A. Ratner, *Chemical Physics Letters* **29** (1974), p. 277

[Ref. 3]   G. Binnig and H. Rohrer, *Helvetica Physica Acta* **55** (1982), p. 726

[Ref. 4]   G. Binnig, H. Rohrer, C. Gerber and E. Weibel, *Physica B & C* **109** (1982), p. 2075

[Ref. 5]   G.Binnig, H. Rohrer, C. Gerber and E. Weibel, *Applied Physics Letters* **40** (1982), p. 178

[Ref. 6]   N. Oncel, A.-S. Hallback, H. J. W. Zandvliet, E. A. Speets, B. J. Ravoo, D. N. Reinhoudt and B. Poelsema, *Journal of Chemical Physics* **123** (2005), p. 044703

[Ref. 7]   L. T. Cai, M. A. Cabassi, H. Yoon, O. M. Cabarcos, C. L. McGuiness, A. K. Flatt, D. L. Allara, J. M. Tour and T. S. Mayer, *Nano Letters* **5** (2005), p. 2365

[Ref. 8]   R. H. M. Smit, Y. Noat, C. Untiedt, N. D. Lang, M. C. van Hemert and J. M. van Ruitenbeek, *Nature* **419** (2002), p. 906

[Ref. 9]   J. Chen, M. A. Reed, A. M. Rawlett and J. M. Tour, *Science* **286** 1999, p. 1550

[Ref. 10]   W. J. Liang, M. Shores, M. Bockrath, J. R. Long and H. Park, *Nature* **417** (2002), p. 725

[Ref. 11]   Z. J. Donhauser, B. A. Mantooth, K. F. Kelly, L. A. Bumm, J. D. Monnell, J. J. Stapleton, D. W. Price, A. M. Rawlett, D. L. Allara, J. M. Tour and P. S. Weiss, *Science* **292** (2001), p. 2303

[Ref. 12]   E. H. Huisman, M. L. Trouwborst, F. L. Bakker, B. de Boer, B. J. van Wees and S. J. van der Molen, *Nano Letters* **8** (2008), p. 3381

[Ref. 13]   G. Meszaros, S. Kronholz, S. Karthauser, D. Mayer and T. Wandlowski, *Applied Physics A* **87** (2007), p. 569

[Ref. 14]   H. B. Akkerman and B. J. de Boer, *Journal of Physics: Condensed Matter* **20** (2008), p. 013001

[Ref. 15]   R. K. Smith, P. A. Lewis and P. S. Weiss, *Progress in Surface Science* **75** 2004, p. 1

[Ref. 16]   Z. Li, S.-C. Chang and R.S. Williams, *Langmuir* **19** (2003), p. 6744

[Ref. 17]   C. J. Chen, *Introduction to Scanning Tunneling Microscopy* (Oxford University Press, New York, 1993)

[Ref. 18]   G. J. Ashwell, B. Urasinska, C. Wang, M. R. Bryce, I. Grace and C. J. Lambert, *Chemical Communications* **45** (2006), p. 4706

[Ref. 19]   W. Haiss, C. S. Wang, I. Grace, A. S. Batsanov, D. J. Schiffrin, S. J. Higgins, M. R. Bryce, C. J. Lambert and R. J. Nichols, *Nature Materials* **5** (2006), p. 995

Gold-induced nanowires on Ge(001)

The structural and the electronic properties of Au induced self-organized nanowires on Ge(001), prepared by different procedures, are investigated with scanning tunnelling microscopy and spectroscopy at room temperature and at 77 K. We found that the Au-induced nanostructures are identical for the different preparation routes. The Au-induced nanowires are comprised of Ge dimers that have their bond aligned in a direction perpendicular to the nanowire. The dimers are buckled, leading to a 2x periodicity along the nanowires. Dimers located at antiphase boundaries are dynamic at room temperature and flip back and forth between two buckled configurations. The troughs between the nanowires have a depth of several atomic layers and are decorated with Au trimers. Finally, the differential conductivities of the nanowires and the troughs are very comparable in magnitude.

Introduction

In the previous Chapters a Pt-modified Ge(001) surface was used as the substrate surface. The most appealing feature of that surface is that it partially contains large areas with perfectly straight dimerized Pt chains with a width of only one atom. Besides the Pt-induced one-dimensional (1D) structures on Ge(001) also gold (Au) induced nanostructures on Ge(001) attracted our interest. Several papers were published in which work on Au-induced nanostructures was reported [Refs. 1-4].

Slightly different preparation methods were used by the different groups that reported on these structures. All procedures have in common that they consist of two parts: (1) evaporation of Au onto Ge(001) and (2) annealing of the Au/Ge surface. In the method used by Schäfer et al. [Ref. 3] these two steps occur simultaneously while Wang et al. [Refs. 1, 2] and Van Houselt et al. [Ref. 4] first evaporate the Au and subsequently anneal the Au/Ge sample. In [Ref. 3], Schäfer and co-workers reported that the deposition of Au on Ge(001) leads to the formation of 1D chains of Au atoms on the Ge surface. They reported that these chains show 1D electron liquid behaviour. These authors report a change of the tunneling conductivity by not less than two orders of magnitude when comparing the ridges of the self-organized chains with the troughs in between the chains.

The electronic properties of low dimensional systems are intimately related to their geometric structure. In ideal 1D or two-dimensional (2D) systems the electron confinement is important, leading to an increased electron correlation with strong deviations from the Fermi liquid model. Particularly in 1D systems the enhanced interaction is accompanied by instabilities. The Fermi liquid theory breaks down spectacularly in 1D [Refs. 5, 6]. It has been predicted that the 1D electron system is much better described by the

Luttinger liquid formalism. Nonetheless, the major problem with 1D electron systems is that they are much harder to realize than their 2D and 3D counterparts.

Hence, the claim by Schäfer et al. that they have found a truly 1D electron system, makes the Au/Ge(001) an exceptionally interesting system. However, their findings are in conflict with results by Van Houselt and co-workers [Ref. 4]. It was suggested by Schäfer et al. that the different preparation routes may be responsible for the discrepancy. Hence, a detailed study is required in which the different preparation methods for the Au-induced nanostructures on Ge(001) are compared.

In this Chapter, the careful study of the Au-induced chains as prepared by two methods is reported, namely (1) deposition of Au while the Ge(001) is at anneal temperature (650 K – 850 K) and (2) deposition of Au while Ge(001) is at room temperature followed by an annealing step (650 K – 850 K). The first method is applied by Schäfer et al. [Ref. 3], whereas Van Houselt et al. [Ref. 4] used the second method. A comparison between the two methods is made. Subsequently, a detailed view on the structural properties of the Au-induced nanostructures is given. We have studied the structural properties at both room temperature and at 77 K. Furthermore, we have studied the electronic properties of the Au-induced nanostructures at both room temperature and at 77 K.

Experimental

Experiments were performed with a low-temperature STM from Omicron (LT-STM), which operates in ultrahigh vacuum (UHV). Ge(001) substrates were cut from nominally flat, 7.6 cm by 0.5 mm, about 25 Ω-cm resistance,

single-side-polished n-type wafers. Samples were mounted on molybdenum or tantalum holders and contact of the samples to any other metal during preparation and experiment has been carefully avoided. The Ge(001) samples were cleaned by prolonged 800 eV Ar$^+$ ion sputtering and annealing via resistive heating at 1050-1100 K. After several cleaning cycles the Ge(001) samples were atomically clean and exhibited a well ordered (2 x 1)/c(4 x 2) domain pattern at room temperature [Refs. 7, 8].

We have applied two methods to prepare the Au-induced self-organized 1D structures. In the first method an equivalent of 0.5 monolayers of Au was deposited onto the Ge(001) surface, while this surface was at an elevated temperature. In subsequent experiments the temperature was varied between 650 K and 850 K. So, the sample was annealed during deposition of Au. Au was evaporated by resistively heating a W wire wrapped with high purity Au (99.995%). For convenience this method is coined the 'hot-method'.

In the second method, again an equivalent of 0.5 monolayers of Au was deposited. However, now the Ge(001) surface was kept at room temperature. After Au deposition the sample was annealed for 2 minutes and then cooled down to room temperature by radiative quenching. This method will later be referred to as the 'room temperature method', abbreviated as the 'RT-method'. Again, the annealing temperature was varied between 650 K and 850 K.

Hot-method vs. RT-method, a comparison
One of the main goals of this study was to see whether the two preparation methods lead to any significant difference. Therefore the topography of the surfaces as prepared by the two different methods is compared.

Firstly, the hot-method will be discussed. Figure 6.1 shows three STM scans of the Au-reconstructed surface, as prepared by the hot method. An equivalent of 0.5 monolayers of Au was deposited on a Ge(001) sample kept at a 775 K. After cooling down to room temperature, the sample was imaged with STM.

Figure 6.1: Filled state STM images of arrays of Au-induced nanostructures on Ge(001) as prepared by the hot-method, imaged at T = 293 K.

In the Figure one can clearly see 1D nanostructures running from the top to the bottom of the images. These Au-induced nanostructures appear as vertical bright rows in the image. The chain-chain separation distance is 1.6 nm. Occasionally defects in the rows are observed. One occasionally also finds noisy appearing dimers in the rows. The depth of the troughs is about 0.4 nm

from the top of the nanowires and thus comprises several atomic layers [Refs. 4, 6]. It should be pointed out already here that one needs a very sharp STM tip in order to measure the depth of the troughs between the densely packed nanowires reliably. With a blunt tip the extracted trough depth will of course be significantly smaller due to convolution effects.

As can be seen in Figure 6.1(a), large substrate areas can fully be covered with the nanowires with this method. Typically, the growth of the nanowires does not stop until the wire runs into the edge of an adjacent substrate terrace.

Less obvious, but present nonetheless, is a zigzagging pattern along the direction of the 1D nanostructures. Like the other mentioned structural properties, this zigzagging pattern will be discussed in more detail later.

Finally, in the troughs in between the Au-induced nanowires there is some atomic structure observed as well. Small blobs are visible that are located both at left and right sides of the troughs.

A variation in sample temperature (between 650 K and 850 K) during deposition of Au did not influence the structural properties of the Au-induced nanostructures at all.

Secondly, the RT-method will be discussed. We deposited 0.5 monolayer of Au on a Ge(001) sample kept at room temperature. After the deposition process the sample was annealed at 750 K for 2 minutes. In Figure 6.2 STM images of the as-prepared Au-induced nanowires are depicted. Similar to the hot-method, this method produces arrays of 1D patterns. The 1D patterns have a mutual separation distance of 1.6 nm as well and here we observe defects occasionally too. Again, the depth of the troughs is about 0.4 nm and the wires are thus comprised of several atomic layers. Similar to the hot-method, large substrate areas can be covered with nanowires by using the RT-

method. Additionally, the STM images in Figure 6.2 show the trough structure as well. Again, by varying the annealing temperature between 650 K and 850 K the structural properties of the formed structures did not change.
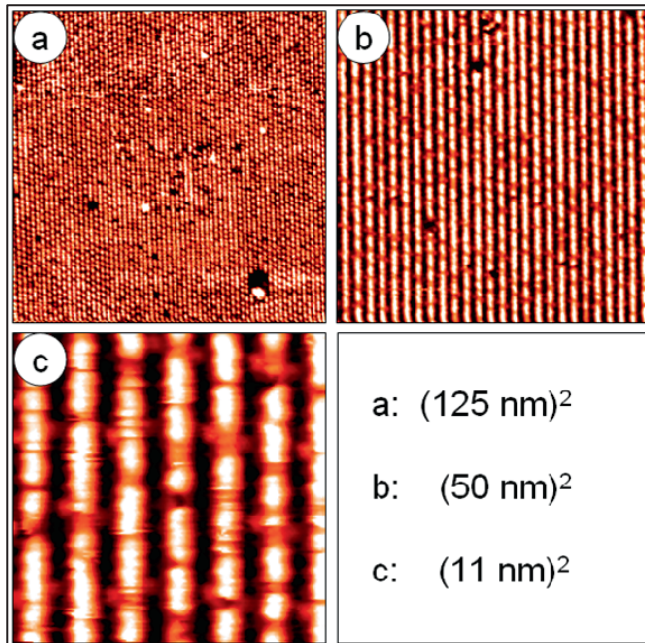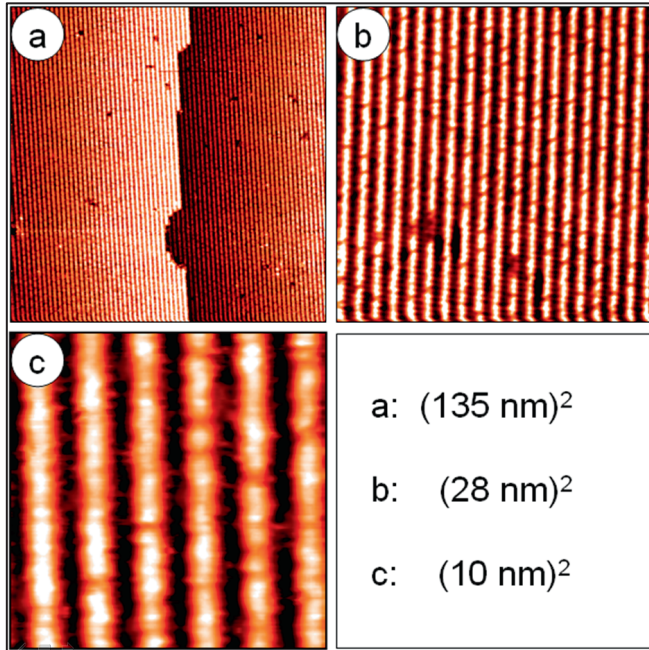

Figure 6.2: Filled state STM images of arrays of Au-induced nanostructures on Ge(001) as prepared by the RT-method, imaged at 293 K.

Above we have seen that the properties of the Au-induced nanowires on Ge(001) were identical for the two different preparation routes. From that we conclude that the moment of sample-annealing (during or after Au deposition) does not have an influence on the eventually obtained nanostructures.

Now, we will discuss the structural properties of the Au-induced nanostructures in more detail. We emphasize that these properties are

identical irrespective of the used method, so we will no more distinguish between the two methods. This also holds for the electronic properties, which will be discussed later.

Nanowire structure

In [Ref. 4] a model was proposed for the Au-induced nanowires. In this model the ridges of the nanowires consist of Ge. The top of these ridges consists of buckled Ge dimers. The idea that the Au-induced nanowires are comprised of buckled dimers, leading to a $2\times$ periodicity along the nanowire direction, has already been put forward in the first papers on the Au/Ge(001) system by Wang et al. [Refs. 1, 2].

Similarly to the atomic Pt chains [see Chapter 3], the separation distance between adjacent nanowires is exactly 1.6 nm. Like the Pt chains, the Au-induced nanowires are aligned along the [111] and the [1$\overline{1}$1] directions. However, the height of the Au-induced nanostructures is about 0.4 nm; this is much higher than the height of the atomic Pt chains, i.e. about 0.1 nm. The height of the Au-induced nanowires thus involves several atomic layers. Commonly, these heights are obtained by surface faceting [Ref. 9]. Actually, it was concluded that the Au-induced nanowires were in fact the microfacets of Ge [Ref. 4]. The incorporated Au induces nanofaceting of the Ge(001) surface into alternating ($\overline{1}$11) and (1$\overline{1}$1) facets. The sides of these facets are Au-trimer decorated Ge(111) micro-facets and have a $\left(\sqrt{3}\times\sqrt{3}\right)R30°$ Au overlayer structure. The model of the formed nanostructures as presented in [Ref. 4] is shown in Figure 6.3.
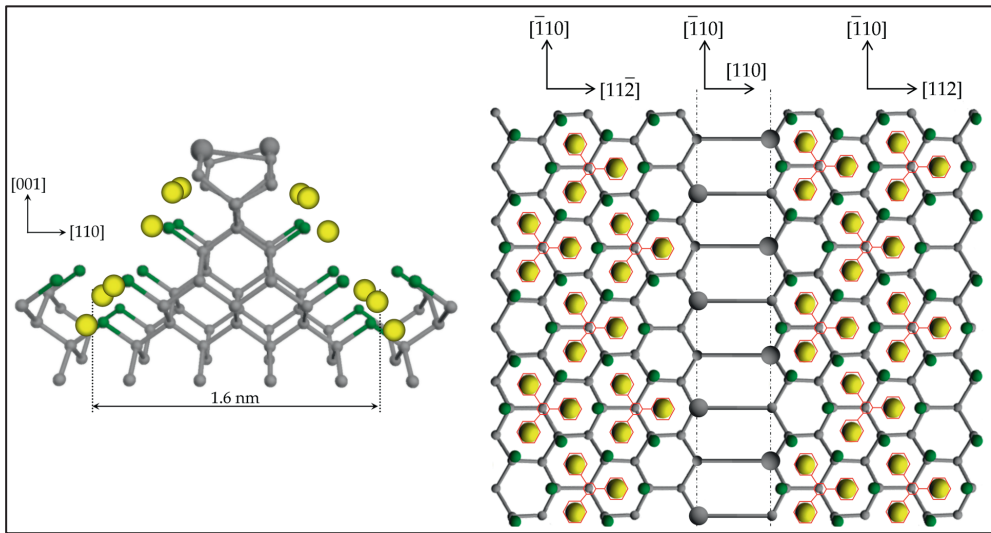
Figure 6.3: Schematic side view (left image) and 'exploded' top view (right image) of the $(\bar{1}11)$ and $(1\bar{1}1)$ facets. The green Ge atoms are the topmost Ge atoms in the $(\sqrt{3}\times\sqrt{3})R30°$ Au overlayer. Note that the Ge dimers on top are buckled; the larger atoms are the higher atoms of the dimers. The Figure is taken from [Ref. 4].

In Figure 6.4(a) small fractions of two Au-induced nanowires are shown. The nanowires exhibit a well visible zigzagging pattern along the direction of the wires. This is due to the buckling registry in the nanowires. In the wire on the right hand side a zigzag line is added as a guide to the eye. The buckling of the dimers leads to a periodicity of 0.8 nm along the nanowires. The same periodicity was reported in [Refs. 1-4]. In the three-dimensional (3D) STM image in Figure 6.3(b) this zigzagging pattern can be seen too.

However, on the basis of an analysis of the Full Width at Half-Maximum (FWHM) of the Au-induced nanowires, which was measured to be 0.72 nm, Schäfer et al. concluded that the nanowires have a width of only one atom. Although the measured value is in agreement with our findings (0.75 nm, Figure 6.4(c)), the accompanying conclusion is very unlikely. This is shown

here via a comparison with both the Ge(001) surface and the Pt induced atomic chains.
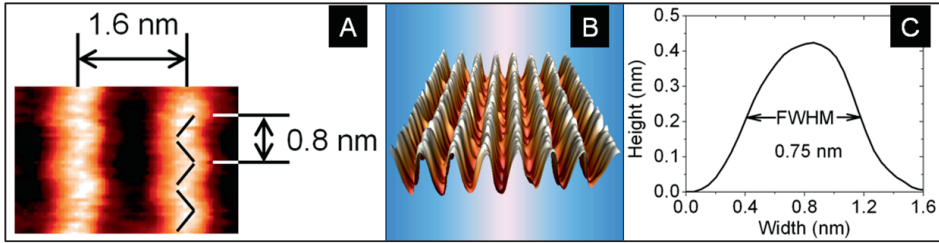

Figure 6.4: Fraction of two Au-induced nanowires, showing the buckling registry along the wires (a). In the chain on the right side a black zigzag line is added as a guide to the eye. 3D representation of an array of Au-induced nanowires (b). Height profile taken across a nanowire, with the FWHM = 0.75 nm (c).

In Figure 6.5 STM images of the Pt-induced chains (a), the Au-induced wires (b) and the Ge(001) surface (c) are presented together with their height profiles (d), (e) and (f), measured as indicated with the arrows in the STM images. Firstly, a comparison between the profiles of the Au-induced nanowires and the atomic Pt chains reveals two things. Both kinds of wires have a chain-to-chain separation distance of exactly 1.6 nm. However, the FWHM of the Pt chain (0.45 nm) is considerably smaller than the FWHM of the Au-induced nanowire. For the atomic chains of Pt it is known that its width is exactly one atom [Chapter Three]. Therefore, it is very improbable that the Au-induced wires have a width of just one Au atom too. Secondly, a comparison is made between the height profile of the Au-induced nanowires with the height profile of the Ge dimer rows of the pristine Ge surface. It is remarkable to see that the width and shape of the top of the Au-induced nanowires is very similar to the width and shape of the profile of the Ge

dimers of the Ge(001) surface. This makes it more logical that the Au-induced nanowires consist of Ge dimers at the top instead of just one Au atom.
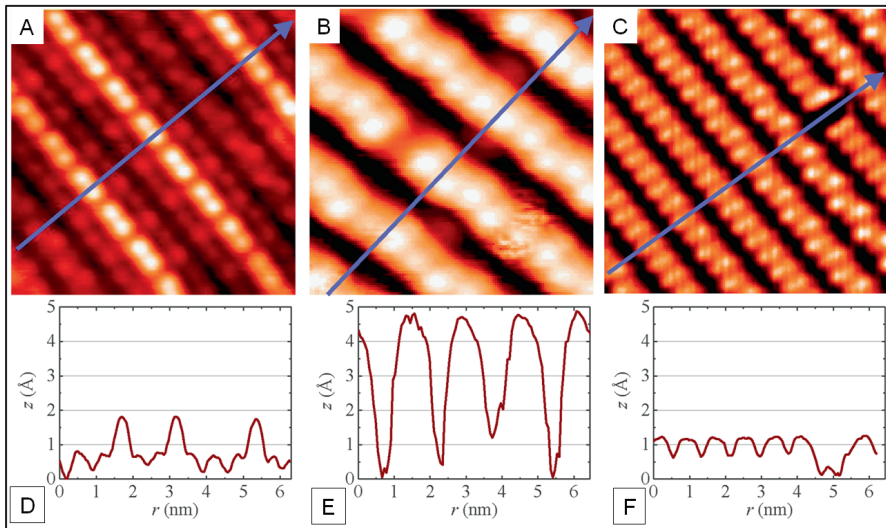
Figure 6.5: STM images of Pt induced (a) and Au induced (b) nanowires and of a pristine Ge(001) surface (c). The images are 5 nm × 5 nm, sample biases are -1.0 V for (a) and (b) and -1.5 V for (c). Tunneling currents are 0.4 nA for (a) and (b) and 0.6 nA for (c). The height profiles in (d), (e) and (f) are measured along the arrows indicated in (a), (b), and (c) respectively.

Flip-flopping dimers and substrate-wire bridges

When we take a closer look at the room temperature STM data of the Au-induced nanowires, some additional features are revealed. Two of these are highlighted in Figure 6.6. This Figure displays an STM image of an array of Au-induced nanowires recorded at room temperature.

A frizzy appearing Ge dimer is present within the white square in the Figure. These frizzy appearing dimers are positioned at antiphase boundaries in the

buckling registry of the nanowires. At these boundaries a single Ge dimer flips back and forth between the two buckled states, since it does not know whether to align with its left or right neighbour. These flip-flopping dimers are also present in the data of Altman [Refs. 1, 2], Schäfer [Ref. 3] and Van Houselt [Ref. 4]. It was reported that this flip-flop process between the two buckled states is a stochastic one [Ref. 4]. The Ge dimers of the pristine Ge(001) surface are also known to exhibit such a stochastic flip-flop motion [Ref. 10].
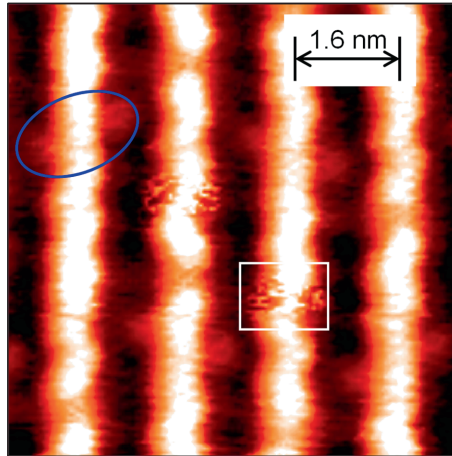
Figure 6.6: Array of Au-induced nanowires. The white square highlights a flip-flopping Ge dimer.

Quite often we also observed *substrate-wire bridges*. In Figure 6.6 an example of such a bridge is surrounded by the blue ellipse. Mostly two protrusions are observed together, one at each side of the nanowire (as the ones presented in Figure 6.6). Occasionally single protrusions were found too. Similar features were also observed in [Refs. 1-4]. Whenever two protrusions are found

together (on different sides of the nanowire) they are not positioned at each other's mirror-positions (considering the wire as a mirror). A straight line from one protrusion to the other makes an angle of approximately 65° with the wire. In [Ref. 4] these *bridges* were attributed to the lowest lying Au trimers on the ridges of the facets, which are located at the bottom of the troughs.

Filled state vs. empty state

Mostly, filled state STM imaging was used to study the structural properties of the Au-induced wires. However, here a comparison is made between filled state and empty state STM images of the nanostructures.
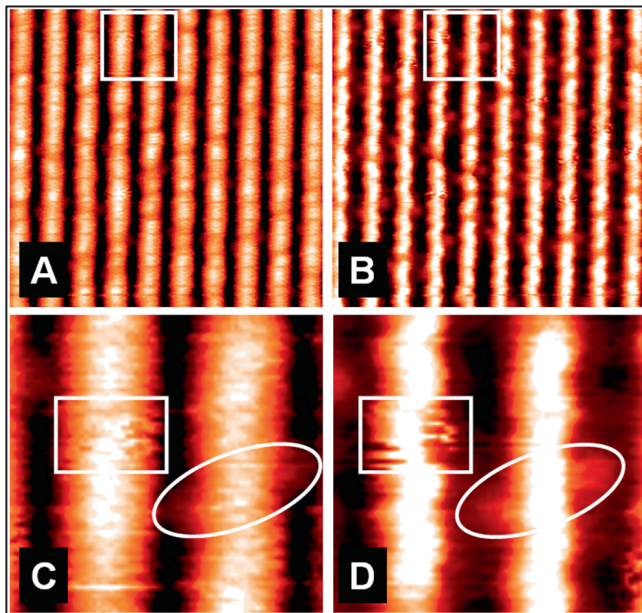

Figure 6.7: STM images of an array of Au-induced nanostructures. (a) displays an empty state image; (b) displays a filled state image of the same area in (a); (c) and (d) are higher magnification images of the squared areas in (a) and (b) respectively. In (c) and (d) a flipflopping dimer (square) and a bridge (ellipse) are highlighted.

In Figure 6.7 four STM images are shown. Figures (a) and (b) are scanned on the same area within the same timeframe; (a) displays an empty state image and (b) displays a filled state image. Figures (c) and (d) are magnified images of the regions highlighted in (a) and (b) respectively.

The zigzagging pattern of the nanowires can clearly be seen in (b); although less obvious this pattern can also be resolved from the empty state image in (a). In Figures (c) and (d) both a flip-flopping dimer as well as a substrate-wire bridge are highlighted by the square and the ellipse respectively.

The fact that we can observe the above-mentioned features at both negative bias and positive bias ensures that they are all topographical features.

Nanowire structure at T = 77 K

Besides a room temperature investigation of the structural properties of the Au-induced nanostructures on Ge(001), we have also studied the Au/Ge(001) surface at 77 K.

In Figure 6.8 a filled state STM image is shown of an array of Au-induced nanowires, imaged at 77 K.

At first sight, a 77 K view of the structures seems to be identical to a RT view. Again, the mutual separation distance between the wires is 1.6 nm, the apparent height of the wires is about 0.4 nm and the periodicity of the wires is about 0.8 nm. However, one major difference between the 77 K data and the RT data can be observed. The flip-flopping dimers, as present in abundance at RT, are not observed at all at 77 K. As mentioned earlier, the dynamics of these dimers is stochastic and behaves Poissonian. Therefore, the number of flip-flopping events decays exponentially with an decrease in

temperature, according to $\propto e^{-E/kT}$. Hence, the flip-flop motion is kinetically frozen at 77 K.
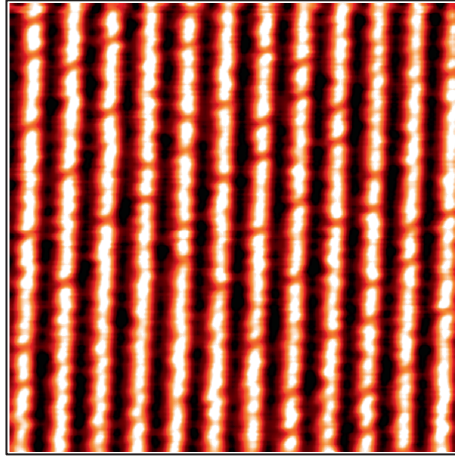
Figure 6.8: Filled state STM image (19 nm x 19 nm) of the Au-induced nanowires, recorded at 77 K

On/off wire differential conductivity

The next focus is on the electronic properties of the Au-induced structures. In [Ref. 4] it was pointed out that the local density of states (LDOS) of the Au-induced nanowires resembles the local density of states of the bare Ge(001) surface very well. In [Ref. 3] Schäfer et al. found that the differential conductivity measured on a wire (4.4 nA/V) was two orders of magnitude higher than the differential conductivity measured in between the wires (0.05 nA/V). Exactly this difference of two orders in the differential conductivity made Schäfer et al. conclude that the wires act as an ideal 1D electron liquid. For that reason, we have studied the electronic properties of the Au-induced structures.

In Figure 6.9 the differential conductivity dI/dV, recorded at 300 K on and in between the Au-induced nanowires is shown. For the entire energy window the differential conductivities measured on the nanowires and in the troughs are very similar in magnitude.
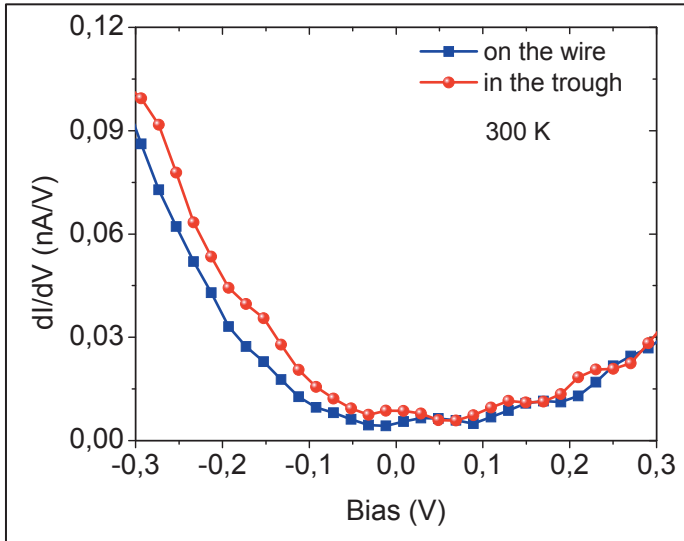
Figure 6.9: Differential conductivity measured both on/off the Au-induced nanowires. Scan settings: V = -1.5 V, I = 0.7 nA.

The results presented here corroborate nicely with the results in [Ref. 4]. In addition, these data corroborate with the data in [Ref. 3] measured in between the wires. Consequently, our data do not match with the data in [Ref. 3] measured on the wires.

In Appendix B we have given a detailed explanation for the fact that in [Ref. 3] a huge difference in the differential conductivity was found between on wire and in between wire measurements. A brief description is given below.

In order to compare the differential conductivities at various locations on the surface in a meaningful way it is important to record the $I(V)$ curves at a fixed sample bias setpoint and a fixed tunneling current setpoint. Unfortunately, Schäfer and co-workers do not give the setpoint values of the sample bias and the tunneling current. Since the actual value of the differential conductivity (around the Fermi level) critically depends on the used setpoint values we have first reconstructed their $I(V)$ curves by integrating the available dI/dV data in [Ref. 3]. From this we extracted the setpoints they most likely have used in their experiments. It appeared that the used setpoints were not identical for the two data sets presented in [Ref. 3]. Presumably, this caused the two orders of magnitude difference in the dI/dV data as reported in [Ref. 3]

In Appendix B we also show what the influence is of a variation in the used setpoints on the experimentally determined differential conductivity.

Electronic properties of Au-induced nanowires @ 77 K

In their paper, Schäfer and co-workers conclude that the Au-induced nanowires act as an ideal model system of a 1D electron system [Ref. 3]. Emblematic of a 1D electron system is a so-called Van Hove singularity. The LDOS of an ideal 1D electron liquid then possesses a discontinuity which shows up as a steep increase of the LDOS at a certain threshold energy followed by a $1/\sqrt{V}$ decay [Ref. 11]. If present, it should in principle be possible to observe a Van Hove singularity at room temperature. This is not observed in neither the present data (previous Sections) nor in the data presented in [Refs. 3, 4]. However, at lower temperatures this anomaly should

be even more easily accessible. For that reason, the electronic behaviour of the Au-induced nanostructures was studied at 77 K as well. Figure 6.10 shows the dI/dV data measured at 77 K. The measurements were performed on a surface similar to the one shown in Figure 6.8 and were recorded both on the Au-induced wires and in between the wires.
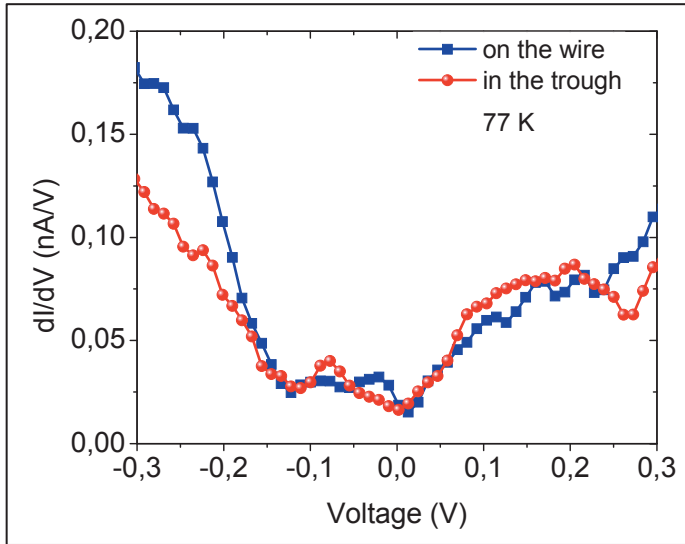
Figure 6.10: Differential conductivity measured at 77 K on top of the nanowires as well as in between the nanowires.

Similar to room temperature, at 77 K the difference between measuring on top of the wires and in between the wires is insignificant. Over the entire voltage window, the dI/dV curves measured on/off wire have similar values. Furthermore, at 77 K the dI/dV values have the same order of magnitude as at room temperature. More interesting however, there is no evidence at all for a Van Hove singularity. Therefore we arrive at the conclusion that the Au-

induced nanowires on Ge(001) bear no signature of a one-dimensional electron liquid.

Conclusions

The structural and the electronic properties of Au-induced nanowires on Ge(001) are investigated with scanning tunneling microscopy and spectroscopy at room temperature and 77 K. Two different preparation routes were used to form these nanowires. It appeared that the use of the different preparation methods results in the same structures, thus having identical electronic and structural properties.

The tops of the ridges of the Au-induced nanostructures consist of buckled Ge dimers. The sides of these ridges are comprised of Ge(111) nano-facets decorated with Au atoms. The wire-to-wire distance is 1.6 nm and the wires have a height of about 0.4 nm with respect to the troughs in between the wires.

The differential conductivities of the nanowires and the regions in between the nanowires measured at room temperature are highly similar and reveal only marginal metallicity. These observations are in marked contrast with a recent claim by Schäfer *et al.* that this system represents an outstanding model system for a 1D electron liquid. This is further corroborated by measurements carried out at 77 K, where we also did not find any evidence for the presence of a 1D electron liquid.

References

[Ref. 1]   J. Wang, M. Li and E.I. Altman, *Physical Review B* **70** (2004), p. 233312

[Ref. 2]   J. Wang, M. Li and E.I. Altman, *Surface Science* **596** (2005), p. 126

[Ref. 3]   J. Schäfer, C. Blumenstein, S. Meyer, M. Wisniewski and R. Claesen, *Physical Review Letters* **101** (2008), p. 236802

[Ref. 4]   A. van Houselt, M. Fischer, B. Poelsema and H. J. W. Zandvliet, *Physical Review B* **78** (2008), p. 233410

[Ref. 5]   S. Tomonaga, *Progress in Theoretical Physics* **5** (1950), p. 544

[Ref. 6]   J. M. Luttinger, *Journal of Mathematical Physics* **4** (1963), p. 1154

[Ref. 7]   H. J. W. Zandvliet, B. S. Swartzentruber, W. Wulfhekel, B.-J. Hattink and B. Poelsema, *Physical Review B* **57** (1998), R6803

[Ref. 8]   H. J. W. Zandvliet, *Physics Reports* **388** (2003), p. 1

[Ref. 9]   D. P. Woodruff, *Journal of Physics: Condensed Matter* **6** (1994), p. 6067

[Ref. 10]   A. van Houselt, R. van Gastel, B. Poelsema, and H. J. W. Zandvliet, *Physical Review Letters* **97** (2006), p. 266104

[Ref. 11]   C. Kittel, *Introduction to Solid State Physics* (John Wiley & Sons, New York, 1971)

Appendix A: Measuring κ

The tunneling current I in STM/STS exponentially depends on both the separation distance between the tip and the substrate, z, and the inverse decay length κ, i.e. $I \propto e^{-2\kappa z}$. The inverse decay length κ provides information on the spatial origin of the tunneling electrons. An electronic state with energy E relative to the Fermi level and parallel wave vector $k_{\parallel}$ will decay into the vacuum with an inverse decay length of

$$\kappa = \sqrt{\frac{2m}{\hbar^2}\left(\frac{\Phi_t + \Phi_s}{2} - E + \frac{e|V|}{2}\right) + k_{\parallel}^2}$$

(A.1)

where Φ_t is the work function of the tip, Φ_s is the work function of the substrate, and V is the sample bias [Refs. 1, 2]. Electronic states with small $k_{\parallel}$ values have the smallest κ and thus contribute most to the tunneling current. However, when the electronic state has a nonzero $k_{\parallel}$ value, κ may substantially increase. A spatial map of κ as a function of V thus provides very relevant information on the details of the electronic states involved in the STM measurement. So far, $I(z)$ spectroscopy has been used as the main technique to extract information on κ. Our newly developed method relies on the Simmons model [Refs. 3, 4], which provides a good approximation of the tunneling current in the low bias range,

$$I(V,z) = \frac{CV}{z}e^{-2\kappa z}$$

(A.2)

where z is the width of the vacuum barrier and C is a constant. Since the exponential term $e^{-2\kappa z}$ dominates over the $1/z$ term, the latter term is often ignored in the standard $I(z)$ spectroscopy technique resulting in $I(V,z) \propto e^{-2\kappa z}$. By plotting $\ln(I)$ as a function of z, the slope gives -2κ. In Figure A.1(b), an experimental $I(z)$ curve (open circles) measured on a Pt/Ge(001) is fitted with Equation (A.2). Although the fit (solid line) looks very good we have to realize that the Simmons model, in contrast to for instance the more realistic Tersoff–Hamann model [Refs. 5, 6] does not take into account the electronic structure of both the tip and the substrate. The latter are, however, unknown.
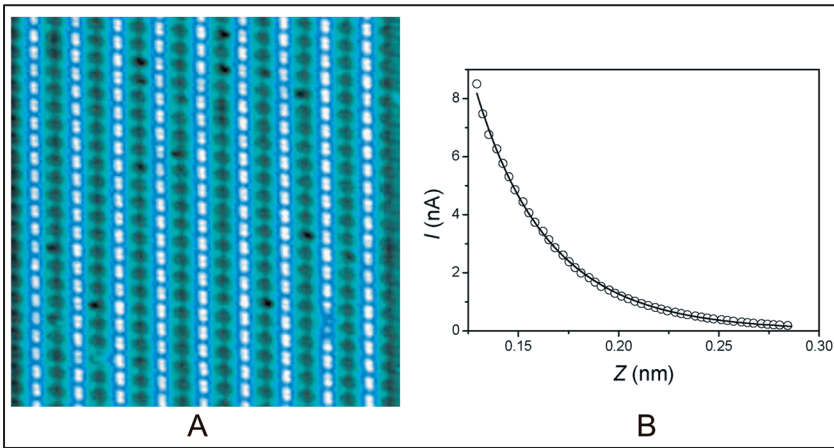
Figure A.1: Filled state STM image of a Pt modified Ge(001) surface recorded at 77 K (a). Sample bias is −1.0 V, tunneling current is 0.4 nA and image size is 15 x 15 nm². In (b) a spatially averaged I-z curve recorded on a Pt modified Ge(001) at 77 K is displayed (open circles). The solid line is a fit based on the Simmons model. The starting distance for the spectroscopy was defined by the current setpoint (1.0 nA, bias voltage −2.0 V). The spectroscopy was performed by subsequently opening the feedback loop, approaching 0.8 Å toward the surface, measuring the current while decreasing the distance over 1.7 Å, and closing the loop again.

When using the conventional $I(z)$ spectroscopy technique in order to make a spatial map of κ, one should measure $I(z)$ curves at each pixel of the topography map. From a practical point of view, this procedure is subject to two major limitations. First, by performing an $I(z)$ measurement at each pixel, the scanning rate dramatically decreases which makes the experiment vulnerable to accidental changes of the tip or the surface during the scanning process. The second drawback is the additional time required to fit the $I(z)$ curve and subsequently extract κ. This data analysis process slows down the determination of κ even more.

Having a closer look at Equation A.2, reveals that κ can be measured in a more efficient way by using the first and second derivatives of the tunneling current to z, i.e. dI/dz and d^2I/dz^2 .

First, we introduce two new parameters, denoted by F_1 and F_2

$$F_1 \equiv \frac{1}{i}\frac{dI}{dz} = -2\kappa - \frac{1}{z} \tag{A.3},$$

$$F_2 \equiv \frac{1}{i}\frac{d^2I}{dz^2} = \left(-2\kappa - \frac{1}{z}\right)^2 + \frac{1}{z^2} \tag{A.4}.$$

For κ this gives

$$\kappa = \frac{-F_1}{2} - \frac{\sqrt{F_2 - F_1^2}}{2} \tag{A.5}.$$

113

In the commonly used I(z) spectroscopy technique, the first term of Equation (A.5) is used. However, the second term in (A.5) represents the normally neglected $1/z$ term. The use of a lock-in amplifier enables the measurement of both dI/dz and d^2I/dz^2 simultaneously with the topography.

Since $\kappa(V)$ depends in principle both on the work functions of the tip and the substrate as well as on the details of the electronic states, we need to find a way to separate these two contributions (the only obvious voltage dependence in κ comes from the $e|V|/2$ term in Equation (A.1). Spatial variations in the work function of the sample are certainly there, but these variations do not depend on the value of the applied voltage V. If, for a certain applied voltage, additional spatial deviations in κ are found that cannot be explained by Equation (A.1), we can ascribe these deviations to variations in the k-space dependence of the electronic states. However, we should keep in mind that changes of the overlap of the wave functions of the tip and the surface might also affect the value of κ.

In order to measure the derivatives dI/dz and d^2I/dz^2, the z-piezo is modulated by a small sinusoidal voltage. The amplitude should not be larger than a few millivolts since the tunneling current exponentially depends on the tip-sample separation distance (see Equation A.2). The modulation frequency should be in the range of several kiloHertz, i.e. somewhat higher than the cutoff frequency of feedback loop, but significantly lower than the bandwidth of the pre-amplifier and the eigenfrequency of the piezo. We chose a modulation voltage on the z-piezo of 2.8–4.0 mV (rms value), corresponding to a z-position modulation of 14–20 pm and a modulation

frequency of 5.0 kHz. The sampling time per pixel point was chosen well in excess of the integration time of the lock-in amplifier. By using a two channel lock-in amplifier the first and second derivative of the current with respect to z can simultaneously be measured at each pixel point of the topographic image. The final results are discussed in Chapter 4.

References

[Ref. 1]   A. Stroscio, R. M. Feenstra and A. P. Fein, *Physical Review Letters* **57** (1986), p.2579

[Ref. 2]   R. M. Feenstra, J. A. Stroscio and A. P. Fein, *Surface Science* **181** (1987), p. 295

[Ref. 3]   J. G. Simmons, *Journal of Applied Physics* **34** (1963), p. 1793

[Ref. 4]   J. G. Simmons, *Journal of Applied Physics* **34** (1963), p. 2581

[Ref. 5]   J. Tersoff and D. R. Hamann, *Physical Review Letters* **50** (1983), p. 1998

[Ref. 6]   J. Tersoff and D. R. Hamann, *Physical Review B* **31** (1985), p.805

Appendix B: Manipulating the differential conductivity

In Chapter Six we have discussed the Au-induced nanowires on the Ge(001) surface. We have seen that in our case the differential conductivity measured on the wires was similar to the differential conductivity measured in between the wires. These data were similar to the data in [Ref. 1], where they only reported values measured on the wires. In addition, our data are also similar to the data in [Ref. 2] measured in between the wires. However, in [Ref. 2], Schäfer and co-workers reported a highly remarkable change of the differential conductivity at the Fermi level by a factor of 10^2 when comparing the nanowires with the troughs in between the nanowires. Since slightly different preparation routes were used, we have compared these routes in Chapter Six. There we have shown that the difference in used preparation routes could not explain the differences between our data (Chapter 6 and [Ref. 1]) and the on-wire data in [Ref. 2].

How can we now explain these differences?

In order to compare the differential conductivities measured at various locations on the surface in a meaningful way it is important to record the $I(V)$ curves with a fixed sample bias setpoint and a fixed tunneling current setpoint. Unfortunately, Schäfer and co-workers do not give the setpoint values of the sample bias and the tunneling current [Ref. 2]. Since the actual value of the differential conductivity critically depends on the used setpoint

values we have first reconstructed their $I(V)$ curves by integrating the available dI/dV data of [Ref. 2].

In Figure B.1(a) the dI/dV data taken from [Ref. 2] are shown, while the reconstructed $I(V)$ curves are depicted in Figure B.1(b) .
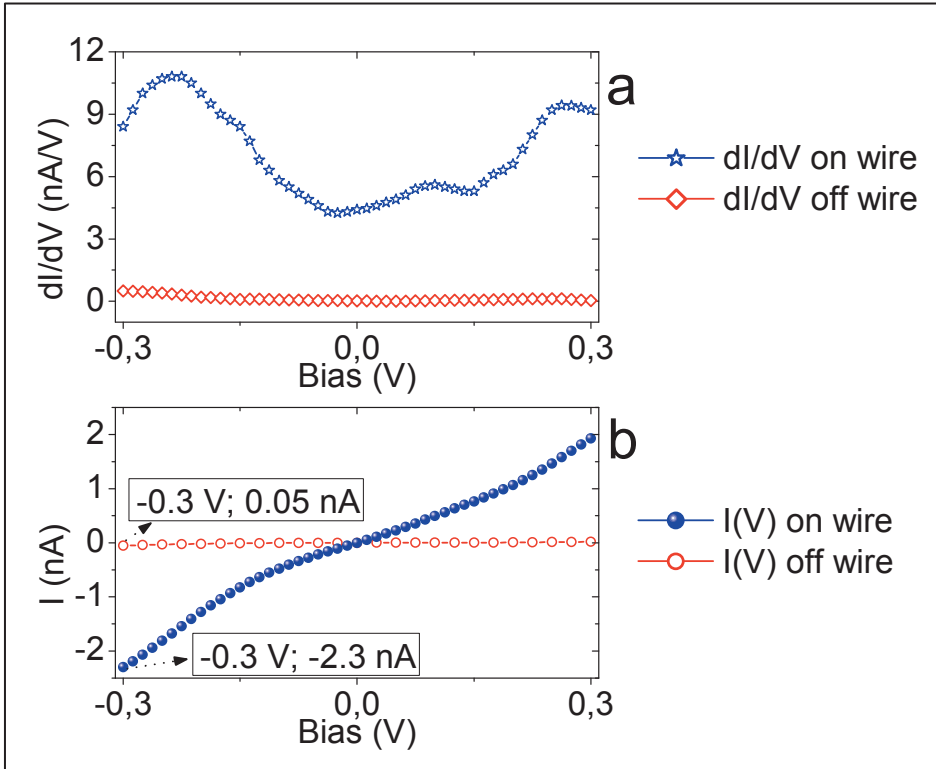

Figure B.1: dI/dV data taken from [Ref. 2] measured both on/off wire (a). The data in (b) are obtained by integration of the data in (a).

In Figure B.1(b) we see that the tunneling current measured in between the Au-induced wires (off wire) ranges from 0.05 nA at -0.3 V to 0.02 nA at 0.3

V. When measuring on top of the nanowires, the tunneling current increased significantly to -2.3 nA at -0.3 V and 1.93 nA at 0.3 V. In addition, in $I(V)$ spectroscopy the chosen setpoint current and voltage determine the starting point of the measured $I(V)$ curve. From taking a first glimpse at the data in Figure B.1(b), it is immediately clear that the starting points of the two $I(V)$ curves are not the same. Consequently, likely these curves were measured with widely varying current and voltage setpoints.

Since the measured differential conductivity at the Fermi level scales with the setpoint current, a difference in used setpoints could well explain the two orders of magnitude difference in the differential conductivity between on-top and in-between the Au-induced nanowires as reported in [Ref. 2]. To illustrate this feature we have performed a series of 'setpoint-dependent' $I(V)$ spectroscopy measurements. The bias setpoint was varied from $-0.3\,V$ to $-1.6\,V$ and the setpoint current ranged from $0.5\,nA$ to $2.0\,nA$.

As clearly shown in Figure B.2(a), the measured $I(V)$ characteristics depend heavily on the chosen setpoints for current and voltage; the slope of the $I(V)$ curves around the Fermi level changes dramatically. Obviously this is also reflected in the numerically derived dI/dV data, which are shown in Figure B.2(b).

Around the Fermi level the dI/dV increases from 0.1 nA/V with -1.6 V and 0.5 nA as the setpoints to 3.6 nA/V using -0.3 V and 2.0 nA. The latter differential conductivity agrees very well with the value presented by Schäfer and his co-workers. Not surprisingly, the setpoints used during the latter experiment (in which the highest differential conductivity, i.e. 3.6 nA/V, was measured) match very nicely with the starting points as were extracted from

the integrated dI/dV curves from [Ref. 2] shown in Figure B.1(b). Therefore, a natural explanation for the reported discrepancy in the differential conductivity measured on the wires and in between the wires in [Ref. 2] is that the two data sets were acquired at different setpoints indeed.
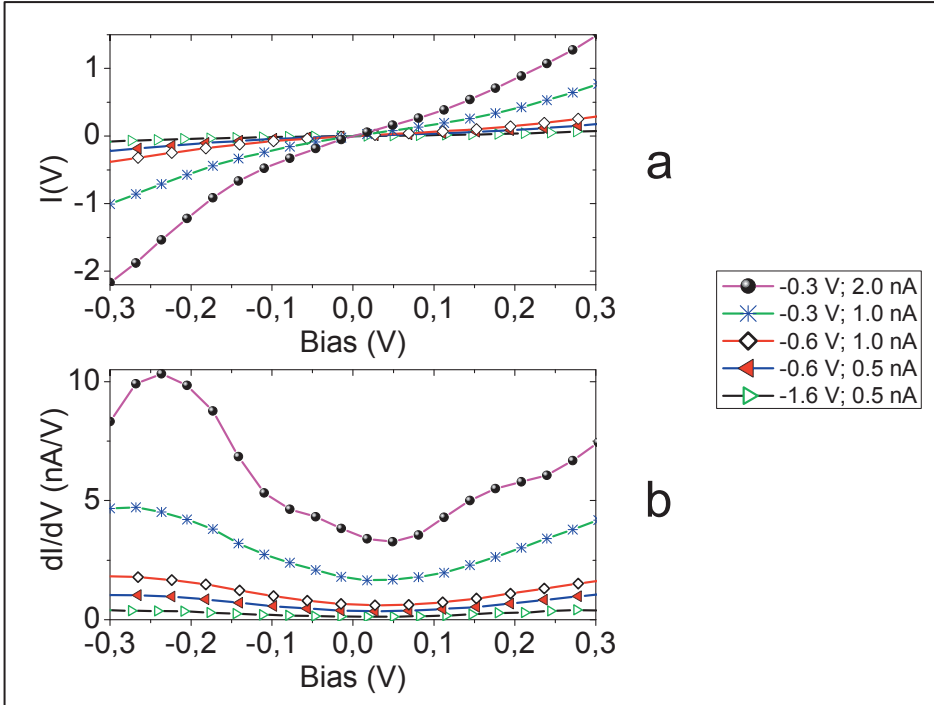
Figure B.2: Current-voltage characteristics measured with various setpoints on Au-induced nanowires (A). The corresponding dI/dV data are shown in B.

Mostly $I(V)$ and dI/dV data are recorded to obtain information on the density of states (DOS). However, as is obvious from the data shown above both $I(V)$ and dI/dV are characteristics of an interplay between the surface under investigation and the used setpoints. Predominantly, this is due to local

variations in the tip-sample distance. In order to obtain a more realistic view of the *DOS*, one can plot the spatially resolved version of the *DOS*, the local density of states (*LDOS*). The *LDOS* can be obtained according to [Ref. 3, 4]:

$$LDOS = \frac{(dI/dV)}{(I/V)} \tag{6.1}$$

Just for confirmation of the above statement, that the *LDOS* represents a materials property purely and should be independent of experimental settings, we have calculated the *LDOS* using the data from Figure B.2. The as-obtained *LDOS* is presented in Figure B.3.
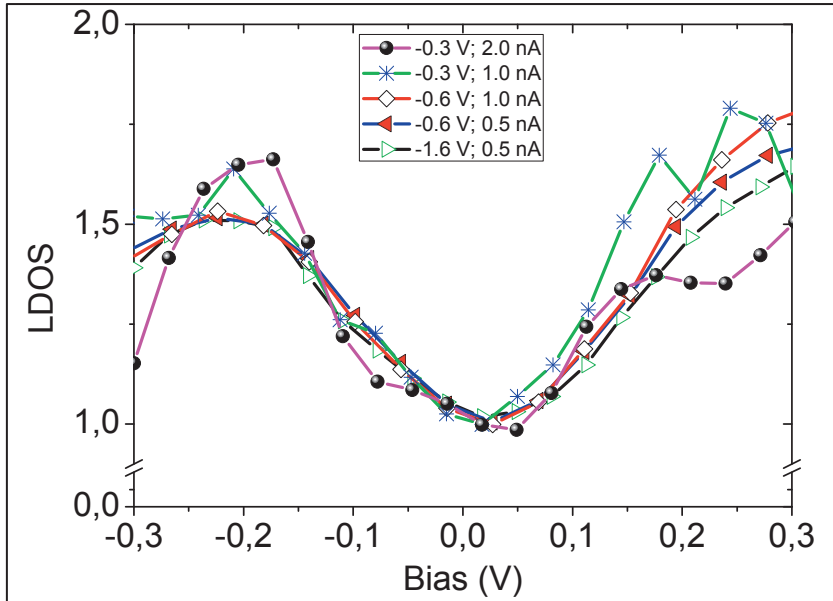
Figure B.3: Local density of states (LDOS) calculated from the data shown in Figure B.2.

In the chart of Figure B.3 it can be seen that the *LDOS* does not change significantly when varying the used current and voltage setpoints.

References

[Ref. 1]   A. van Houselt, M. Fischer, B. Poelsema and H. J. W. Zandvliet, *Physical Review B* **78** (2008), p. 233410

[Ref. 2]   J. Schäfer, C. Blumenstein, S. Meyer, M. Wisniewski and R. Claesen, *Physical Review Letters* **101** (2008), p. 236802

[Ref. 3]   A. Stroscio, R. M. Feenstra and A. P. Fein, *Physical Review Letters* **57** (1986), p.2579

[Ref. 4]   R. M. Feenstra, J. A. Stroscio and A. P. Fein, *Surface Science* **181** (1987), p. 295

Summary

The ongoing miniaturization of (components of) electronic devices will eventually need a totally new preparation route for these (components of) devices. It is thought that the ultimate miniaturization requires the use of functional molecules and their incorporation into nanostructured templates. For that reason it is interesting to study nanostructured surfaces and the behaviour of adsorbed molecules on these surfaces.

In this dissertation results are described on two different nanostructured surfaces. Their structural and electronic properties were studied with scanning tunneling microscopy (STM) and scanning tunneling spectroscopy (STS). In Chapter Two these experimental techniques were discussed.

In Chapter Three the structural and electronic properties of the Pt-modified Ge(001) surface are discussed. After evaporation of Pt on Ge(001) and a subsequent annealing procedure three types of terraces were formed.

The α-terrace is believed to consist of both symmetric and asymmetric Ge dimers and contains a large amount of vacancy-defects.

The β-terrace is comprised of both Ge dimers and Ge-Pt dimers and contains a large number of vacancy-defects too. However, here the defects are clustered in lines.

Large arrays of atomic Pt chains were found on the β-terraces. During Pt deposition the Pt occupies subsurface positions. When the surface is annealed the surface dimer rows widen and the Pt pops up in pairs of two atoms. After a subsequent rotation by 90° the Pt dimers form chains with a width of only one atom. Mostly, the chains have a mutual separation distance of exactly 1.6 nm. The chemical nature of the chains was confirmed via selective adsorption of CO.

The Pt chains undergo a structural transition from a 2× to 4× periodicity when cooled down from 293 K to 4.7 K. STS experiments revealed that this transition is accompanied by a reduction in the differential conductivity of the Pt chains. We concluded that the transition is driven by a Peierls instability.

At room temperature the Pt/Ge(001) surface was decorated with CO molecules. This system was studied with STM at 77 K; this is described in Chapter Four. It appeared that CO binds preferentially, if not exclusively, to the Pt chains and not to the underlying surface. At this temperature CO occupies two different adsorption sites. A long-bridge site showed up as a protrusion at both positive and negative bias. An on-top or short-bridge site showed up as a depression at positive bias and as a protrusion at negative bias.

By comparing the distribution of the separation distance between adsorbed CO molecules with a no-interaction model we found that the CO molecules show a remarkably long-ranged mutual repulsion, i.e. they repel each other up to about 4 nm.

By spatially mapping the inverse decay length of the CO-decorated Pt/Ge(001) surface we found that at positions where CO is adsorbed the inverse decay length is small.

The decoration of the Pt/Ge(001) surface with octanethiol molecules is discussed in Chapter Five. Octanethiol preferentially adsorbs on the Pt chains.

By performing STS on various positions above the adsorbed molecules we were able to distinguish between the thiol-head and the octane-tail of the molecule. Hereby, we were able to resolve the adsorption geometry of the molecule.

During I(t) experiments recorded above an adsorbed octanethiol molecule, the molecule occasionally wagged its tail upwards. In this event, the molecule contacted the tip of the STM. Then, the electrons now longer tunnel through the vacuum but flow through the molecule. This allowed us to determine the single octanethiol molecule resistance, i.e. 100-150 MΩ.

In Chapter Six we focused on Au-induced nanostructures on Ge(001). They were prepared using two different preparation routes. Subsequently, the structural and electronic properties of the formed structures were studied at 293 K and at 77 K. We showed that these were independent of the used preparation method.

The Au-modified Ge(001) surface consists of nanowires. The tops of the ridges of these nanowires appear to consist of buckled Ge dimers. The sides of these ridges are comprised of giant Ge(111) nano-facets decorated with Au atoms. The wire-to-wire distance is 1.6 nm and the wires have a height of about 0.4 nm with respect to the troughs in between the wires.

The differential conductivities of the nanowires and the regions in between the nanowires at room temperature are highly similar and reveal only marginal metallicity. These observations are in marked contrast with a recent claim by Schäfer *et al.* that this system represents an outstanding model system for a 1D electron liquid. This is further corroborated by the measurements carried out at 77 K, where we also did not find any evidence for the presence of a 1D electron liquid.

Samenvatting

De voortdurende miniaturisatie van (componenten van) elektronica apparaten zal uiteindelijk een compleet nieuwe preparatie methode voor deze (componenten van) elektronica apparaten nodig hebben. Er wordt verwacht dat voor de ultieme verkleining, men functionele moleculen en hun incorporatie in nano-gestructureerde patroon oppervlakken nodig heeft. Daardoor is het interessant om nano-gestructureerde oppervlakken en het gedrag van geadsorbeerde moleculen op deze oppervlakken te bestuderen.

In dit proefschrift staan resultaten beschreven over twee verschillende nano-gestructureerde oppervlakken. Zowel hun structurele als hun elektronische eigenschappen zijn bestudeerd met behulp van scanning tunneling microscopie (STM) en met scanning tunneling spectroscopie (STS). Deze experimentele technieken staan beschreven in Hoofdstuk Twee.

De structurele en de elektronische eigenschappen van het platina (Pt) gemodificeerde Ge(001) oppervlak zijn besproken in Hoofdstuk Drie. Na verdamping van Pt op Ge(001) en een daaropvolgende verwarmingsprocedure worden er drie verschillende soorten terrassen gevormd.

Het α-terras bestaat waarschijnlijk uit zowel symmetrische als asymmetrische Ge dimeren en het terras bevat een groot aantal vacature defecten. Het β-terras bestaat zowel uit Ge dimeren als uit Ge-Pt dimeren en bevat ook een groot aantal vacature defecten. Echter, de defecten zijn nu geclusterd in lijnen.

Grote arrays van atomaire Pt ketens zijn gevonden op de β-terrassen. Gedurende de depositie van Pt, neemt het Pt posities in net onder het Ge oppervlak. Wanneer het oppervlak verwarmd wordt, verwijden de dimeer rijen zich en komt het Pt in paren van twee atomen naar boven. Na een daaropvolgende rotatie van 90°, vormen de Pt dimeren een keten met een breedte van exact één atoom. De onderlinge scheidingsafstand tussen de ketens is meestal exact 1.6 nm. Het chemische karakter van de ketens werd bevestigd door selectieve adsorptie van koolmonoxide (CO) op de ketens.

De Pt ketens ondergaan een structurele overgang van een $2\times$ naar een $4\times$ periodiciteit bij afkoeling van 293 K ($20\,°C$) naar 4.7 K ($-268\,°C$). STS experimenten hebben aangetoond dat deze transitie bijgestaan wordt door een reductie in de metalliciteit. We concludeerden dat de overgang aangestuurd wordt door een Peierls instabiliteit.

Op kamertemperatuur werd het Pt/Ge(001) oppervlak gedecoreerd met CO moleculen. Dit systeem is bestudeerd met STM bij 77 K ($-196\,°C$); dit staat

beschreven in Hoofdstuk Vier. Het is gebleken dat CO preferentieel, zo niet exclusief, op de Pt ketens adsorbeert en niet op het onderliggende oppervlak. Bij deze temperatuur bezet CO twee verschillende adsorptie posities. Een 'long-bridge' positie, die zichtbaar is als verhoging bij zowel positieve als negatieve spanning, en een 'on-top' of 'short-bridge' positie, die zichtbaar is als depressie bij positieve spanning en als verhoging bij negatieve spanning.

Door vergelijking van de distributie van de scheidingsafstand tussen de geadsorbeerde CO moleculen met een 'geen-interactie model', vonden we dat de CO moleculen een opmerkelijk verstrekkende onderlinge repulsie ondervinden; ze stoten elkaar af tot op een afstand van ongeveer 4 nm. Door een ruimtelijke plattegrond van de inverse vervallengte te maken van het met CO gedecoreerde Pt/Ge(001) oppervlak, zagen we dat op posities waar CO geadsorbeerd zit de inverse vervallengte klein is.

De decoratie van het Pt/Ge(001) oppervlak met octaanthiol moleculen staat beschreven in Hoofdstuk Vijf. Octaanthiol adsorbeert preferentieel op de Pt ketens.

Door het uitvoeren van STS experimenten op verschillende posities boven de geadsorbeerde moleculen konden we onderscheid maken tussen de thiol-kop en de octaan-staart van het molecuul. Hierdoor konden we de adsorptie geometrie van het molecuul achterhalen.

Tijdens I(t) experimenten opgenomen boven een geadsorbeerd octanethiol molecuul, kwispelde het molecuul zijn staart af en toe omhoog. Gedurende deze actie maakte de staart van het molecuul contact met de tip van de STM. Nu tunnelen de elektronen niet meer door het vacuüm, maar vindt het transport van de elektronen plaats door het molecuul. Hierdoor konden we

de weerstand van één enkel octaanthiol molecuul bepalen, nl. $100-150 \, M\Omega$.

In Hoofdstuk Zes lag onze focus bij de goud (Au) geïnduceerde nanostructuren op Ge(001). Deze zijn gemaakt op twee verschillende preparatie methodes. Daaropvolgend zijn de structurele en de elektronische eigenschappen van de gemaakte structuren bestudeerd op 293 K en op 77 K. We hebben aangetoond dat de eigenschappen onafhankelijk zijn van de gebruikte preparatie methodes.

Het Au-gemodificeerde oppervlak bestaat uit nanodraden. De bovenkant van de draden lijkt uit Ge dimeren te bestaan die afwisselend links en rechts naar beneden hellen. De flanken van de draden bestaan uit Ge(111) facetten gedecoreerd met Au atomen. De draad tot draad afstand is 1.6 nm en de hoogte van de draden is ongeveer 0.4 nm.

De metalliciteit van de draden en van de regio's tussen de draden is bij kamertemperatuur gelijkwaardig en is zeer marginaal. Deze observaties staan in contrast met een recente claim door Schäfer en zijn collega's. Zij beweren namelijk dat het Au/Ge(001) systeem een buitengewoon goed modelsysteem is van een eendimensionaal (1D) elektron vloeistof. Onze bevindingen zijn verder bevestigd door STM/STS metingen bij 77 K; hier werd ook geen bewijs gevonden voor de aanwezigheid van een 1D elektron vloeistof.

List of publications

Parallel electron-hole bilayer conductivity from electronic interface reconstruction;
R. Pentcheva, M. Huijben, K. Otte, W.E. Pickett, J. E. Kleibeuker, J. Huijben,
H. Boschker, <u>D. Kockmann</u>, W. Siemons, G. Koster, H. J. W. Zandvliet, G.
Rijnders, D. H. A. Blank, H. Hilgenkamp, A. Brinkman;
Physical Review Letters **104** (2010), p. 166804

*Comment on "New model system for a one-dimensional electron liquid: Self-organized
atomic gold chains on Ge(001)";*
A. van Houselt, <u>D. Kockmann</u>, T.F. Mocking, B. Poelsema, H.J.W. Zandvliet;
Physical Review Letters **103** (2009), p. 209701

Structural and Electronic properties of Au induced nanowires on Ge(001);
<u>D. Kockmann</u>, T.F. Mocking, A. van Houselt, B. Poelsema, H.J.W. Zandvliet;
Journal of Physical Chemistry C **113** (2009), p. 17156

Transport through a single octanethiol molecule;
<u>D. Kockmann</u>, B. Poelsema, H.J.W. Zandvliet;
Nano Letters **9** (2009), p. 1147

*Remarkably long-ranged repulsive interaction between adsorbed CO molecules on Pt-
modified Ge(001);*
<u>D. Kockmann</u>, B. Poelsema en H.J.W. Zandvliet;
Physical Review B **78** (2008), p. 245421

Reappraisal of variable-range hopping in quantum-dot solids;
A.J. Houtepen, <u>D. Kockmann</u> en D. Vanmaekelbergh;
Nano Letters **8** (2008), p. 3516

Spatial mapping of the inverse decay length in real-time;
R.J. de Vries, A. Saedi, <u>D. Kockmann</u>, A. van Houselt, B. Poelsema en H.J.W. Zandvliet;
Applied Physics Letters **92** (2008), p. 174101

Peierls instability in Pt chains on Ge(001);
A. van Houselt, T. Gnielka, M. Fischer, J. Aan de Brugh, N. Oncel, <u>D. Kockmann</u>, R. Heid, K.-P. Bohnen, B. Poelsema en H.J.W. Zandvliet;
Surface Science **602** (2008), p. 1731

Formation of atomic Pt chains on Ge(001) studied by scanning tunnelling microscopy;
M. Fischer, A. van Houselt, <u>D. Kockmann</u>, B. Poelsema en H.J.W. Zandvliet;
Physical Review B **76** (2007), p. 245429

Effect of C6-olefin isomers on pi-complexation for purification of 1-hexene by reactive extractive distillation;
A.E. Wentink, <u>D. Kockmann</u>, N.J.M. Kuipers, A.B. de Haan, J. Scholz en H. Mulder;
Separation and Purification Technology **43** (2005), p. 149

Dankwoord

Promoveren doe je alleen, maar niet zonder de hulp van velen. Vandaar dit Dankwoord, waarschijnlijk het meest gelezen deel van dit proefschrift (lees: doe een poging en lees de rest ook, het valt wel mee).

Als eerste wil ik uiteraard mijn promotoren bedanken. Harold en Bene, bedankt voor de kans die jullie mij, als 'chemicus', hebben gegeven. De afgelopen jaren heb ik met veel plezier gewerkt aan het onderzoek dat in dit proefschrift beschreven staat. Ondanks dat een binding met het onderzoek hieraan heeft bijgedragen, was dit voor mij niet mogelijk geweest zonder een prettige werkomgeving. Ten grondslag hiervan ligt vooral de manier waarop jullie de zaak runnen. Bedankt hiervoor.

Harold, als 1^e promotor heb ik de laatste jaren vooral met jou gewerkt. Officieel was je mijn baas, maar gelukkig voelde dit niet altijd zo. Met jou omgaan is niet onderhevig aan hiërarchische verstoring. Je was altijd aanspreekbaar en stond direct klaar wanneer ik met een probleem zat. Jouw betrokkenheid is zeker van essentieel belang geweest voor het verloop mijn onderzoek en daarnaast had je ook altijd wel een leuke mop te vertellen.

Amir, gedurende vrijwel de volle vier jaren op de UT waren wij kantoorgenoten. In het begin nog met ons tweeën, zodat we zelfs nog meer kantoorruimte hadden dan *onze baas*. Bedankt voor de gesprekken over STM, Iran en de islam en andere zaken en voor de vermakelijke/hilarische films waarin jij de laatste jaren een hoofdrol speelde. Onze verschillende professionele interesses/instelling hebben er voor gezorgd dat we veel van elkaar hebben kunnen leren.

Akram, ruim tweeënhalf jaar hebben wij een kantoor gedeeld. Onze gesprekken gingen voornamelijk over de verschillende software programma's en ik denk dat we veel van elkaar geleerd hebben. Regelmatig hebben we ook de situaties in jouw thuisland besproken en ik hoop dan ook dat de vooruitgang in Pakistan zich de komende jaren voortzet.

Tijs, voordat je als promovendus plaats nam in ons kantoor was je natuurlijk *mijn student*. Nogmaals wil ik je bedanken voor jouw bijdrage aan mijn promotieonderzoek. Een jaar lang heb ik je mogen begeleiden tijdens jouw afstudeeronderzoek. Ik vond het een leuke, maar daarnaast ook een leerzame ervaring. En, niet onbelangrijk, jouw werk heeft bijgedragen aan twee mooie publicaties en uiteindelijk geleid tot je diploma en tot je huidige job.

Arie, wij kenden elkaar al van onze studie in Utrecht en dat schiep direct een band in Twente. Ik baalde er altijd van dat jij, ondanks dat je helemaal uit Barneveld moest komen, eerder *op vloer 5* aanwezig was dan ik. Sinds je bij CPM zit, is die tijd gelukkig voorbij. Maar serieus, op Harold na, ben jij degene van wie ik het meest geleerd heb. Zowel op technisch als op theoretisch vlak wist je me altijd uit de brand te helpen. Ik vind het daarom ook erg leuk dat je in mijn promotiecommissie zit.

Niet zelden gaat een technisch promotieonderzoek gepaard met behoorlijke technische problemen. Gelukkigerwijs ben ik hiervan geschoond gebleven. De minuscule technische mankementen die er wel waren, werden echter snel opgelost door Hans en Herman. Hiervoor dank. (En Hans, bedankt voor de gezamenlijke rookpauzes).

Verder wil ik iedereen bedanken die een bijdrage heeft geleverd aan de goede sfeer binnen de afdelingen PNE en VSF.

Dat ik zou promoveren zullen er vroeger maar weinigen hebben gedacht. Dat dit toch gaat lukken (!?) komt hoofdzakelijk door de altijd aanwezige stimulering (vroeger vaak tot ongenoegen van de auteur) en steun van mijn ouders. Pap en mam, bedankt.
En tenslotte Marijn. De afgelopen jaren heb jij ervoor gezorgd dat ik me in tijden van stress (?) kon ontspannen en dankzij jou ben ik *zo lekker gewoon gebleven*.

<p align="center">Iedereen bedankt!</p>

Curriculum Vitae

Daan Kockmann werd geboren op 16 juli 1978 te Feldkirch (Oostenrijk). Aan het Twents Carmel Lyceum te Oldenzaal behaalde hij zijn HAVO en VWO diploma's, in respectievelijk 1995 en 1997.

In 1999 begon hij bij de Saxion Hogeschool IJsseland aan de studie Algemene Chemie. Na een stage bij de Separation Technology Group (Universiteit Twente) en een afstudeerstage bij het Debye Instituut voor Nanomateriaalonderzoek (Universiteit Utrecht), werd in 2003 het ingenieursdiploma (ing.) Chemie behaald.

Daaropvolgend werd in maart 2006 het Master of Science diploma behaald door de mastertrack *Chemistry and Physics* aan de Universiteit Utrecht te voltooien. Zijn afstudeerproject heeft hij uitgevoerd bij de afdeling *Chemie en Fysica van Nanostructuren*. Hier heeft hij gewerkt aan de synthese van halfgeleidende nanokristal materialen en heeft hij de optische, de elektronische en de electrochemische eigenschappen hiervan bestudeerd.

In januari 2006 trad hij in dienst van de Universiteit Twente om daar een promotieonderzoek uit te voeren bij de vakgroep *Physical Aspects of NanoElectronics.* Een deel van het daar uitgevoerde werk staat beschreven in dit proefschrift en in enkele wetenschappelijke artikelen. Daarnaast bezocht hij enkele conferenties waar (een deel) van het werk is gepresenteerd:
- 71st Annual Meeting of the Deutsche Physikalische Gesellschaft and DPG - spring meeting of the Division Condensed Matter, 2007 Regensburg (Duitsland),
- The 22nd Conference of the Condensed Matter Division of the European Physical Society, 2008 Rome (Italië),
- 56th International Symposium and Exhibition of the American Vacuum Society, 2009 San Jose (VS).

Tenslotte is Daan twee jaar actief geweest als bestuurslid van het Promovendi Netwerk Universiteit Twente.